Micro Gas Turbine Performance Evaluation

by

Francis Oppong

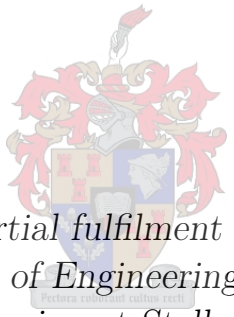

Thesis presented in partial fulfilment of the requirements for the degree of Master of Engineering (Mechanical) in the Faculty of Engineering at Stellenbosch University

Supervisors:

Prof. S.J. van der Spuy
Prof. T.W. von Backström

December 2016

Declaration

By submitting this thesis electronically, I declare that the entirety of the work contained therein is my own, original work, that I am the sole author thereof (save to the extent explicitly otherwise stated), that reproduction and publication thereof by Stellenbosch University will not infringe any third party rights and that I have not previously in its entirety or in part submitted it for obtaining any qualification.

Date: . December 2016

Abstract

Micro Gas Turbine Performance Evaluation

F. Oppong

Department of Mechanical and Mechatronics Engineering,
University of Stellenbosch,
Private Bag X1, Matieland 7602, South Africa.

Thesis: MEng (Mech)

December 2016

The performance of the BMT 120 KS micro gas turbine engine is investigated in this thesis. The study includes component matching of the engine elements using compressor and turbine characteristic maps to analyse the engine's performance. Analytical and numerical calculations were used to assess the various thermodynamic parameters of the engine and loss of engine power exacerbated by poor performance of the engine components. Engine performance was modelled using commercial simulation software GasTurb and Flownex SE and an in-house one-dimensional code. Using the numerical computations, a component sensitivity and matching analysis was performed for the engine using the various engine components. The theoretical performance of the engine was validated with experimental engine tests. The comparison of engine simulation results and experimental test data showed a consistent trend. A thrust difference of between 0.5% and 6% was achieved between the experimental and simulated results for the baseline engine. The experimental and simulated exhaust gas temperature of the BMT engine showed differences between 1.4% and 6%. Furthermore, a mean-line turbine design analysis was undertaken to study the possibility of improving the performance of the engine's axial turbine. Simulations that made use of the mean-line turbine predicted a thrust of approximately 190 N and exhaust gas temperature of 993 K at a speed of 120 000 rpm.

Uittreksel

Mikro Gasturbine Performance Evaluation

("Micro Gas Turbine Performance Evaluation")

F. Oppong

Departement Meganiese en Megatroniese Ingenieurswese,
Universiteit van Stellenbosch,
Privaatsak X1, Matieland 7602, Suid Afrika.

Tesis: MIng (Meg)

Desember 2016

Die werksverrigting van die BMT 120 KS mikro gasturbine word in hierdie tesis ondersoek. Die studie behels onder andere die gebruik van kompressor-en turbinekaarte om komponentpassing van enjinonderdele te doen ten einde die werksverrigting van die enjin te analiseer. Analitiese en numeriese berekeninge is gebruik om die verskillende termodinamiese parameters van die enjin, asook werkverrigtingverliese as gevolg van die swak lewering van enjinonderdele te ondersoek. Die enjinwerkverrigting is gemodelleer met behulp van GasTurb en Flownex SE sagteware, asook 'n in-huis enn-dimensionele kode. Deur gebruik te maak van die numeriese berekeninge is 'n sensitiwiteitspassing analise ook uitgevoer vir die verskillende enjin komponente. Die teoretiese werksverrigting van die enjin is bevestig met behulp van eksperimentele enjin toetse. Die vergelyking tussen die eksperimentele-and simulasie resultate wys 'n deurlopende neiging. 'n Verskil in stukrag van tussen 0.5% en 6% is behaal tussen die eksperimentele en simulasie resultate. 'n Vergelyking van die eksperimentele en simulasie resultate vir die enjin uitlaatgas temperatuur van die BMT enjin het verskille van tussen 1.4% en 6% getoon. 'n Middellyn analise van die turbine is gedoen om die moontlikhede vir die verbetering van die enjin se aksiaalturbine te ondersoek. 'n Analise wat gebruik maak van die turbine se middellyn resultate dui aan dat 'n stukrag van 190 N en uitlaatgas temperatuur van 993 K by 'n rotasiespoed van 120 000 opm behaal kan word.

Acknowledgements

I would like to express my sincere gratitude to Almighty God for his guidance, grace and wisdom. Furthermore, special appreciation goes to my committed supervisors Prof. T.W. von Backström and Prof. S.J. van der Spuy for their patience, guidance and hope in me.

My heartfelt thanks to my wife Salamatu Karim and son Kwaku Yeboah for their support.

I would also like to thank David Krige, Gareth Erffort, Dr Francois Louw and Dr. Lacina Diaby for their support, time and all the sacrifices they made for me.

I want to thank my parents and siblings for their encouragement and support.

I acknowledge the support, prayers and the advice of my church small group. Thanks peers for the coffee and testimonies about God and his son Jesus Christ.

My thanks also go to Severin Azankpo, Emmanuel Bwembya, Michael Wilkinson, Bernard Effah, Fredua Agyeman, Prince Gyebi, Christiaan Burger, Felix Asoba, Samuel Asante, Emmanuel Assiamah Yeboah and all my friends for their immense contribution towards the completion of this thesis.

Lastly, I acknowledge the support of CSIR for funding the project and for the provision of GasTurb and also MTech and ESTEQ for providing Flownex SE for the project.

Dedication

To my wife Salamatu Karim and son Kwaku Yeboah

Contents

List of Figures

List of Tables

Nomenclature

Constants

π	3.1416	[−]
R	287	[J/kgK]
c_{pa}	1.4	[−]
c_{pg}	1.333	[−]

Variables

A	Area	[m^2]
C_a	Velocity	[m/s]
C_d	Discharge coefficient	[−]
c_{pa}	Air specific heat at constant pressure	[J/kgK]
$\dot{Q}$	Energy	[J]
u_e	Exhaust jet velocity	[m/s]
u_0	Free stream velocity	[m/s]
f	Fuel-air ratio	[−]
c_{pg}	Gas specific heat at constant pressure	[J/kgK]
r	Radius	[m]
$\dot{m}$	Mass flow rate	[kg/s]

F_{net}	Net thrust	[N]
N	Rotational speed	[rpm]
p	Pressure	[Pa]
P	Power	[W]
R_e	Reynolds number	[−]
W_θ	Relative velocity	[m/s]
ε_R	Rotor deflection angle	[Degrees]
ξ_R	Rotor loss coefficient	[−]
U	Rotational velocity	[m/s]
r_s	Shroud radius	[m]
R	Specific gas constant	[J/kgK]
ε_S	Stator deflection angle	[Degrees]
ξ_S	Stator loss coefficient	[−]
T	Temperature	[K]
C_θ	Tangential velocity	[m/s]
$\dot{W}$	Work	[J]

Subscripts

a	Air, axial
cv	Control volume
$corr$	Corrected
d	Discharge
des	Design

e	Exit
f	Fuel
g	Gas
h	hub
in	Inlet
$isen$	Isentropic
m	Mean
p	Propulsion
R	Rotor
s	shroud
S	Stator
0	Total
tt	Total-to-total
th	Thermal
T	Turbine

Greek Symbols

β	Blade angle	[Degrees]
ε	Deflection angle	[Degrees]
Λ	Degree of reaction	[−]
ρ	Density	[kg/m^3]
β	Diameter ratio	[−]
Δ	Difference	[−]

η	Efficiency	[%]
α	Flow angle	[Degrees]
ϕ	Flow coefficient	[−]
ψ	Loading coefficient	[−]
ξ	Loss or power coefficient	[−]
σ_s	Slip factor	[−]
γ	Specific heat ratio	[−]

Acronyms

AFCC	Axial Flow Compressor Code
APU	Auxiliary Power Unit
BMT 120 KS	Baird Micro Turbine 120 Kerosene Start
CFD	Computational Fluid Dynamics
CPR	Compressor Pressure Ratio
EGT	Exhaust Gas Temperature
GPA	Gas Path Analysis
GT	Gas Turbine
GSP	Gas Turbine Simulation Program
GSU	Ground Support Unit
HV	Heating Value
IGV	Inlet Guide Vane
IPR	Impeller Pressure Ratio
KF	Kalman Filtering

KKK	Kuhnle, Kopp and Kausch
MLD	Mean-Line Design
MLA	Mean-Line Analysis
MGT	Micro Gas Turbine
NGV	Nozzle Guide Vane
PROOSIS	Propulsion Object-Oriented Simulation Software
SE	Simulation Environment
SFC	Specific Fuel Consumption
TCU	Turbine Control Unit
TIT	Turbine Inlet Temperature
TPM	Turbo Power Match
TPR	Turbine Pressure Ratio
UAV	Unmanned Aerial Vehicle

Chapter 1

Introduction

In recent years Micro Gas Turbine (MGT) engines have become popular technologies in commercial aviation and hobby industries. They are used on unmanned aerial vehicles (UAVs) and as auxiliary power units (APUs) for modern aircraft. MGTs are also used in hybrid electric vehicles and small electricity generating plant applications. They are suited for such applications due to their high power to weight ratio, multi-fuel capability and simplicity in design. These engines have interrelated components which have nonlinear characteristics. The individual engine component's performance contributes to the overall engine performance. Researchers are therefore motivated to develop and design highly efficient MGT components. In this regard, considerable research has focused on the performance improvement of the compressor and turbine stages of the Baird Micro Turbine (BMT 120 KS) engine at Stellenbosch University's Department of Mechanical and Mechatronic Engineering. This project investigates component matching of the BMT engine and the modified compressor and turbine stages. Analytical and numerical analyses are used to review the BMT thermodynamic cycle through a detailed assessment of the engine's previous theoretical and experimental evaluations. This serves as a basis for improved component matching of the engine.

1.1 Motivation

Although MGTs have gradually emerged as popular elements of small-scale propulsion systems, their full potential has not yet been exploited. In recent years, research projects have been undertaken to redesign the turbine and

compressor stages of the BMT engine in order to increase the engine's thrust output. Despite the improved component performance, the engine suffers from high exhaust gas temperatures (EGT), high fuel consumption and fails to reach the design rotational speed. A possible reason for these issues might be mismatching of the compressor and turbine components. Component matching, which involves the use of the compressor and turbine characteristic maps for gas turbine (GT) analysis is used to investigate the engine's performance. The results of this study will lead to research questions and solutions that will contribute towards improving the BMT engine's fuel consumption, exhaust gas temperature and the engine's overall performance.

1.2 Objectives

The focus of this study is to evaluate the performance of the BMT 120 KS engine. An in-depth engine performance analysis provides a better understanding of the limitations and merits of the engine components and their impact on performance. Consequently, various engine components will be assessed via system performance simulations. The project's objectives are as follows:

1. Perform an experimental test of the baseline engine (BMT 120 KS).
2. Perform analytical calculations (one-dimensional code) to validate the thermodynamic performance of the baseline engine.
3. Model and simulate the baseline engine in both GasTurb (Gas turbine simulation software) and Flownex SE (Thermodynamic system analysis software).
4. Analyse the modified compressor and turbine components in Flownex SE.
5. Compare numerical, analytical and experimental results of the various engine configurations.
6. Suggest a preliminary turbine stage design improvement.

1.3 Thesis Overview

The thesis is divided into six chapters and structured as follows:

Chapter 2 details the literature review of micro gas turbine technologies. The literature includes micro gas turbine performance improvement options and gas turbine performance modelling methods. This chapter also gives an overview of the BMT engine and gas turbine performance parameters.

The experimental evaluation of the engine is presented in chapter 3. The engine experimental assessment captures the experimental procedures, data measurements and the calibration of the measuring instruments. The engine performance analyses are discussed in chapter 4. The analytical and numerical calculations of the engine performance parameters are presented in this chapter. Also, the numerical softwares used for the engine analyses are described. The simulated engine results are compared to the experimental data sets of the engine.

Chapter 5 presents preliminary turbine design improvements for the BMT turbine stage. The turbine design analysis involved turbine mean-line evaluation, which includes calculation of the turbine performance parameters.

Finally, Chapter 7 provides discussions, conclusions and recommendations for engine performance improvement.

Chapter 2

Literature Review

This chapter presents an overview of MGT technologies. An overview of the BMT engine and literature from academic research projects that have been undertaken to improve MGT performance is presented. The thermodynamic principles and performance parameters of a simple gas turbine are also reviewed. Lastly, gas turbine performance modelling is discussed.

2.1 The BMT 120 KS Engine

The BMT 120 KS engine shown in Figure 2.1 is a single spool (shaft) MGT.

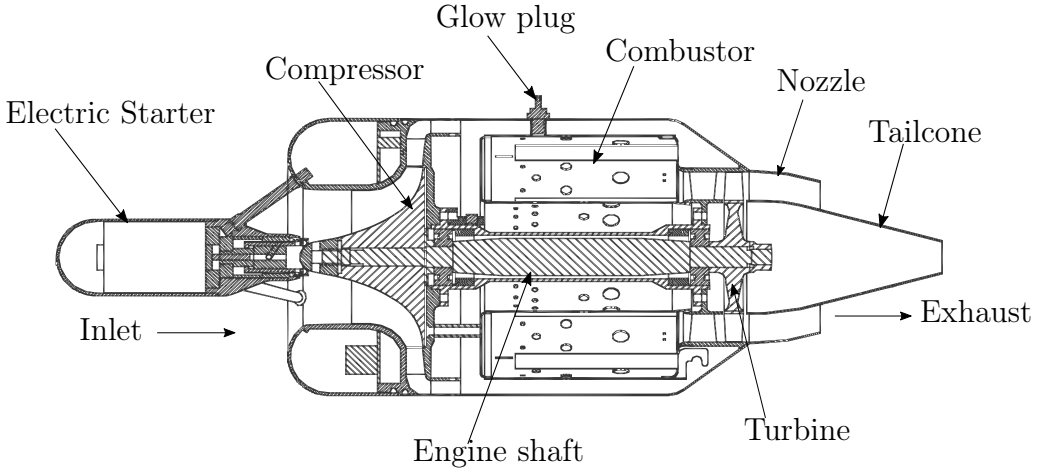

Figure 2.1: BMT 120 KS engine, (Burger, 2016).

The main elements of the engine are a centrifugal compressor, annular combustor, single axial flow turbine and fixed converging nozzle. The engine compressor rotor originates from the KKK K27.2 turbocharger with a diameter of 70 mm. The BMT 120 engine employs a 14 vaned aluminium wedge diffuser having a 90-degree vaneless bend and 43 axial de-swirl blades. The compressor rotor combined with the diffuser forms the complete compressor stage. The single axial flow turbine has 23 blades and can withstand high rotational speeds. The turbine and the nozzle guide vanes are made of Inconel 713 (Bassson, 2014).

The engine combustor employs a low-pressure fuel vaporising system (Burger, 2016). The BMT engine runs on kerosene or Jet (A1) fuel and does not require gas for starting. The MGT uses part of the fuel mixed with lubricant for lubrication of the engine shaft bearings. The shaft of the engine is made of high quality heat treated tool steel and is supported by two high speed hybrid ceramic ball bearings (Baird, 2011). The BMT uses an electric starter, which can sustain the engine up to a speed of 30 000 rpm. The engine has a microprocessor turbine control unit (TCU) used for control and protection of the engine (Baird, 2011).

The centrifugal compressor draws in air from the surroundings into the engine. The air is then compressed, hence increasing the total pressure and temperature of the air. The diffuser increases the static pressure of the air and lowers its velocity as it passes through the diverging passages. The low velocity air then enters the combustion chamber and mixes with fuel to burn continuously. The turbine expands the high temperature gas from the combustion process, hence producing mechanical power to drive the compressor. The converging exhaust nozzle reduces the exhaust gas pressure and increases the kinetic energy to create thrust for propulsion.

2.2 Background

In recent years different academic research projects have been undertaken on micro gas turbines with the purpose of improving gas turbine performance. The intent of these projects was to optimise performance parameters such as the specific fuel consumption, pressure ratio, cycle peak temperature, system pressure losses, turbine and compressor efficiencies and the engine thrust and power. Most of these gas turbines (GT) have power output values of less than 100 kW. Some of the techniques considered for the performance improvements are discussed.

2.2.1 *Compressor Stage Improvements*

Ling *et al.* (2007) designed and improved the compressor stage of the KJ66 micro jet engine using ANSYS CFX. The authors increased the pressure ratio of the centrifugal compressor at a lower mass flow rate. They claimed that the new design outperformed the original compressor stage.

Jie and Guoping (2010) re-designed 11 cm diffuser of an MGT compressor stage. They focused on investigating the effect of varying the cross-sectional area distribution along the flow path on the redesigned diffuser's performance. The new diffuser configuration was equipped with main and splitter blades. The Computational fluid Dynamics (CFD) and experimental results confirmed that the new diffuser showed improvement, with an 11% thrust increase and 9% reduction in specific fuel consumption for the jet engine.

Krige (2012) redesigned the vaned diffuser of the BMT 120 KS engine. He aimed to maximise the compressor stage pressure recovery in order to increase the engine's total-to-static pressure ratio, mass flow and thrust output. The experimental and numerical examination of the baseline and modified diffusers showed that the pressure recovery increased from 0.48 to 0.73. The static-to-static pressure ratio across the diffuser increased from 1.39 to 1.44.

Van Der Merwe (2012) designed and optimised a centrifugal compressor impeller for the BMT engine. The author sought to achieve a total-to-total pressure ratio of 4.72 and an isentropic compressor efficiency of 79.8% at a mass flow rate of 0.325 kg/s. The new impeller performance was validated by comparing its mean-line, experimental and CFD results. He showed that the experimental and numerical data correlated well.

De Villiers (2014) incorporated a 1D (1-dimensional) mean-line code and CFD software codes $FINE^{TM}$/Turbo and $FINE^{TM}$/Design3D to design a centrifugal compressor stage for the BMT engine. According to the author, the new compressor stage yielded a total-to-static pressure ratio of 3.0, and efficiency of 76.5% and a thrust of 170 N at a rotational speed of 119 000 rpm compared to the origininal BMT engine.

Burger (2016) designed and optimised a crossover diffuser for the BMT engine. The crossover diffuser combined with Van der Merwe's impeller improved the compressor stage total-to-static pressure ratio from 2.62 to 3.65.

2.2.2 *Combustor Improvements*

Guidez *et al.* (2009) investigated the feasibility of combustion in a miniature combustor. Their aim was to study combustion stability and efficiency.

They applied Raman spectroscopy and 1D Rayleigh scattering and standard thermodynamic measurements to estimate the temperatures and main species concentration along radial profiles at the combustor outlet. They measured combustion efficiency of 80%.

Chaudhari *et al.* (2012) report the design and simulation of a miniature annular combustion chamber applying ANSYS CFX. They evaluated the impact of flow patterns and temperature distributions on the combustion chamber liner walls. The numerical results showed that the combustion chamber walls were significantly affected by combustion flames which can cause combustor failure.

Gieras (2012) conducted a 3D numerical simulation of the aerodynamic flow through a GTM-120 micro jet engine combustor. They considered the effect of engine downsizing on the mass flow, pressure losses and heat transfer in the combustor. The aim of their research was to maximise thermal efficiency by minimising fuel consumption and controlling emissions.

Krieger *et al.* (2012) discuss the design, numerical and experimental evaluation of a combustion chamber for micro gas turbines. They analysed the behaviour of heat transfer on the flow and temperature patterns in the combustion chamber. The authors argued that the numerical and experimental results correlate well.

According to Armstrong and Verstraete (2014), a semi-constant volume combustor increases the pressure in the combustor and reduces engine fuel consumption. The authors re-designed a constant volume combustor for a micro jet engine. They choked the turbine nozzle guide vanes (NGV) to slow down the combustion chamber velocity in order to a create pressure rise in the combustor. They contend that the new design predicted a specific fuel consumption and thrust improvement of 27% and 35% for a combustor pressure ratio of 1.1.

2.2.3 *Wave Rotor Cycle*

The wave rotor technique employs a pressure exchanging device which uses pressure waves to transfer energy between a gas turbine engine's working fluids (Akbari and Müller, 2003). The pressure and temperature of the low working fluid of the GT is then increased. This tool can either be a rotating drum or disc attached to the compressor/turbine or the combustor of the engine. The wave rotor concept can either be in radial or axial form.

Wilson and Paxson (1993) investigated the performance of a simple turbojet engine with the wave-rotor enhanced technique. They obtained an increase of 1 to 2% for the engine thermal efficiency and 10 to 16% for the specific power.

Snyder and Fish (1996) evaluated the performance benefits of the wave rotor cycle in a small turboshaft engine. The engine topped with wave rotor showed a considerable reduction of 22% in specific fuel consumption (SFC) compared to the baseline engine.

Akbari and Müller (2003) suggest that the wave-rotor technique is the efficient approach to improve small jet engine thermodynamic cycle performance. The authors investigated and evaluated the performance of a small turbojet engine at different thermodynamic conditions with a four-port wave rotor. According to the authors, the outcome of their investigation showed significant improvement in the combustion pressures and temperatures compared to the baseline engine.

According to Iancu *et al.* (2005), the wave-rotor cycle increases the overall gas turbine compression and expansion ratio. They argued that the wave-rotor technique can achieve a 50 to 83% increase in compression efficiency for ultra-micro and small gas turbines.

2.2.4 *Turbine Stage Improvements*

Bar and Czarnecki (2009) performed a mean line and CFD analysis of a micro jet axial turbine. The Concept NREC AXCENT code was used for aerodynamic computations to develop 2D and 3D entropy performance contours for the turbine. The authors assert that a lower tip clearance, higher Reynolds Number, and specific speed coefficient boost turbine efficiency and overall engine performance.

Verstraete *et al.* (2010) investigated and improved the overall performance of the KJ66 turbojet engine. A spherical dimple vortex turbine blade profile was adapted for the axial turbine stage in order to obtain the required performance improvement. The authors claim that the improved engine showed an efficiency increase of 2 to 6% compared to the baseline engine.

Basson (2014) designed new turbine stages as the replacement for the existing turbine of the BMT 120 KS engine. He performed 1D and 3D numerical analyses on the new turbines. Smit (2014) manufactured Basson's turbines, and obtained experimental results for the newly designed turbines.

2.3 Simple Gas Turbine Thermodynamic Cycle

The standard Brayton open-air cycle is the thermodynamic representation of a gas turbine engine. The cycle is described with the T-s and p-v diagrams depicted in Figure 2.2. Ideally, the cycle has isentropic air compression, constant pressure heat addition, isentropic gas expansion and constant pressure heat rejection. In practice, the compression, heat addition, expansion and heat rejection processes are not isentropic.

The cycle can either be an open or closed cycle. In the closed cycle, the engine working fluid is kept in the system in that the engine exhaust gas temperature is cooled and reused in the cycle. For the open cycle, the engine working fluid exits the cycle after expansion in the turbine. The working fluid is assumed to be calorically perfect at all working conditions with specific heat ratio (γ) and specific heat capacity (c_p) constant throughout the cycle.

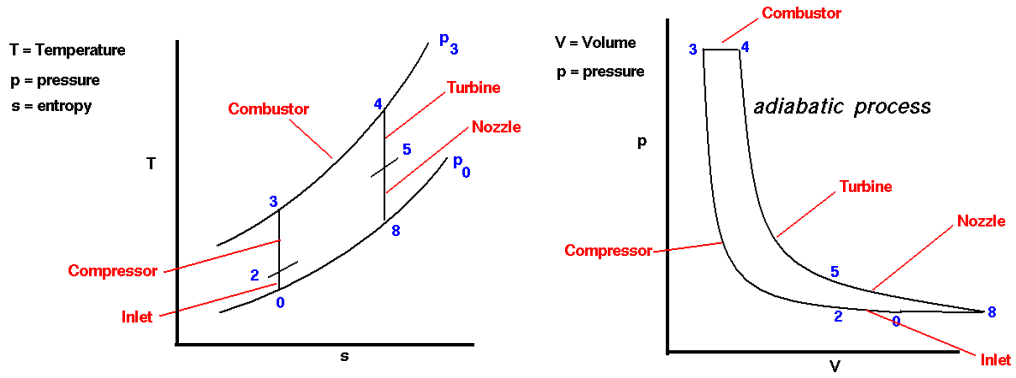

(a) T-s diagram

(b) p-v diagram

Figure 2.2: Brayton thermodynamic cycle, (NASA, 2016).

The Brayton cycle T-s and p-v thermodynamic processes are described as follows:

- 0-3 Isentropic compression in the compressor.
- 3-4 Constant pressure heat addition in the combustor.
- 4-5 Isentropic expansion in the turbine.
- 5-8 Isentropic work done in the nozzle.
- 8-0 Constant pressure heat rejection to the atmosphere.

Referring to Figure 2.2, the GT as a turbomachinery device can be analysed at the various stations using the energy equation:

$$\frac{dE_{cv}}{dt} = 0 = \dot{Q}_{cv} - \dot{W}_{cv} + \dot{m}_i\left(h_{si} + \frac{V_i^2}{2}\right) - \dot{m}_e\left(h_{se} + \frac{V_e^2}{2}\right) \tag{2.3.1}$$

$$= \dot{Q}_{cv} - \dot{W}_{cv} + \dot{m}_i h_{0i} - \dot{m}_e h_{0e}$$

$$h_{0i} = \dot{m}_i\left(h_{si} + \frac{V_i^2}{2}\right) \tag{2.3.2}$$

$$h_{0e} = \dot{m}_e\left(h_{se} + \frac{V_e^2}{2}\right) \tag{2.3.3}$$

For a steady flow process in the engine:

$$\dot{m}_e = \dot{m}_i = \dot{m} \tag{2.3.4}$$

Hence the energy equation can be simplified as:

$$0 = \dot{Q}_{cv} - \dot{W}_{cv} + \dot{m}c_p(T_{0i} - T_{0e}) \tag{2.3.5}$$

The thermodynamic parameters at the various engine station points can be computed by applying equation 2.3.5.

2.4 Gas Turbine Performance Parameters

Gas turbine performance can be evaluated by means of experimental tests or theoretical, analytical and numerical simulations. These engine assessment methods analyse the engine performance parameters. The output of a gas turbine is characterized by the thrust, specific thrust, specific fuel consumption, propulsive efficiency, thermal efficiency and overall efficiency (Farokhi, 2014).

Thrust: Gas turbine engines are designed to create thrust for propulsion at different flight conditions. The engine air mass flow and the fuel added in the combustion chamber create the desired thrust via a burning process to release higher kinetic energy at the propelling nozzle outlet. The thrust of a turbine jet engine is influenced by the ram effect, altitude, air mass flow, air speed, and propelling nozzle dimensions. The engine thrust can be obtained by describing the engine as a control volume and applying momentum and mass conservation laws to the boundaries as shown in Figure 2.3.

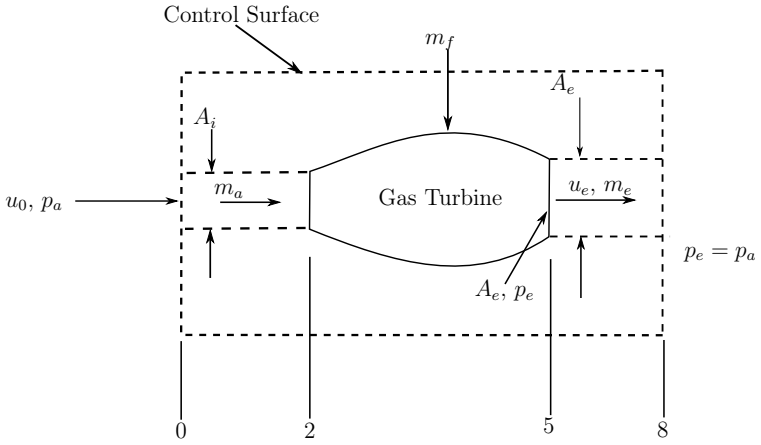

Figure 2.3: Aero engine thrust.

The engine thrust is mathematically expressed as:

Net thrust = Momentum thrust + Pressure thrust - Momentum drag

$$F_{net} = (\dot{m}_a + \dot{m}_f)u_e - \dot{m}_a u_0 - (p_e - p_a)A_e \tag{2.4.1}$$

The engine thrust is governed by the choked and unchoked condition of the propelling nozzle. For a choked nozzle, the engine nozzle pressure ratio is higher than the engine critical pressure ratio. Therefore the pressure thrust is included in the thrust equation. On the other hand, in a non-choked nozzle, the engine exit flow expands to ambient pressure. The thrust equation converts to:

$$F_{net} = (\dot{m}_a + \dot{m}_f)u_e - \dot{m}_a u_0 \tag{2.4.2}$$

Ideally, the fuel-to-air ratio is assumed negligible and then thrust is given as:

$$F_{net} = \dot{m}_a(u_e - u_0) \tag{2.4.3}$$

For stationary or test rig engines the free stream air velocity reduces to zero. The engine thrust is then given as:

$$F_{net} = \dot{m}_a u_e \tag{2.4.4}$$

Specific thrust: The specific thrust of the engine is the thrust of the engine per unit mass flow of air. According to Cohen *et al.* (1996) the specific thrust of the engine determines the engine size, weight, frontal area, and drag on the engine. It is therefore important to maximise the specific thrust of an engine in order to generate thrust with the smallest amount of airflow and minimum engine frontal area. Specific thrust is expressed as:

$$F_{specific\ thrust} = \frac{F_{net}}{\dot{m}_a} \tag{2.4.5}$$

Specific fuel consumption: The engine specific fuel consumption is the ratio of mass of fuel to net thrust or power of the engine. Producing higher thrust or power at a lower rate of fuel consumption reduces engine weight and fuel cost. Reduced SFC in a gas turbine engine is also related to better engine efficiency. The specific fuel consumption is given as:

$$SFC = \frac{\dot{m}_f}{F_{net}} \tag{2.4.6}$$

Propulsive efficiency: This is the engine thrust power per the power transferred to the engine airflow. The propulsive efficiency of an engine depends on the engine combustion process and the amount of energy wasted in the nozzle. The propulsive efficiency is expressed as:

$$\eta_p = \frac{\dot{m}_a(u_e - u_0)}{\dot{m}_a[u_0(u_e - u_0) + (u_e - u_0)^2/2]} \tag{2.4.7}$$

Thermal Efficiency: This is the ratio of the mechanical power output produced by the engine to the heat energy input. The thermal efficiency of a gas turbine is increased by increasing the compression pressure ratio and the turbine inlet temperature. The overall cycle efficiency depends on the thermal efficiency. For a simple Brayton cycle, thermal efficiency can be increased by the addition of a heat recovery cycle to the baseline cycle. The thermal efficiency of a Brayton cycle for a gas turbine is given as

$$\eta_{th} = 1 - \frac{1}{\left(p_{03}/p_{01}\right)^{\frac{\gamma-1}{\gamma}}} \tag{2.4.8}$$

2.5 Gas Turbine Performance Modelling

The performance of an engine at the design and off-design points can be obtained from gas turbine performance modelling. Off-design evaluation is required to model the operating range of gas turbines due to the engine's non-linear thermodynamic behaviour. Off-design behaviour is also used to examine the impact of a change in engine component characteristics on engine output. Cumpsty (2003) agrees that a gas turbine's performance at off-design conditions should be satisfactory and safe irrespective of its non-linear behaviour. El-Sayed (2008) emphasises that although gas turbines are designed to operate effectively at specific design points, the engine should also work acceptably at off-design conditions. According to Asgari (2014), off-design modelling is the most suitable means of optimising, maintaining and predicting the performance of a gas turbine.

The off-design performance of a gas turbines involves performance predictions, condition monitoring and degradation analysis. The engine diagnosis and degradation analysis are normally executed based on the performance predictions (Suraweera, 2011). The off-design performance of gas turbines can be evaluated using the following methods: component matching, stage stacking, gas path analysis, computational fluid dynamics and the Wittenberg method (Thirunavukarasu, 2013). These modelling methods are mathematically formulated with linear and non-linear equations into computer programs for performance simulations.

2.5.1 *Component Matching*

Among the off-design performance prediction methods, the conventional component matching method is the most popular and easily implementable. It

forms the basis for the other performance prediction techniques. According to Cohen *et al.* (1996), component matching is suitable for the non-linear off-design simulation of gas turbines due to its flexibility, consistency, simplicity and better accuracy. Component matching combines momentum, mass and energy conservation theory to generate engine thrust and power. Accordingly, component matching depends on the compatibility of engine mass flow, work, and rotational speed taking into account mechanical losses. Component matching is accomplished using the compressor, turbine and nozzle characteristics shown in Figure 2.4 and 2.5. The maps are defined by the pressure ratio, efficiency, non-dimensional mass flow and speed.

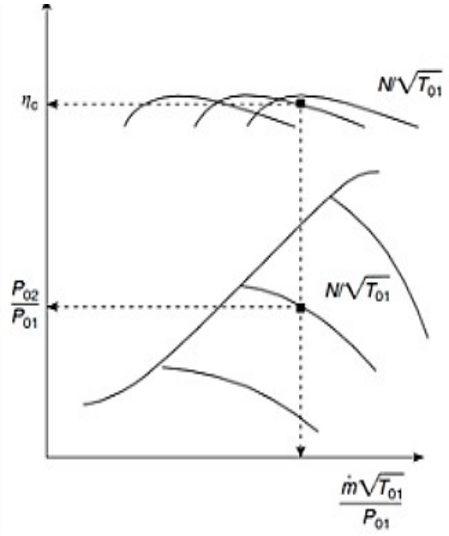

Figure 2.4: Compressor characteristic map, (El-Sayed, 2008).

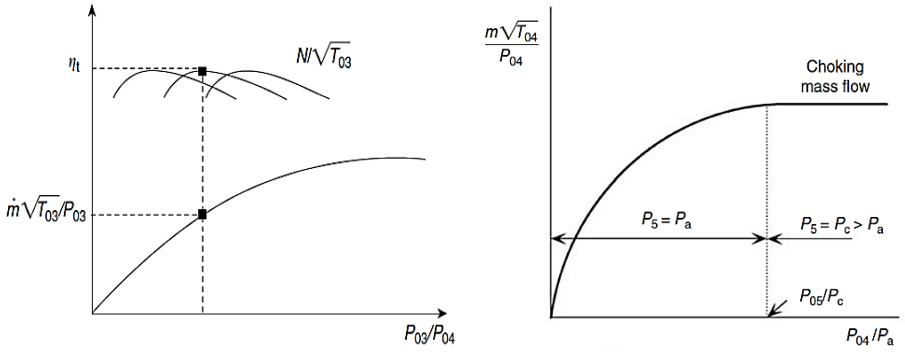

(a) Turbine map

(b) Propelling nozzle map

Figure 2.5: Turbine and nozzle characteristic maps, El-Sayed (2008).

Substantial gas turbine performance analyses have been performed with component matching. Walsh and Fletcher (2004), Cohen *et al.* (1996) and Cump-

sty (2003) in their books give detailed literature on performance evaluation of turbojet engines using component matching. Pinkel and Karp (1947) did a turbojet engine performance analysis employing the component matching technique. Flack (1990) also discusses performance evaluation of a gas turbine using component matching. The author asserts that the method was effective in determining the operating range of the engine. Bringhenti and Barbosa (2004) used component matching to investigate the performance of a 1MW industrial gas turbine. Tsoutsanis *et al.* (2015) discusses the simulation of a gas turbine with non-linear adaptation of the compressor and turbine maps based on component matching.

The component matching method is categorised as either a nested loop or a matrix iteration method. The nested-loop matching technique is easy to understand and implement. However, this method becomes computationally unstable for larger loops (Walsh and Fletcher, 2004). To determine the power or thrust of a gas turbine with the nested-loop technique, the operating points are selected from the compressor characteristic shown in Figure 2.4. Subsequently, the turbine and nozzle parameters are then computed with these variables. Using flow and speed compatibility between the compressor, turbine and nozzle the engine thrust or power are determined. The procedure is iterated repeatedly until convergence is reached.

The matrix iteration method is used for advanced gas turbine off-design performance simulations. Unlike the nested loop,the method of matrix iteration is computationally efficient for larger loops. The method is widely implemented in gas turbine simulation programs such as GasTurb, Flownex SE, PROOSIS, GSP and TURBOMATCH. The method uses equal values of matching guesses and constraints. The guessed variables are updated continuously until the constraint parameters are fulfilled. The matrix iteration method is executed for a gas turbine as follows:

1. Guess initial operating point for the compressor and turbine inlet temperatures (matching guess).
2. Calculate the turbine and nozzle operating points (matching constraints).
3. Calculate the error between matching constraints and the matching guess.
4. Make a small change in the matching guesses and repeat the process.
5. Combine the errors from the matching guess and constraints to form a matrix of partial derivatives.
6. Invert the matrix and change all matching guesses by the amounts given by multiplying the inverted partial derivatives matrix by the errors matrix.

7. Repeat the procedure until the errors between calculated values of the matching constraints and guesses converge.

The matrix iteration technique normally uses the multi-variable Newton-Raphson method, Gaussian elimination, QR and LU decomposition to generate the partial derivatives and find solutions.

2.5.2 *Gas Path Analysis*

Gas Path Analysis (GPA) is one of the oldest engine off-design modelling methods proposed by Urban in the late 1960s. The progress made by this method in the gas turbine industry has led to different derivatives of GPA being used in the gas turbine industry. GPA is used for evaluating non-linear performance parameters such as flow capacities, efficiencies and pressure ratio. The GPA of an engine does performance analysis making use of independent and dependent variables (Li, 2002). The dependent parameters are temperature and pressure whereas the independent variables are mass flow rate and efficiency (Thirunavukarasu, 2013). The independent variables are affected by changes in the dependent variables. The independent values are constantly updated until the dependent variables converge.

Stamatis (2011) investigated a twin-shaft gas turbine with GPA methods. His aim was to evaluate the effectiveness of the GPA method for modelling the performance of the engine. He found that the classical GPA method was ineffective.

Bauwens (2015) used GPA to assess the performance of a micro gas turbine engine. He concluded that although the method is effective for performance modelling, diagnostic of multiple faults and measurement of engine degradation is difficult.

2.5.3 *Stage Stacking*

Stage stacking performance is similar to the conventional component matching method and is normally used for compressor performance prediction. The stage stacking method is a simple and effective tool for compressor performance estimation to determine a gas turbine engine's performance (MacIsaac and Langton, 2011). The method requires characteristic performance maps for its implementation. The ordered stage parameters can be determined with gas dynamics equations with known first stage compressor inlet conditions

(Suraweera, 2011). The outlet conditions of the preceding stage are used as input values for the next stage.

Cerri *et al.* (1993) discuss the performance deterioration of a compressor with an inverse stage stacking technique. They confirm that good results were accomplished with the performance modelling technique.

Procacci and Rispoli (1995) analysed the performance deterioration of an axial flow compressor with the stage stacking technique. The purpose of the investigation was to evaluate the performance of a variable geometry compressor with single constant rotational speed.

Abdel-Fattah and Frith (1995) considered the derivation of individual stage characteristics for a multi-stage axial compressor. The results obtained correlates with the manufacturer's data.

Tomita and Barbosa (2003) integrated the stage stacking method into the Axial Flow Compressor Code (AFCC) to assess the performance of an axial compressor with different inlet guide vanes (IGV) and stator setting. The simulation results correlate well with the experimental data.

2.5.4 *Wittenberg Method*

In 1976 Wittenberg developed a performance modelling method which does not require a compressor, turbine and nozzle maps for performance prediction. Unlike the component matching method the Wittenberg approach applies gas dynamic equations to evaluate a gas turbine's performance. Although the method does not require characteristic maps, it can be implemented with compressor maps to assess the effects of compressor efficiency variation on the engine. Mirza-Baig and Saravanamuttoo (1991) examined the performance of the Garrett 731-2 turbofan engine based on this method. Their approach required design point parameters only. They concluded that the obtained results agree well with the available engine data.

2.5.5 *Computational Fluid Dynamics*

Computational fluid dynamics (CFD) is a finite numerical simulation volume method that employs the mass, momentum and energy equations to evaluate gas turbine performance. Detailed complex flow physics in the engine can be captured with CFD . This includes the study of flow behaviour in the compressor, combustion chamber and the turbine. The CFD method of evaluating engine performance does not require engine characteristic maps.

Pachidis *et al.* (2006) performed turbofan engine performance analysis with ANSYS FLUENT. They concluded that good correlation was established between the baseline engine PYTHIA simulation and the CFD results.

Amirante *et al.* (2007) optimised the intake of the Pegasus small jet engine. They analysed and improved the effects of boundary layer on the engine intake nozzle and velocity profile using ANSYS FLUENT combined with the progressive optimisation technique. They conclude that the numerical and experimental data match well.

Trebunskikh *et al.* (2012) examined the performance of the KJ66 micro turbine engine with the FloEFD, CFD software code. The authors concluded that the numerical results correlate well with the experimental test results. However, they reported that non-uniform fluid temperature distributions at the combustor outlet, and wedge diffuser inefficiencies contribute towards poor performance of the engine.

Badami *et al.* (2013) used ANSYS FLUENT to analyse the performance of the SR-30 micro jet engine. The intent was to investigate the engine thermodynamic cycle performance. According to the authors, the CFD data showed consistent matching with the experimental values. The nozzle and turbine pressure ratios showed differences of less than 5% and the mass flow rate and thrust values showed differences close to 2% and 10% respectively.

Krivcov *et al.* (2014) studied the performance of a micro gas turbine engine with ANSYS CFX. The authors claim that good agreement was established between the computational results and the thermodynamic 1D code for the engine.

2.6 Closing Remarks

The chapter provided background information on MGTs. Gas turbine engine performance modelling methods were discussed. Gas turbine elements work in unison with each other and hence the overall engine performance depends on the individual component operational outputs. This section also presented previous research studies undertaken to improve the performance of MGT engines. Gas turbines basically apply the Brayton cycle thermodynamic principle to convert fuel energy into useful work. The thrust or power output of a gas turbine engine depends on the gas generator's performance. Good performance modelling of a gas turbine components ensure accurate prediction of the operation of the gas turbine.

Chapter 3

Baseline Tests

This section discusses the experimental evaluation of the standard BMT engine. The experimental set-up and procedure are described. The aim of the experimental test was to measure engine performance values such as thrust, fuel consumption, inlet and exhaust gas temperatures and air mass flow rate at various speeds and compare to available BMT engine data to evaluate engine parameters that are repetitive. These parameters are used to validate the numerical simulations. The engine is arranged with a bell-mouth at the engine inlet to measure the air mass flow into the engine and an exhaust extraction tube at the rear of the engine to prevent recirculation of the exhaust gases.

Two sets of test runs were conducted in the experiment. The tests were performed at an intervals of 45 s for various speeds at a speed interval of 20 krpm. Test 1 attained a maximum speed of 103 krpm. The reason for lower speed is attributable to problems with the engine fuel injection nozzle. This caused a loss of flame in the combustion system and stopped the engine. Test run 2 reached a maximum engine speed of 120 krpm. During test run 2 it was observed that fuel was leaking from the engine exhaust and due to that no further test was performed. Figure 3.1 depicts the engine arrangement on the test rig.

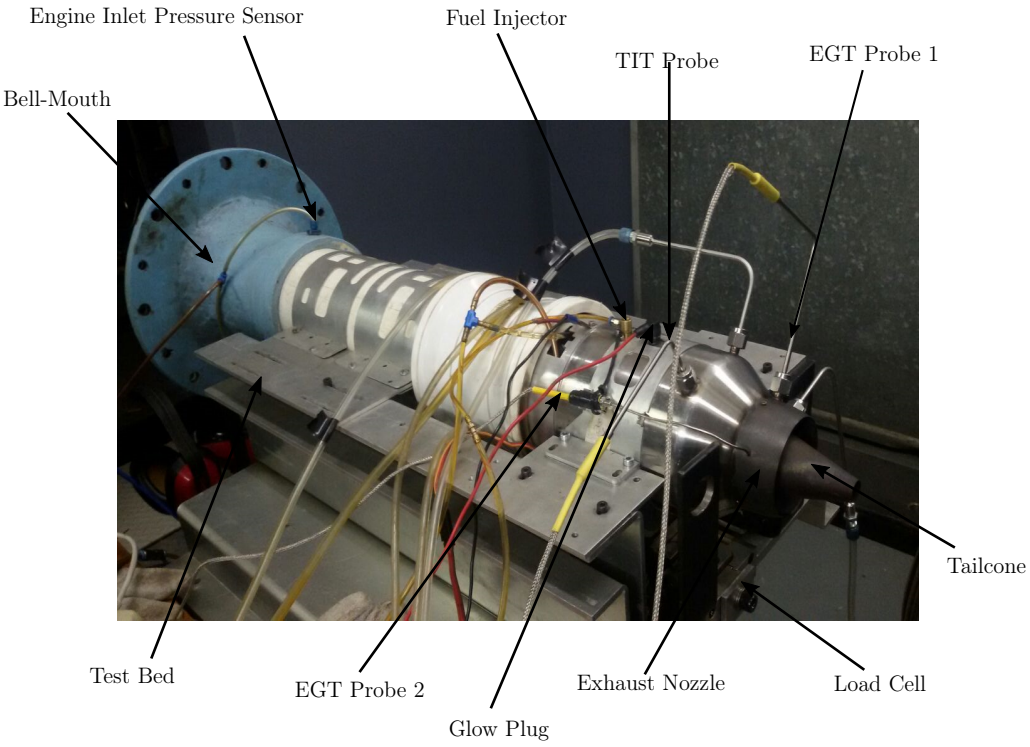

Figure 3.1: BMT experimental test setup.

3.1 Calibration and Data Acquisition

In order to get accurate data readings from the experiment, the measuring devices had to be calibrated. The calibration involved the pressure transducers and temperature thermocouples. These sensors and thermocouples are connected to a personal computer using an HBM Spider 8 data logger. Catman software was used to interpret the readings from the data logger into the respective units for the measured parameters. All the measurements are recorded and saved using Catman software.

3.1.1 *Temperature Measurement*

A K-Type thermocouple was used for the engine temperature measurements. K-Type thermocouples are accurate to $\pm$ 2.2 °C and have a sensitivity of 41 $\mu V/$°C. The temperatures were measured at the turbine inlet and the exhaust. The exhaust temperatures were measured at two positions with two different temperature probes. The probes are named as probe 1 and 2 as shown in Figure 3.1. Temperature probe 1 is a thick sheath thermocouple of

sheath diameter 3 mm and 110 mm long while temperature probe 2 is a thin sheath type of diameter 1.5 mm and 110 mm long. Figure 3.2 depicts the measuring positions of the turbine entry and outlet temperatures. Lastly, the ambient temperature in the test laboratory was measured with a thermometer.

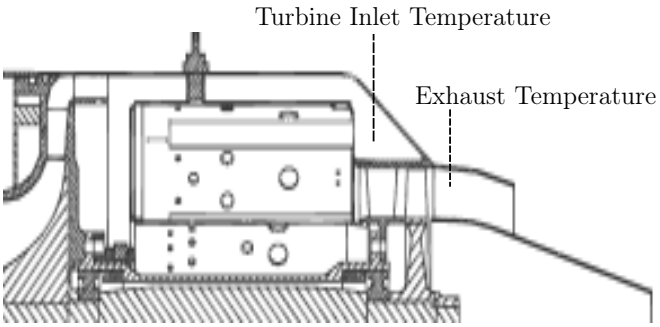

Figure 3.2: Turbine inlet and outlet temperature measurement.

3.1.2 *Pressure Measurement*

Pressures in the BMT engine were measured with HBM P8AP transducers. These sensors have an accuracy of 0.3% and repeatability of 0.1%. They were calibrated with a pressure gauge at minimum and maximum pressures of 100 kPa and 500 kPa. The pressures were measured at the bell-mouth, the compressor outlet, turbine inlet and outlet. The laboratory environment ambient pressure was measuerd with a pressure barometer.

3.1.3 *Fuel Flow Measurement*

The mass rate of the fuel consumed by the engine was measured with an HBM U2A 50 kg/s load cell. The fuel was contained in a 5-litre capacity fuel container and suspended on a load cell. The load cell has a sensitivity of ± 0.02 kg/s. The measured fuel consumption is captured on the PC.

3.1.4 *Air Mass Flow Measurement*

The air mass flow rate is determined by measuring the difference between the local static pressure and the ambient pressure at the engine bell-mouth as shown in Figure 3.3. These pressures are determined at three points as shown in Figure 3.3. The mean value of the three readings is then used to calculate the mass flow rate into the engine.

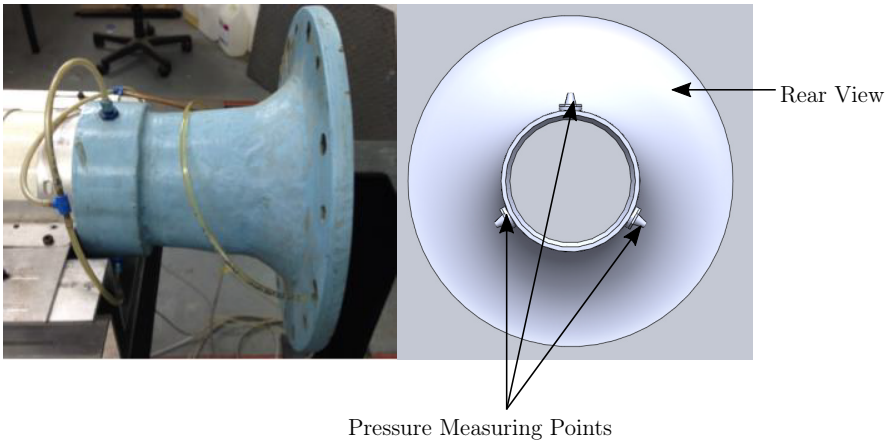

Figure 3.3: Bell-mouth for air mass flow measurement.

With a known pressure difference at the inlet of the bell-mouth, the velocity of the flow can be deduced as:

$$C_a = \sqrt{\frac{2\Delta p}{\rho_a}} \tag{3.1.1}$$

Hence the mass flow rate into the engine can be computed from the relation:

$$\dot{m} = \rho_a C_d A_{duct} C_a \frac{1}{\sqrt{1-\beta^4}} \tag{3.1.2}$$

$$\dot{m} = \rho_a C_d A_{duct} \sqrt{\frac{2\Delta p/\rho_a}{1-\beta^4}} \tag{3.1.3}$$

The discharge coefficient (Krige, 2012) and diameter ratio are given as:

$$C_d = 0.9975 - 0.00653\sqrt{\frac{(10^6)\beta}{Re}} \tag{3.1.4}$$

$$\beta = \frac{d_2}{d_1} \tag{3.1.5}$$

3.1.5 *Thrust Measurement*

The thrust was measured with a load cell placed beneath the engine as indicated in Figure 3.1. The load cell measures the engine thrust as the engine accelerates and move on the test bench. The load cell is a 500 N HBM RSCC S-type. It has a sensitivity of ± 0.2%. The load cell is calibrated with a spring loaded weight scale. The load cell had already been calibrated by the laboratory technician, therefore it was not recalibrated.

3.2 Test Results

The BMT experimental results are illustrated in Tables 3.1 and 3.2 and through Figures 3.5 and 3.8. The experimental results are compared to the available experimental data of the engine measured by Krige (2012). The current experiment is named as experiment 2 whereas the previous experiment (Krige, 2012) is denoted as experiment 1. The BMT engine thrust performance is displayed in Figure 3.4. Thrust measured in experiment 2 is between 3.2% and 7.3% higher than experiment 1 thrust. Table 3.1 shows that the engine mass flow rate increases with increasing engine speed. The same trend is realised for the fuel consumption. The correlation between the mass flow rates for both experimental results is depicted in Figure 3.5. The mass flow rate shows a percentage difference that varies between 0.04% and 1.88%.

Table 3.1: BMT experimental test results.

Speed (krpm)	Thrust (N)	Mass Flow (kg/s)	Fuel Flow (kg/s)
120	136.6	0.293	0.0063
100	78.4	0.233	0.0041
80	43.4	0.175	0.0029

Figure 3.6 illustrates the comparison between the fuel flow rate for the two tests. The difference between the fuel flow rates measured for the two tests is between 15.5% and 17.2%. It was observed that the combustor was leaking fuel at the exhaust of the engine during experimental test 2. This probably contributed to high fuel consumption in experiment 2, as the combustor required more fuel to provide stable combustion due to its poor performance.

Figure 3.7 shows a plot of the BMT turbine inlet temperatures. The turbine inlet temperature (TIT) was measured with a thin sheath thermocouple of diameter 1.5 mm and 110 mm long, at the passage between the combustor and the stator of the turbine stage as shown in Figure 3.2 in section 3.1.1. A single temperature probe measurement was done, unlike the EGT measurement. A

percentage difference of between 12% and 21% is observed compared to experiment 1. The turbine inlet temperature depicts a fluctuating temperature profile and is highly susceptible to heat transfer losses. Radiative heat transfer is also more pronounced at the turbine inlet. These effects might contribute towards the large deviation in temperature readings at the turbine inlet.

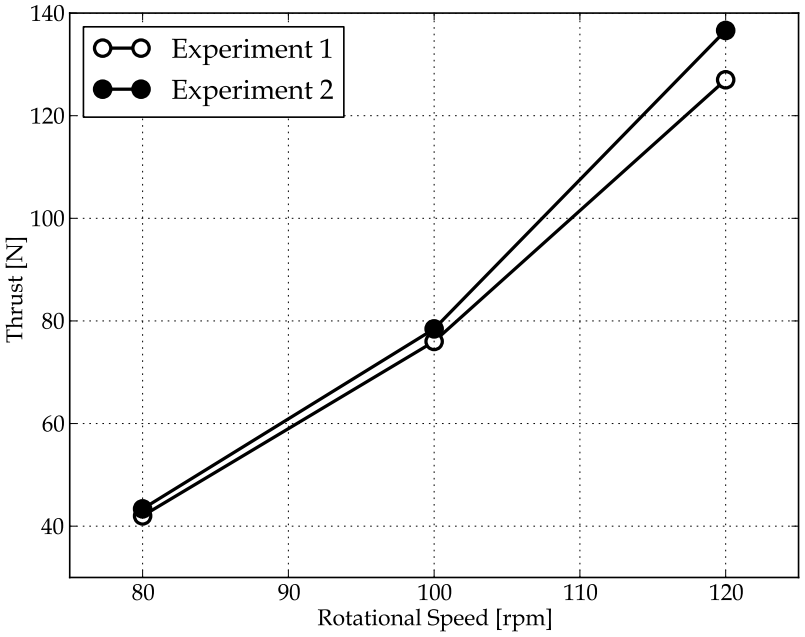

Figure 3.4: Plot of BMT thrust.

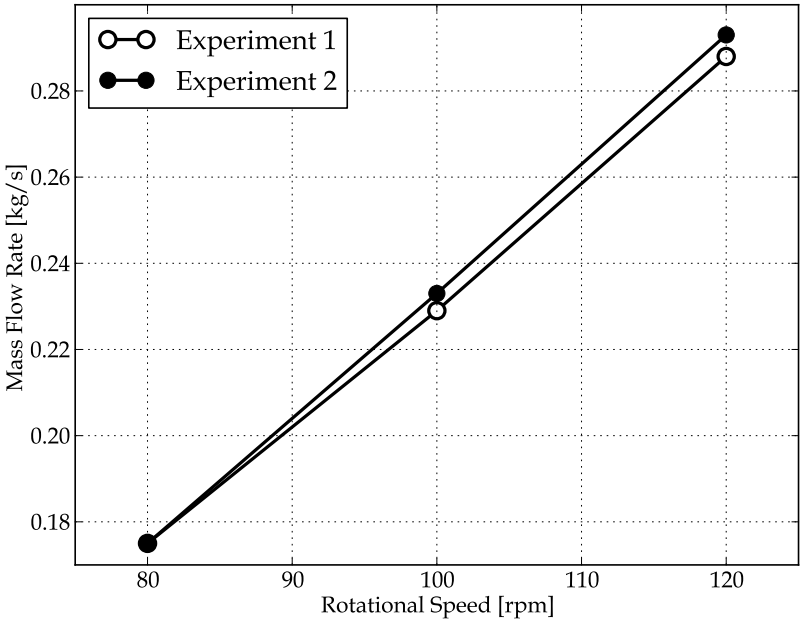

Figure 3.5: Plot of BMT air mass flow rate.

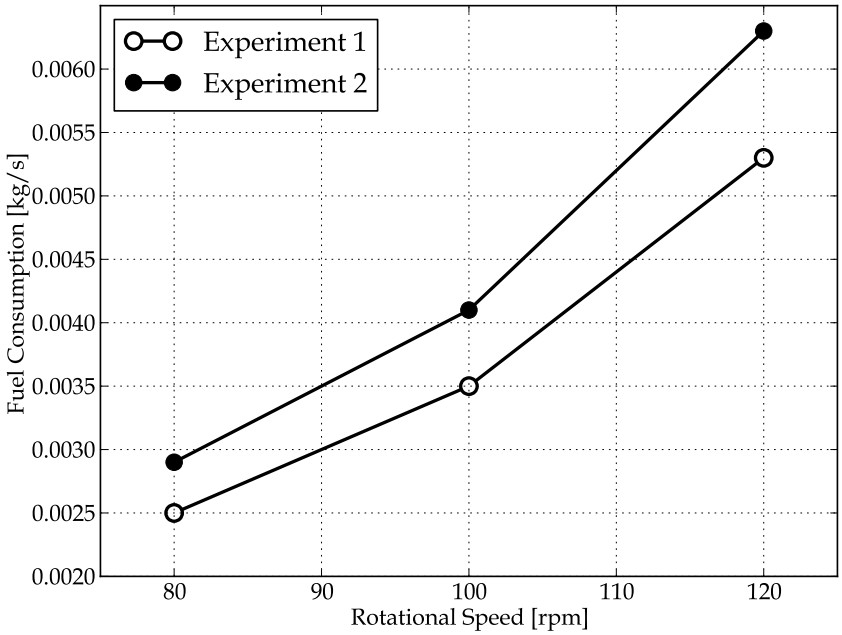

Figure 3.6: Plot of BMT fuel flow rate.

In Figure 3.8 the EGTs of experiment 2 are compared. The EGTs were measured at two positions as shown in Figure 3.1. The position 1 thermocouple is a thick sheath temperature probe labelled as probe 1 while position 2 thermocouple is of the thin sheath type named as probe 2. The probe 2 measured higher EGT values than the probe 1. The reason is that the thick probe has a slower response due to the thicker coating material. The wide deviation in the EGTs could also be caused by an uneven temperature profile or circumferential distribution of the engine exhaust gases or the presence of cold or hot spots in the exhaust gases. The existence of hot or cold spots in the exhaust gases could be as a result of a poor mixture of air and fuel in the combustion chamber. Becker (2015) made similar observations when performing a temperature measurement study of the BMT engine. A minimum percentage difference of 1% and maximum deviation of 17% was observed when the EGTs of the probes were compared. Table 3.2 shows the comparison between experiment 1 and experiment 2 EGTs. The difference between probe 1 and experiment 1 EGTs is in the range of 16-23.2% while probe 2 recorded a deviation of 6.4-15.3%. Based on this evidence, it was decided to use probe 2 data for future comparison, if required.

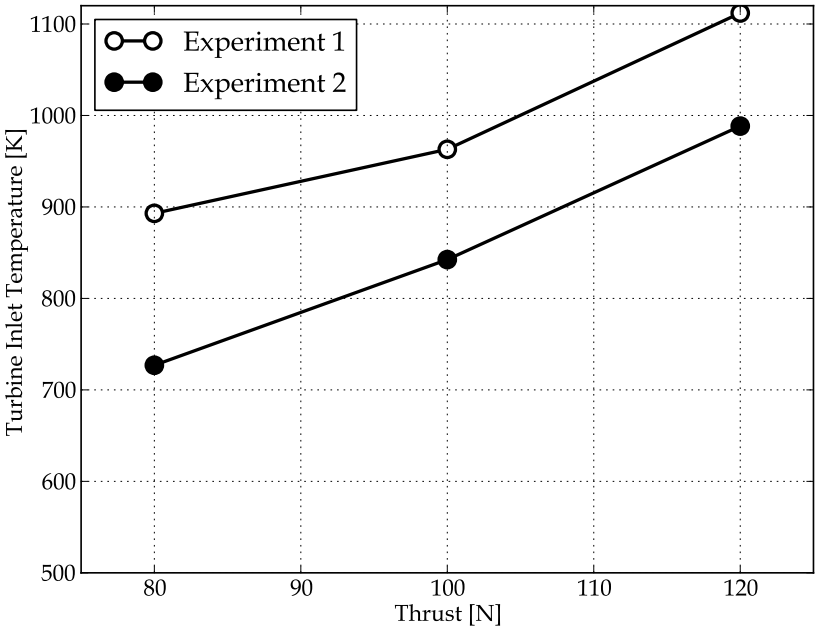

Figure 3.7: BMT experimental TIT.

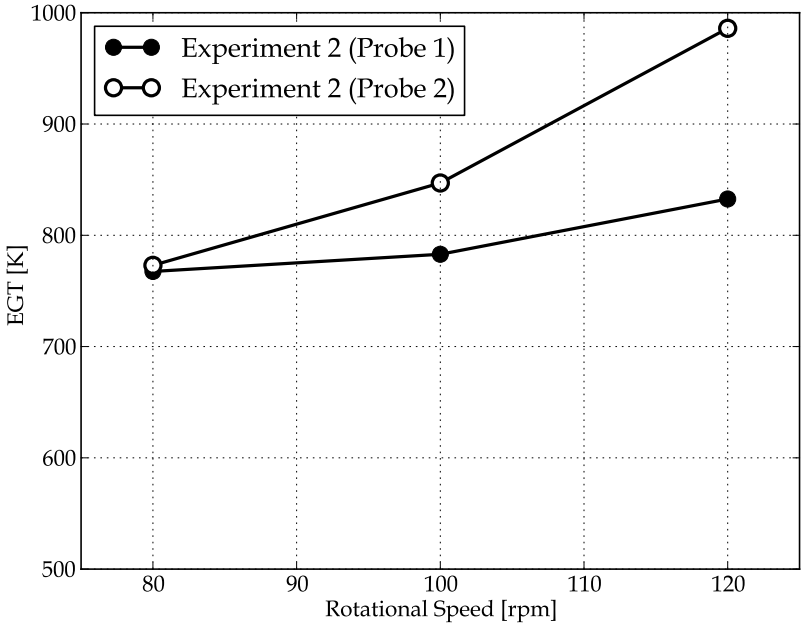

Figure 3.8: BMT experimental EGTs.

Table 3.2: BMT experimental EGT.

Speed (rpm)	Exp 1	Probe 1	Difference (%)	Probe 2	Difference (%)
120	1051	832	23.2	986	6.4
100	935	783	17.7	847	9.9
80	901	767	16.0	773	15.3

3.3 Closing Remarks

This section described the experimental test for the BMT engine. This includes the test procedure and calibration of the measuring devices and data acquisition. The experimental test results were compared to the available engine data. Two sets of test run were done with test run 1 only attaining a maximum speed of 103 krpm as a result of failure of the fuel nozzle causing a loss of flame. Test run 2 successfully reached the engine maximum speed of 120 krpm but it was observed that the engine was leaking fuel from the exhaust during the tests. It was found that the combustor was not in a good condition and therefore the test could not be repeated. The experimental thrusts and mass flow rate showed a consistent trend with the available engine data.

The turbine inlet temperature was measured at only one position on the engine. The measurement was done with a 1.5 mm thin sheath thermocouple and 110 mm long. The turbine inlet temperature recorded a low temperature compared to the available TIT values measured by Krige (2012). The turbine inlet is prone to heat transfer losses and unstable radial and circumferential temperature profile. Therefore the effect of radiative heat transfer between the probe and the hot gases could result in recording inaccurate turbine inlet temperatures. Radiation effects can cause temperature errors of between 50 and 160 °C (Figliola and Beasley, 2015). Brohez *et al.* (2004) also reports temperature errors of up 200 °C due to the effect of radiation. Referring to Figures 3.7 and 3.8, it is evident that due to the uneven circumferential distribution of hot gases at the turbine inlet, a temperature value close to the probe 2 exhaust temperature was measured at the turbine inlet.

The exhaust temperature of the engine was measured at two positions on the engine. These measuring probes were labelled as temperature probe 1 and 2. Probe 1 was of the thick sheath type of 3 mm diameter and 110 mm long whereas probe 2 is a thin sheath type of diameter 1.5 mm and 110 mm long. Temperature probe 1 measured EGTs lower than the EGTs measured by temperature probe 2. Based on observations as discussed, the thin thermocouple temperature measurement was used as the preferred engine EGT value. It is therefore also recommended to use the thin sheath temperature probe for future EGT measurement. Using the thick sheath thermocouple with a low sensitivity can cause the engine to operate too hot or overheat. This can cause

premature failure of turbine blades and other engine components. Furthermore, the thermocouples will be shielded from radiation for future temperature measurments as both the turbine inlet and outlet temperature readings were affected by disparities due to radiation losses.

Chapter 4

Engine Cycle Analysis

This chapter describes the various engine performance cycle analyses. It presents the simulation methodologies and software programs used for the numerical analyses. The objective of the cycle analysis was to obtain approximations for the engine's primary performance parameters.

4.1 Theoretical Analysis

The standard Brayton open air cycle thermodynamic equations were used to determine the engine performance parameters at the engine elements' boundaries. The goal was to establish engine overall performance parameters such as the turbine inlet stagnation temperature, compressor efficiency, thrust and specific fuel consumption. Each engine component was treated as a separate control volume for the various interface thermodynamic analyses.

The engine was considered to be a stationary or test rig engine at standard sea level conditions. The origin of the free stream air at the inlet and exit of the engine was chosen far away to ensure that the pressures at these stations of the control volume are uniform with the surrounding conditions as shown in Figure 2.3. Thence, considering no losses at the engine inlet the stagnation pressure and temperature at the compressor inlet are equivalent to the ambient conditions $p_{02} = p_a$ and $T_{02} = T_a$. Also, the engine free stream speed u_0 and Mach number M_0 are negligible with respect to the ambient conditions. The cycle parameters were calculated based on the station points defined in Figures 2.2 and 2.3. In order to obtain a good approximation for the engine parame-

ters, an iterative one-dimensional calculation was done in a Python program to compute the performance parameters. Detailed calculations involving the entire engine are presented in the appendix A. The performance computations were executed using data acquired from literature, available BMT experimental data and standard ambient conditions at sea level as summarized in Table 4.1. The compressor parameters are discussed later.

Table 4.1: BMT basic parameters.

Parameter	Name of Parameter	Value	Unit
Ambient Parameters	Ambient temperature	288.15	K
	Ambient pressure	101.325	kPa
BMT Parameters	Total-total pressure ratio	3.15	-
	Combustion efficiency	90	%
	Mechanical efficiency	98	%
	Total-total turbine efficiency	85	%
	Mass flow rate	0.288	kg/s
	Fuel consumption	0.0053	kg/s
	Combustor pressure loss	10	%
	Rotational speed	120 000	rpm
	Impeller outer diameter	70	mm
	Impeller outlet blade angle	40	°
	Impeller outlet flow angle	59.6	°
Other parameters	Cold air specific heat	1005	J/kgK
	Gas specific heat	1148	J/kgK
	Cold air specific heat ratio	1.4	-
	Gas specific heat ratio	1.33	-
	Gas constant	287	J/kgK
	Fuel heating value	43.1	MJ/kg

In MGTs and conventional larger GTs, the engine combustion efficiency and combustor pressure loss have an essential contribution towards obtaining a higher thrust or power output. The literature survey done on MGT combustion efficiency and pressure loss did not conclusively specify a defined value for the efficiency and the pressure loss. In a study done by Suchocki *et al.* (2014) for the GTM-140 MGT combustor, they found the combustion pressure loss to be 9% of the inlet pressure. Toro *et al.* (2008) analysed the KJ66 combustor and established combustion pressure loss to be 12%. Armstrong and Verstraete (2014) also report that the combustion pressure loss for the KJ66 is approximately 12%. Gieras (2012) concur that the pressure drop for the GTM-120 micro combustor is 10%. The BMT engine's available experimental data show that a burner pressure drop of 11% was measured.

Söhret *et al.* (2015) agree that the combustion efficiency of MGTs ranges from 75% to 98%. Bakalis and Stamatis (2012) measured a combustion efficiency of 85% for the Olympus HP micro jet engine. Guidez *et al.* (2009) determined a combustion efficiency of 80% for a miniature combustor. Meyers (2016) BMT combustor expert at the CSIR Pretoria office recommended a combustion efficiency of 90% for the engine. On this basis, a combustor pressure loss and efficiency of 10% and 90% respectively were chosen for the BMT engine calculations as stated in Table 4.1.

4.1.1 *Compressor Parameters*

The compressor parameters are calculated from the impeller inlet to the diffuser outlet. The compressor annulus area, mass flow rate ($\dot{m}_a$) and the ambient density of air were used to determine an initial estimate of the absolute velocity of air trapped in the compressor. The exact velocity, static pressures and temperatures were then determined iteratively. The annulus area and velocity are expressed as follows:

$$A_{in} = \pi(r_s^2 - r_h^2) \tag{4.1.1}$$

$$C_{in} = \frac{\dot{m}_a}{\rho_{02} A_{in}} \tag{4.1.2}$$

With a known absolute velocity, the static temperature and pressure at the inlet are calculated as:

$$T_2 = T_{02} - \frac{C_{in}^2}{2c_p} \tag{4.1.3}$$

$$p_2 = p_{02}\left(\frac{T_2}{T_{02}}\right)^{\frac{\gamma}{\gamma-1}} \tag{4.1.4}$$

The actual static density is then determined after obtaining the actual static pressure and temperature at the inlet of the compressor. The static density is computed as:

$$\rho_2 = \frac{p_2}{RT_2} \tag{4.1.5}$$

Using the assumption of adiabatic flow in the diffuser the overall compressor stage temperature T_{03} was denoted by the impeller outlet temperature. The compressor outlet temperature is then determined as:

$$T_{03} = T_{02} + \frac{\sigma_s \psi U C_{\theta 2}}{c_{pa}} \tag{4.1.6}$$

The slip factor is calculated Using Stanitz relation:

$$\sigma_s = 1 - \frac{0.63\pi}{Z} \tag{4.1.7}$$

where σ_s is the slip factor, ψ is the power coefficient and Z is the number of impeller blades. The power coefficient was assumed to be unity.

The stagnation pressure at the outlet of the compressor is calculated using the known compressor pressure ratio and the compressor inlet stagnation pressure. The stagnation pressure is determined by making use of this formula:

$$p_{03} = p_{02} CPR_a \tag{4.1.8}$$

Using T_{03}, CPR_a, T_{02} and γ the compressor stage total-to-total isentropic efficiency is computed as:

$$\eta_c = \frac{T_{02}(CPR_a^{\frac{\gamma-1}{\gamma}} - 1)}{T_{03} - T_{02}} \tag{4.1.9}$$

4.1.2 *Combustion Chamber Parameters*

The combustor outlet temperature which also serves as the turbine inlet temperature can simply be calculated using the conservation of energy. On the basis of energy in the fuel being equal to the energy of the burnt gas the combustor outlet temperature is determined using the relation:

$$T_{04} = T_{03} + \frac{f \eta_b HV}{c_{pg}} \tag{4.1.10}$$

Knowing the burner pressure loss, the pressure of the high temperature combustion gases coming out of the combustor can be computed using:

$$p_{04} = p_{03}(1 - \Delta p) \tag{4.1.11}$$

4.1.3 *Turbine Parameters*

There is no clearly established data for MGT shaft mechanical efficiency in the literature. A mechanical efficiency in the range of 92% to 98% was used by Rahman and Whidborne (2008) and Gao and Huang (2011) in a performance evaluation of MGTs. A mechanical efficiency of 98% was arbitrarily chosen for the BMT. Taking into account the mechanical losses in the engine shaft bearings, the BMT compressor work is equal to the turbine work. Applying this relation the turbine outlet pressure is computed as:

$$T_{05} = T_{04} - \frac{\dot{m}_a c_{pa}}{\dot{m}_g \eta_m c_{pg}}(T_{03} - T_{02}) \tag{4.1.12}$$

The stagnation pressure after the turbine is then computed from the relation:

$$p_{05} = p_{04}\left[1 - \frac{(1 - T_{05}/T_{04})}{\eta_T}\right]^{\frac{\gamma_g - 1}{\gamma_g}} \tag{4.1.13}$$

The static temperature after the turbine is expressed as:

$$T_5 = T_{05}\left(\frac{p_5}{p_{05}}\right)^{\frac{\gamma - 1}{\gamma}} \tag{4.1.14}$$

4.1.4 *Nozzle Parameters*

Isentropic conditions are assumed between the inlet and outlet of the BMT's converging nozzle. The stagnation pressure and temperature after the nozzle are therefore given as:

$$p_{08} = p_{05} \text{ and } T_{08} = T_{05} \tag{4.1.15}$$

As stated in section 3.1, the control volume was chosen far away from the engine inlet and outlet. Hence, the hot gases in the nozzle outlet expand to ambient pressure, $p_8 = p_a$. In addition to this information, the static pressure in the nozzle throat was higher than the critical pressure at the nozzle throat. Therefore the nozzle flow is unchoked and the exhaust pressure of the exit is equal to the ambient pressure. The corresponding static temperature after the nozzle was then computed as:

$$T_8 = T_{05}\left(\frac{p_8}{p_{05}}\right)^{\frac{\gamma_g - 1}{\gamma_g}} \tag{4.1.16}$$

Combining equation 3.19 and 3.14 the nozzle exhaust velocity, density and area are calculated as follows.

Exhaust velocity:

$$u_e = \sqrt{2c_{pg}(T_{08} - T_8)} \tag{4.1.17}$$

Exhaust gas density:

$$\rho_e = \frac{p_8}{RT_8} \tag{4.1.18}$$

Exhaust area:

$$A_e = \frac{\dot{m}_g}{\rho_e u_e} \tag{4.1.19}$$

4.1.5 *Performance Parameters*

The engine thrust and the specific fuel consumption are determined as follows.

Thrust:

$$F_{net} = \dot{m}_a(u_e - u_0) \tag{4.1.20}$$

where u_0 reduces to zero for a test rig or stationary engine as already mentioned in section 4.1. Consequently, the engine thrust reduces to:

$$F_{net} = \dot{m}_a u_e \tag{4.1.21}$$

The specific fuel consumption is calculated using:

$$SFC = \frac{\dot{m}_f}{F_{net}} \tag{4.1.22}$$

4.1.6 *Analytical Results*

Tables 4.2 and 4.3 collate the analytical results and the two sets of experimental performance data of the BMT engine at a design speed of 120 krpm. As mentioned in section 3.2, the available experimental test data measured by Krige (2012) is defined as experiment 1 and the current experiment results referred to as experiment 2. The initial performance analysis yielded a thrust of 140 N and thrust percentage difference within 11% of experiment 1. Micro gas turbine engines use about 5-10% of the engine fuel consumption for lubrication of the engine's bearings (Leylek *et al.*, 2013). In order to get an approximate analytical thrust value comparable to the experiment 1 data, a value of 10% of the measured fuel massflow rate is assumed to be used for the BMT engine bearing lubrication. The new fuel flow value of 0.00477 kg/s was then used to calculate the baseline engine parameters. With the new fuel flow value, the calculation predicted a thrust value of 128 N. Table 4.2 shows the comparison between experiment 1 data and the analytical results. Percentage differences in the range of 0.8% to 17.8% were obtained.

Table 4.2: Comparison of analytical and experiment 1 results.

Parameter	Experiment 1	Analytical	Difference (%)
Thrust(N)	127	128	0.8
Exhaust Gas Temperature (K)	1051	864	17.8
Specific fuel consumption (g/kNs)	41.7	37.3	11.0

Table 4.3 compares experiment 2 and the analytical results. Percentage differences in the range of 1.0% to 16.3% was established. Due to the problems experienced with the fuel flow rate measurement, the experiment 1 data was used as standard data for the analytical calculations.

Table 4.3: Comparison of analytical and experiment 2 results.

Parameter	Experiment 2	Analytical	Difference (%)
Thrust(N)	137	128	6.6
Exhaust Gas Temperature (K)	986	864	12.4
Specific fuel consumption (g/kNs)	45.9	37.3	18.8

4.2 Numerical Analysis

This section reports the numerical simulation methodologies. GasTurb (Gas turbine simulation software) and Flownex SE (Thermodynamic system simulation software) were used for the numerical modelling and simulation. Design and off-design point simulations were performed in both GasTurb and Flownex SE. Flownex SE was used for the engine component matching due to easier introduction of engine characteristic maps into the program.

4.2.1 *GasTurb Simulation Environment*

GasTurb is a numerical simulation program designed specifically for both aircraft and industrial gas turbine cycle analysis. It is easy and flexible to evaluate engine thermodynamic cycle performance at design and off-design conditions (Kurzke, 2012). The program also has geometric engine designs that permit disk stress calculation. GasTurb can handle different categories of engines such as single and twin spool turbojets, turboprops, turbofans and turboshafts. Figure 4.1 illustrates a single spool turbojet engine layout such as the BMT engine in GasTurb. The numbers 0 to 8 indicate the station points of the engine from

the front to the rear of the engine. These points describe the engine configuration and show where exactly the thermodynamic properties of the flow occurs in the engine.

The program use the work, speed and mass flow compatibility, applying the matrix iteration component matching method to compute the engine performance parameters. The engine model starts with the selection of a rotational speed, and other boundary conditions such as the compressor inlet mass flow rate, inlet pressure and temperature, the combustor outlet temperature and the turbine efficiency. The system fuel flow rate and turbine mass flow rate are determined based on the combustor outlet temperature, fuel heating value and the compressor mass flow rate. The simulated combustion outlet temperature was determined from the BMT theoretical analysis. Therefore, the GasTurb simulation accounted for the 10% loss of fuel flow used for the engine's bearing lubrication. The engine model parameters stated in Table 4.4 were used for the GasTurb simulation at a design speed of 120 krpm. These parameters were established from the analytical calculations and the available experiment data (Krige, 2012). Bleed flow was not included in the GasTurb performance simulation.

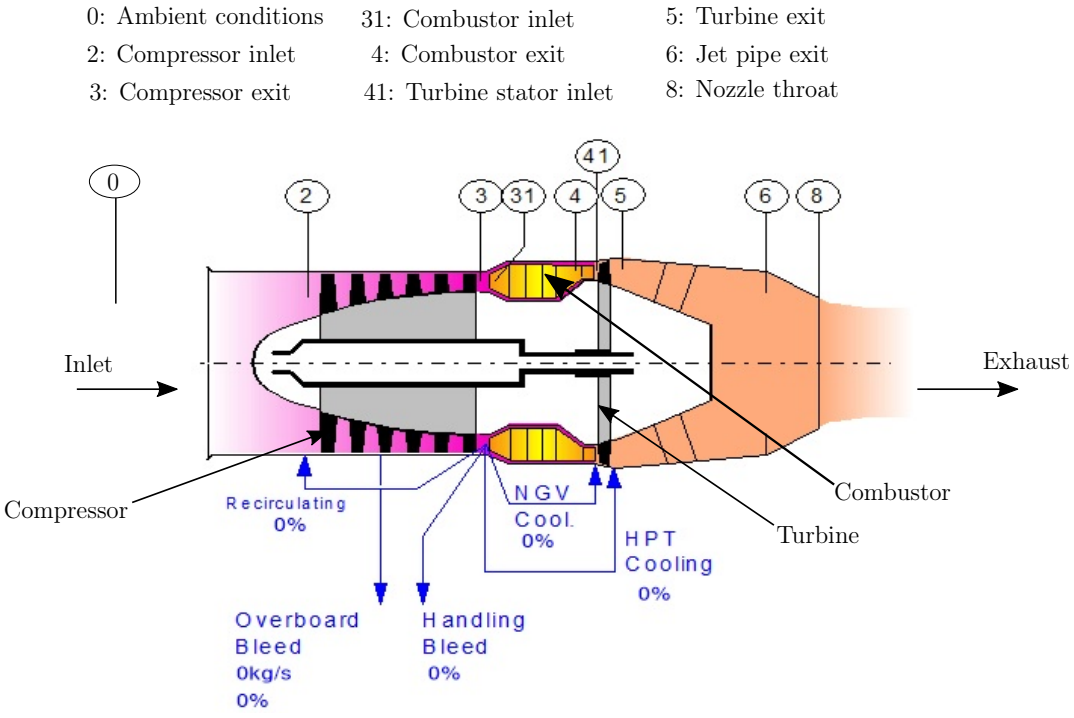

Figure 4.1: GasTurb generic turbojet engine schematic.

Table 4.4: BMT GasTurb model parameters at design point.

Parameter	Name of parameter	Value	Unit
Ambient conditions	Ambient temperature	288.15	K
	Ambient pressure	101.25	kPa
BMT parameters	Pressure Ratio	3.15	-
	Compressor efficiency	81	%
	Turbine efficiency	85	%
	Mechanical efficiency	98	%
	Combustion efficiency	90	%
	Rotational speed	120 000	rpm
	Turbine exit duct pressure ratio	0.999	-
	Turbine inlet temperature	1047	K
	Number of turbine stages	1	-

4.2.2 *GasTurb Results*

GasTurb engine performance results are shown in Figures 4.2 to 4.4. Figure 4.2 shows the GasTurb simulation results at the engine design point. The simulated results achieved a thrust value of 130 N at the engine design speed of 120 krpm at a mass flow rate of 0.288 kg/s.

Station	W kg/s	T K	P kPa	WRstd kg/s
amb		288,15	101,325	
1	0,288	288,15	101,325	
2	0,288	288,15	101,325	0,288
3	0,288	424,38	319,174	0,111
31	0,288	424,38	319,174	
4	0,293	984,88	287,256	0,191
41	0,293	984,88	287,256	0,191
49	0,293	864,95	154,444	
5	0,293	864,95	154,444	0,333
6	0,293	864,95	154,290	
8	0,293	864,95	154,290	0,333
Bleed	0,000	288,15	101,325	

P2/P1 = 1,0000	P4/P3 = 0,9000		P6/P5	0,9990
Efficiencies:	isentr	polytr	RNI	P/P
Compressor	0,8160	0,8427	1,000	3,150
Burner	0,9000			0,900
Turbine	0,8500	0,8396	0,668	1,860
Spool mech Eff	0,9800	Nom Spd	120000	rpm

FN	=	0,13	kN
TSFC	=	35,7004	g/(kN*s)
FN/W2	=	452,22	m/s
Prop Eff	=	0,0000	
eta core	=	0,1449	
WF	=	0,00465	kg/s
s NOx	=	0,05839	
XM8	=	0,8120	
A8	=	0,0015	m²
P8/Pamb	=	1,5227	
WBld/W2	=	0,00000	
Ang8	=	20,00	°
CD8	=	0,9372	
WClN/W2	=	0,00000	
WClR/W2	=	0,00000	
Loading	=	100,00	%
e45 th	=	0,85000	
far7	=	0,01614	
PWX	=	0,00	kW

Figure 4.2: BMT GasTurb results.

Figure 4.3 displays the correlation between GasTurb simulated results and the experiments thrust data. A consistent trend is achieved between the simulated and the experiments thrust. Comparing the results, a percentage deviation in the range of 2.2% to 17% was achieved for the GasTurb simulation and

experiment 1 thrust. The experiment 2 thrust is 5% to 20% higher than the GasTurb thrust. GasTurb simulation predicted lower thrust at 80 krpm compared to the experiments.

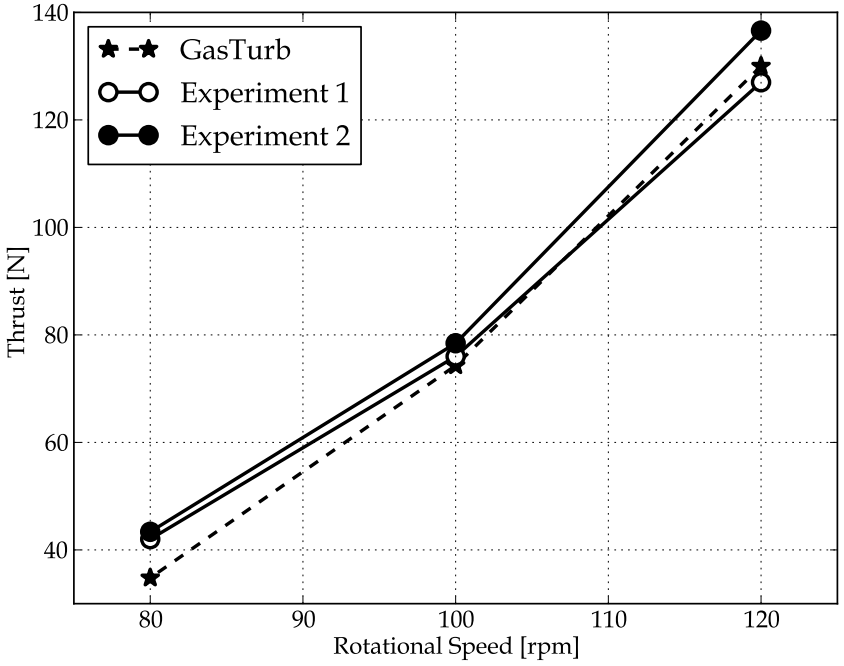

Figure 4.3: BMT GasTurb simulation and experiments thrust line.

Figure 4.4 illustrates the thermodynamic characteristic behaviour of the MGT performance parameters. The figure details the changes in the mass flow, the static and total pressures and temperatures at the different stations of the engine. The total mass flow in the engine remains constant throughout the engine after combustion. The stagnation pressure and temperature also follow the same trend after expansion of the gases in the turbine, unlike the static pressure and temperature which changes through the entire engine cycle.

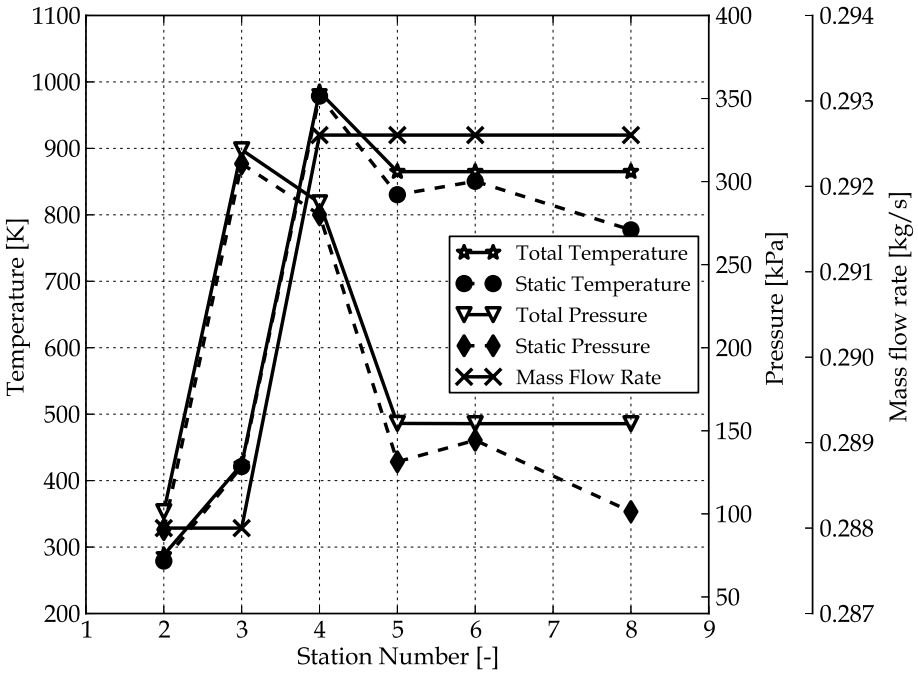

Figure 4.4: BMT GasTurb station properties.

4.2.3 *Flownex Simulation Environment*

Flownex SE is used for thermodynamic and CFD analysis and modelling of turbomachinery problems (M-Tech, 2015). The software is locally developed in South Africa by M-Tech Industrial (Pty) Ltd and distributed by ESTEQ (Pty) Ltd. The software is suitable for design and simulation of aerospace and other related industry thermodynamics and turbomachinery network problems. Flownex SE is well suited for on-design and off-design modelling and simulation of gas turbine engines. The software has standard library components such as turbines, compressors, pipes, and heat transfer elements, which allows easy forming of turbomachinery networks. A Flownex user can analyze a standard turbomachine and add and analyze additional components. Figure 4.5 describes the Flownex BMT engine arrangement. The engine network model consists of an inlet boundary properties, compressor, fuel suply, combustor, turbine, thrust nozzle and exhaust boundary conditions. The connecting nodes in the network system join the network elements smoothly and ensure good network communication between the components.

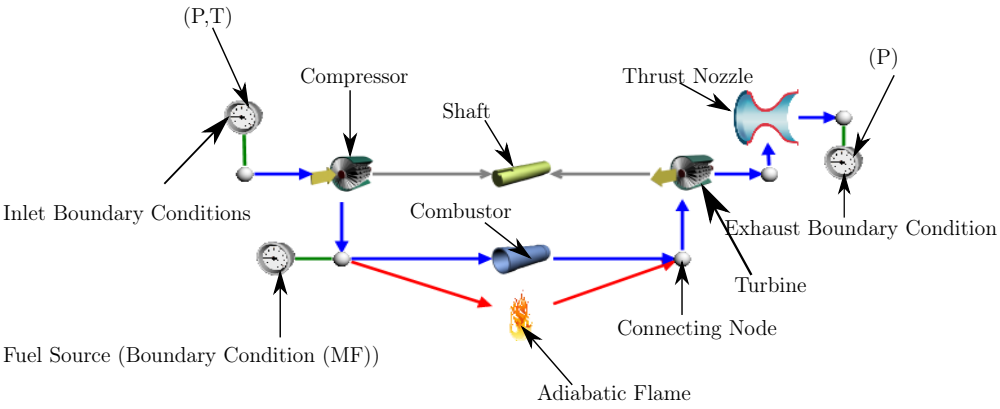

Figure 4.5: Flownex SE engine layout.

4.2.4 *Compressor Unit*

Figure 4.6 displays the gas turbine compressor unit in Flownex. The compressor section is made up of an airflow gauge and the compressor. The inlet gauge monitors the mass of airflow into the engine. The inlet boundary conditions were set to ambient conditions for both pressure and temperature.

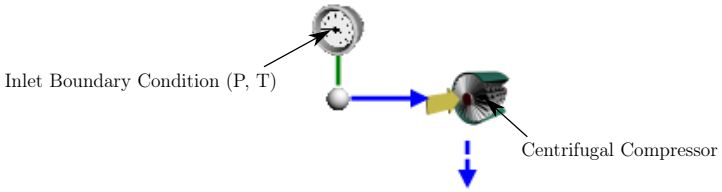

Figure 4.6: Compressor unit.

4.2.5 *Combustor Model*

There are two combustion modelling methods in Flownex, namely, the adiabatic flame element and the Flownex combustion model which uses combustion characteristic maps. Due to unavailability of combustion performance maps for MGTs, the adiabatic flame element model was used for the engine combustion modelling. The adiabatic flame element determines the cycle peak temperature and off-gas composition. The Gordon-McBride program, a secondary program integrated into Flownex SE calculates the cycle off-gas composition and the maximum temperature. This program does not account for the combustor geometry in determining the peak temperature. The combustion pressure loss is computed separately by the Flownex program. This is established by placing the combustor geometry (pipe) parallel with the adiabatic flame as shown in Figure 4.7. The combustion pressure loss is determined by Flownex using the

combustor geometry and the roughness value of the combustor material and Darcy equation. The Gordon-McBride program uses Flownex input (reactant pressure, inlet temperature, and mass fraction) upstream of the combustor to generate the output data. Flownex then retrieves the calculated peak temperature and mass fractions and delivers them to the combustor downstream nodes. As mentioned in section 2.1, BMT engine uses Jet (A1) or Kerosene as fuel therefore Jet (A1) was used for the combustion system. The mass flow of fuel into the network model was specified.

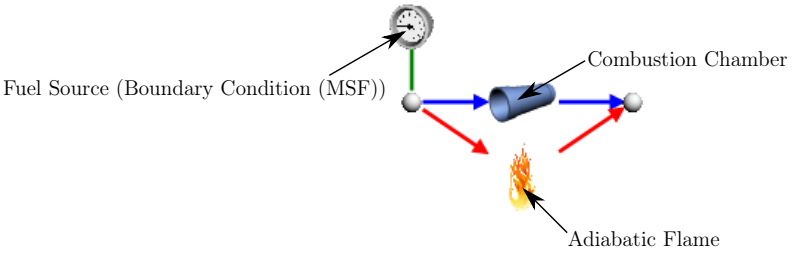

Figure 4.7: Adiabatic flame combustion system.

4.2.6 *Turbine Unit*

The turbine unit consists of the axial flow turbine, thrust nozzle and the exhaust boundary condition. The thrust nozzle determines the thrust output from the engine. A converging-diverging nozzle with identical throat and the exit areas were used to represent the converging nozzle of the BMT engine.

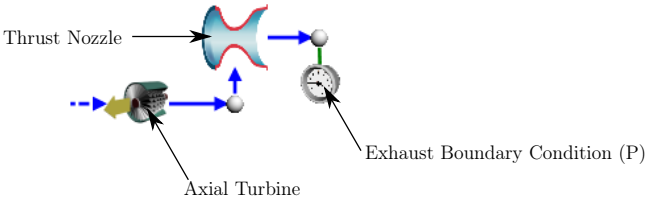

Figure 4.8: Turbine unit.

4.2.7 *Setting of Parameters*

The engine model parameters presented in Table 4.5 were introduced into the Flownex simulation environment for the engine simulation. All engine network simulations were executed at the various ambient conditions measured by the respective authors. The geometry of the combustor is not accounted for by the adiabatic flame temperature, therefore the combustor thickness for this model was arbitrarily set at 1 mm.

Table 4.5: Flownex BMT model parameters.

Parameter	Name of parameter	Value	Units
Ambient conditions	Ambient temperature	288.15	K
	Ambient pressure	101.325	kPa
BMT parameters	Combustor length	70	mm
	Combustor diameter	84	mm
	Combustor thickness	1	mm
	Nozzle area	0.04323	m^2
	Mechanical efficiency	98	%
	Combustor pressure drop	10	%

4.3 Flownex Component Matching

The component matching methods in Flownex SE are presented in this section. The Flownex direct design functionality and turbo power match tools were used for the engine component matching.

4.3.1 *Flownex Direct Design Functionality*

Flownex SE design is a functionality tool that allows automatic computation, sizing and matching of turbomachine units to obtain suitable system conditions. The design functionality uses the matrix iteration technique. The functionality tool utilises the effective multi-variable Newton-Raphson and orthogonal and upper triangular matrix (QR) decomposition for its matrix iteration and computations. The design functionality tool performs the component matching using an equal number of constraints and independent variables. The matching rule follows the same procedure already explained in section 2.4.1 for the matrix iteration method. The independent variables are guessed at the begin of the calculation. These values are continually updated with a relaxation factor. The engine matching was executed using the outlined procedure below.

1. Select the designer configuration menu from the Flownex library.
2. Set the name of the designer, relaxation value and maximum iteration.
3. Set the convergence criteria and steady state solver values.
4. Set the equality constraints and independent variables.
5. Run the simulation until convergence is attained.

The equality constraints were set as the engine shaft excess power and the turbine mass flow rate while the turbine geometry and the rotational speed scaling factor were set as the independent variables. The excess shaft power is zero after convergence.

4.3.2 *Turbo Power Match*

Turbo Power Match (TPM) enables easy and flexible matching of turbomachinery components. Component matching is either performed in the steady state or transient mode. This design tool is used when the turbo unit's inlet guide vanes (IGV) or the shaft speed are varied to execute matching. Activation of this tool is done through the power matching and speed category on the shaft or gearbox input property window shown in Figure 4.9. Matching elements such as the turbine, compressor, pump or fan are specified in the property window. The power matching and speed category on the shaft element is activated for networks with only a shaft connecting turbo units. However, for networks with both a shaft and gearbox connecting turbo elements, power matching and speed category of the gearbox element is activated. The excess shaft power produced from the matching process is expressed as:

$$P_{excess} = \eta_m \sum P_{positive} - \sum P_{negative} \tag{4.3.1}$$

where η_m is the mechanical efficiency, $\sum P_{positive}$ is the power supplied by power providing components such as the turbine and $\sum P_{negative}$ is the power required by power absorbing components such as the compressor.

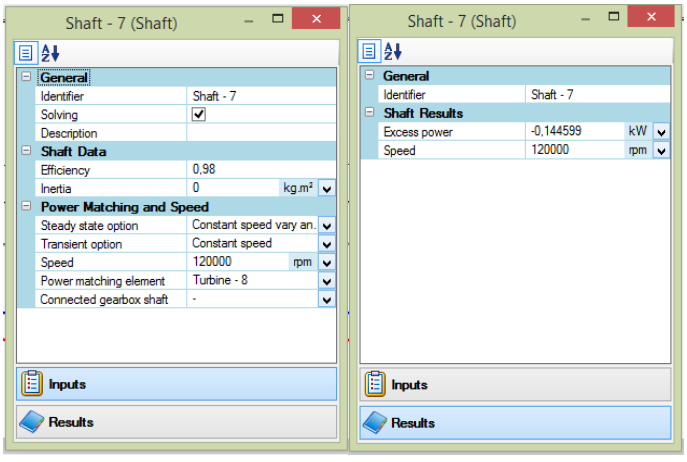

Figure 4.9: Turbo power matching.

4.3.3 *Flownex Engine Network Models*

The engine modelling and simulation in Flownex includes the following.

1. Baseline BMT engine simulation
2. Modified engine simulations
    - Simulations using Burger's and De Villiers' compressor stages and the various BMT turbine stages .
    - Simulations of the engine with variable nozzle and turbine area using Burger's compressor stage and the original BMT turbine stage.

4.3.4 *Engine Characteristic Maps*

In order to assess the performance of the BMT engine using the component matching technique, characteristic maps of the compressor and turbine are required. Figure 4.10 through 4.13 to 4.19 present the engine compressor and turbine stage characteristic maps. Figures 4.10 and 4.11 represent the standard BMT compressor maps published by Krige (2012). Figure 4.10 describes the pressure ratio and corrected mass flow performance while Figure 4.11 presents the plot of efficiency against corrected mass flow. These maps were imported into Flownex for the baseline BMT engine performance evaluation. Figures 4.12 and 4.13 illustrate the original BMT turbine maps developed by Basson (2014). Figure 4.12 shows the pressure ratio and the corrected mass flow rate through the turbine. Figure 4.13 describes the efficiencies of the turbine plotted against the corrected mass flow rate.

Basson (2014) re-designed the turbine stage of the BMT engine using different load coefficients. The load coefficients chosen for the turbine design are 95%, 100% and 105% respectively. Figures 4.14 and 4.15 display the performance curves developed by Basson (2014) for the re-designed turbine stages of the engine. These maps describe the efficiency, pressure ratio and the corrected mass flow plots of the 95%, 100% and 105% loading coefficients. The maps were individually introduced into Flownex and simulated with the different engine compressor stages to evaluate engine performance outputs.

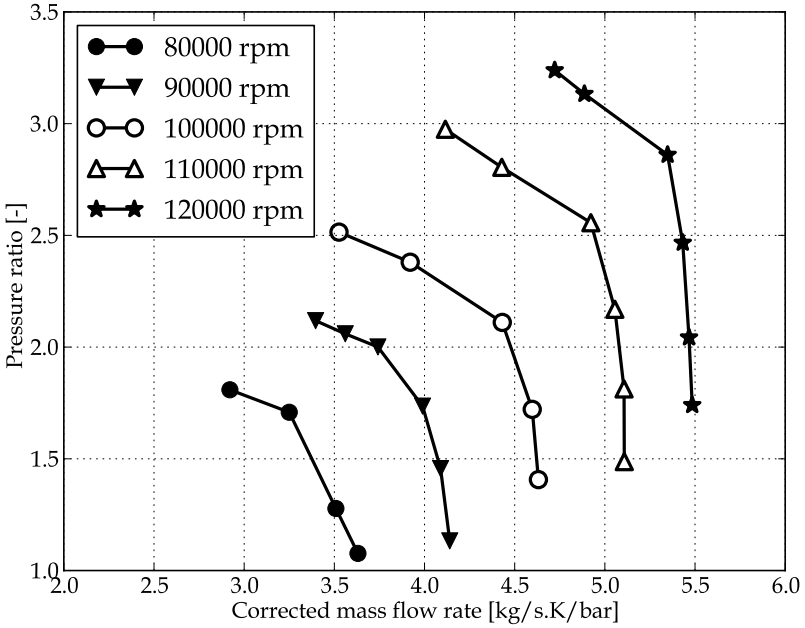

Figure 4.10: BMT compressor map (Pressure ratio vs Corrected mass flow).

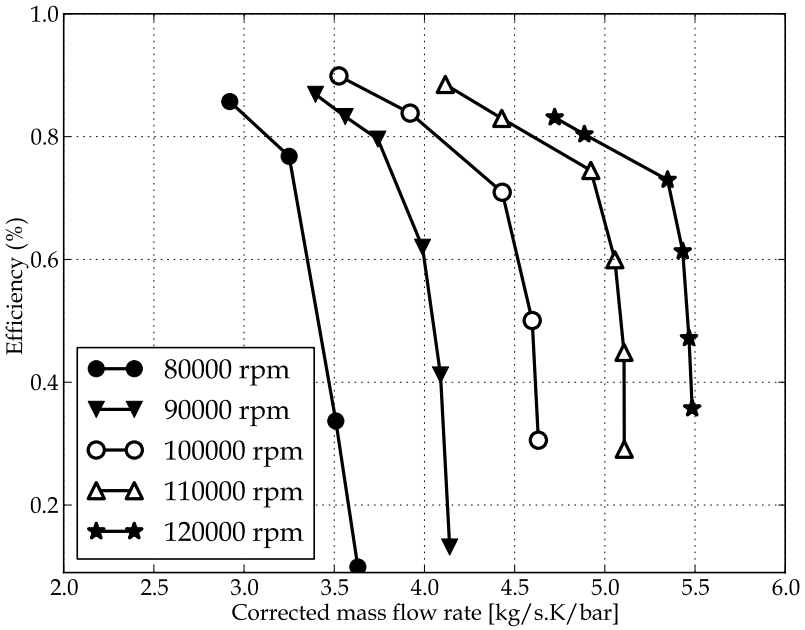

Figure 4.11: BMT compressor map (Efficiency vs Corrected mass flow).

Figures 4.16 and 4.17 describe the compressor pressure ratio, efficiency and corrected mass flow rate performance maps published by De Villiers (2014). These maps were developed for the re-designed compressor stage for the BMT engine using NUMECA CFD software. The characteristic maps were introduced into the Flownex simulation environment to evaluate the behaviour of

the engine. The initial simulation was performed with the standard BMT turbine and subsequently the re-designed turbine stages by Basson.

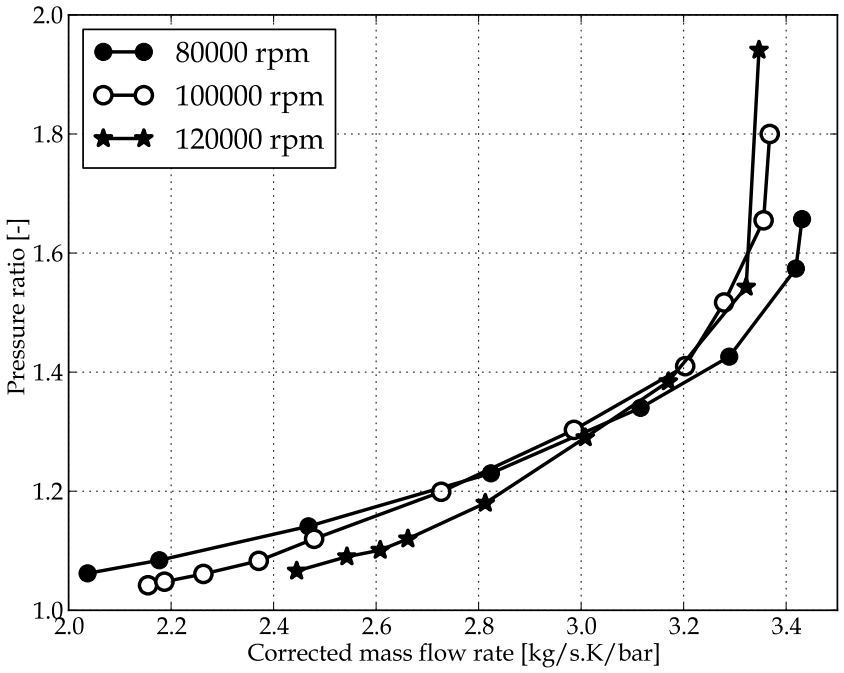

Figure 4.12: BMT turbine map (Pressure ratio vs Corrected mass flow rate).

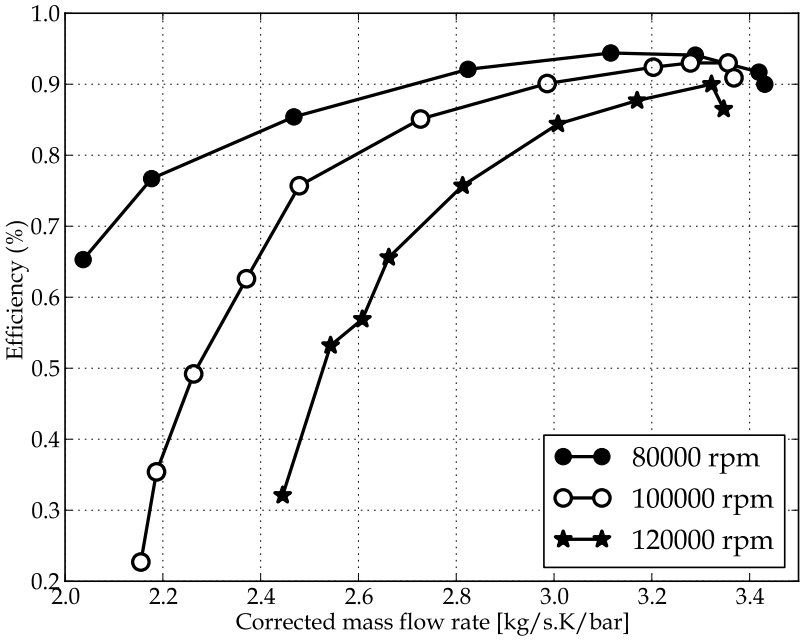

Figure 4.13: BMT turbine map (Efficiency vs Corrected mass flow rate).

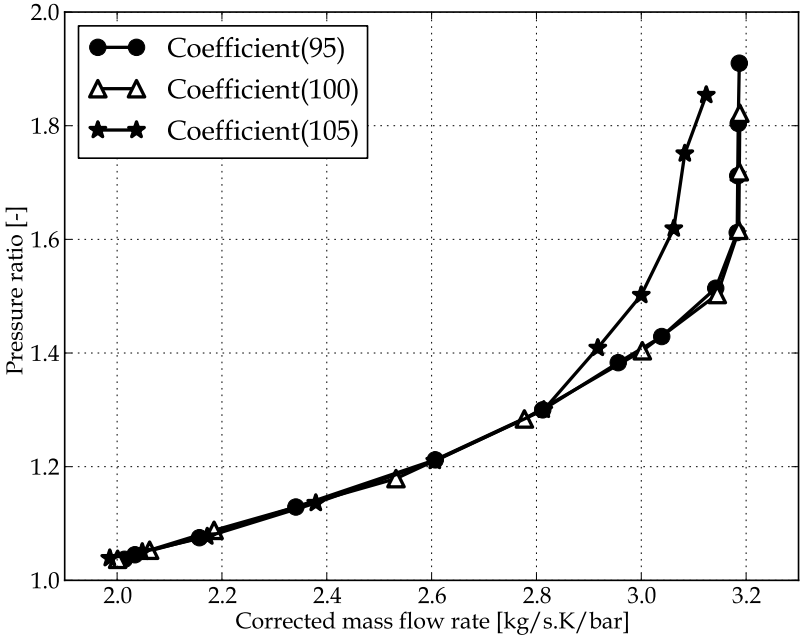

Figure 4.14: Pressure ratio and corrected mass flow rate maps, (Basson, 2014).

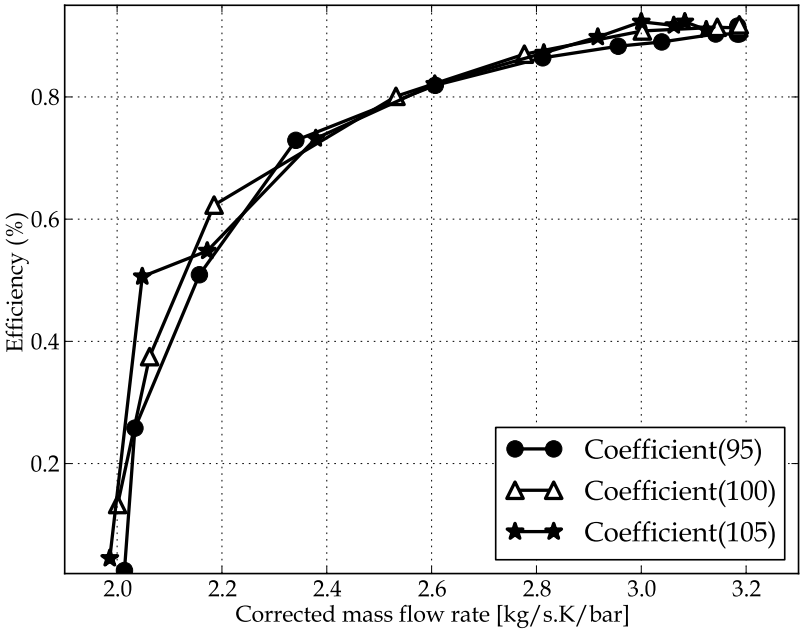

Figure 4.15: Efficiency and corrected mass flow rate maps, (Basson, 2014).

Figures 4.18 and 4.19 illustrate the compressor characteristic maps published by Burger (2016) using NUMECA CFD for his re-designed compressor stage. Figure 4.18 presents the plot of pressure ratio against the corrected mass flow rate of the compression stage. Figure 4.19 shows the efficiency and the cor-

rected mass flow rate contour plot. The performance maps were introduced into the Flownex SE to evaluate the performance of the engine.

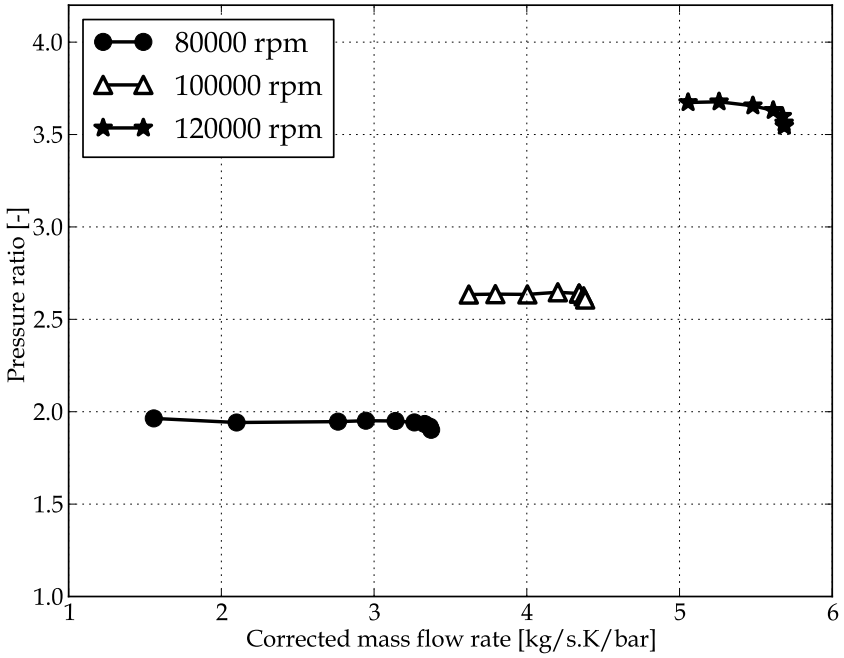

Figure 4.16: Pressure ratio and corrected mass flow rate, (De Villiers, 2014).

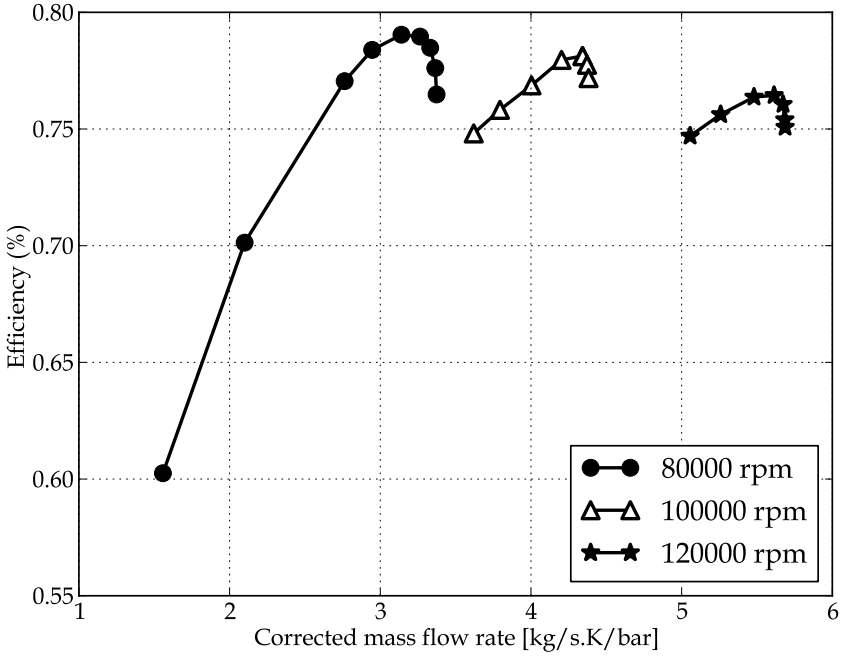

Figure 4.17: Efficiency and corrected mass flow rate maps, (De Villiers, 2014).

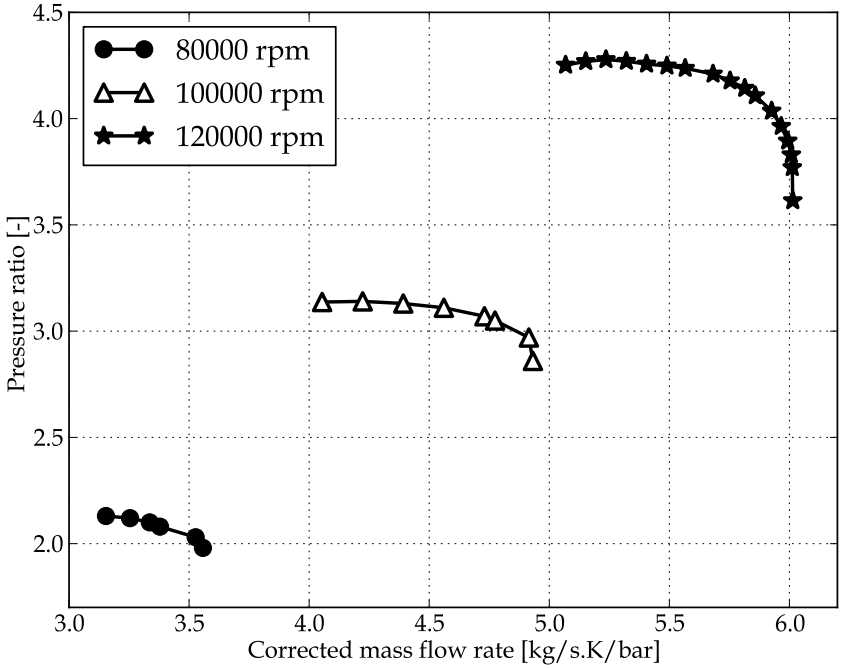

Figure 4.18: Compressor map (pressure ratio and corrected mass flow rate).

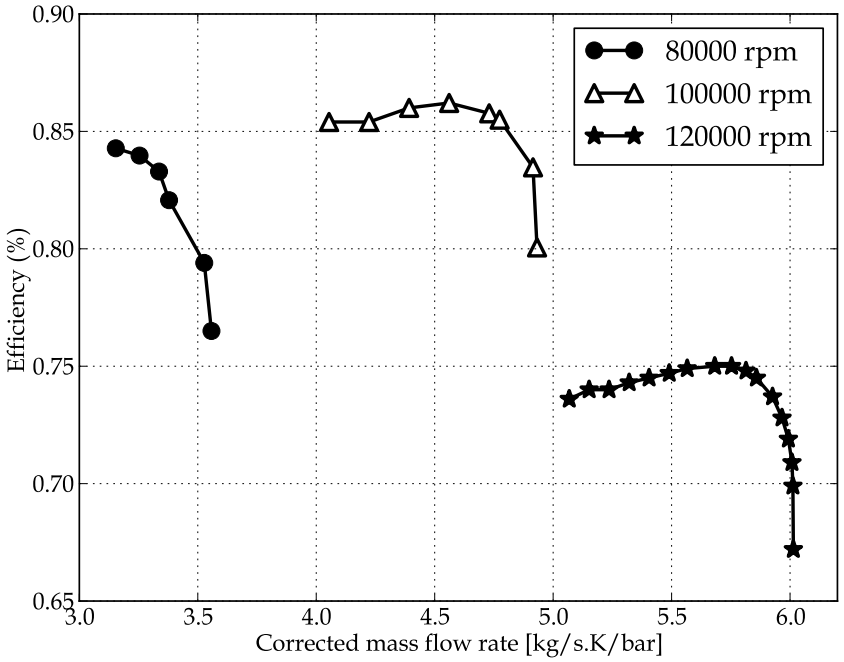

Figure 4.19: Compressor map (efficiency and corrected mass flow rate).

4.4 Baseline Engine Simulation Results

This section presents the results for the sensitivity and matching analysis for the standard BMT engine. This includes simulation results of the baseline

engine and the original BMT compressor stage with the three turbine stages designed by Basson (2014). Figure 4.20 and Table 4.6 show a comparison of the baseline engine simulated and the available experimental thrust values. As stated in section 3.2, the BMT experiment test by Krige (2012) is defined as experiment 1 whereas the new experimental test is named as experiment 2. A minimum and maximum percentage deviation of 3% and 10% are obtained between the simulation and experiment 1 thrust. A thrust difference between 0.5% and 6% was obtained when comparing experiment 2 and the simulation results.

The simulation and the experimental EGTs are compared in Table 4.6 and Figure 4.21. With reference to Figure 4.21, deviations in the range of 1.4-6% are obtained when experiment 2 EGTs are compared to the simulated EGTs. The difference is probably due to uneven distribution of the exhaust gases at the engine exhaust as mentioned in section 3.2. As shown in Table 4.6, differences of 11.7-16% are obtained for experiment 1 and the simulated EGTs. The highest temperature differences occur at speeds between 110 and 80 krpm. Figure 4.22 shows the correlation between the Flownex simulation and the experiment's specific fuel consumption as a function of the engine rotational speed. The simulation predicted higher thrust with less fuel consumption. Percentage deviations ranging from 14-20% and 25-29% were obtained for experiment 1 and 2 when compared to the simulated SFCs.

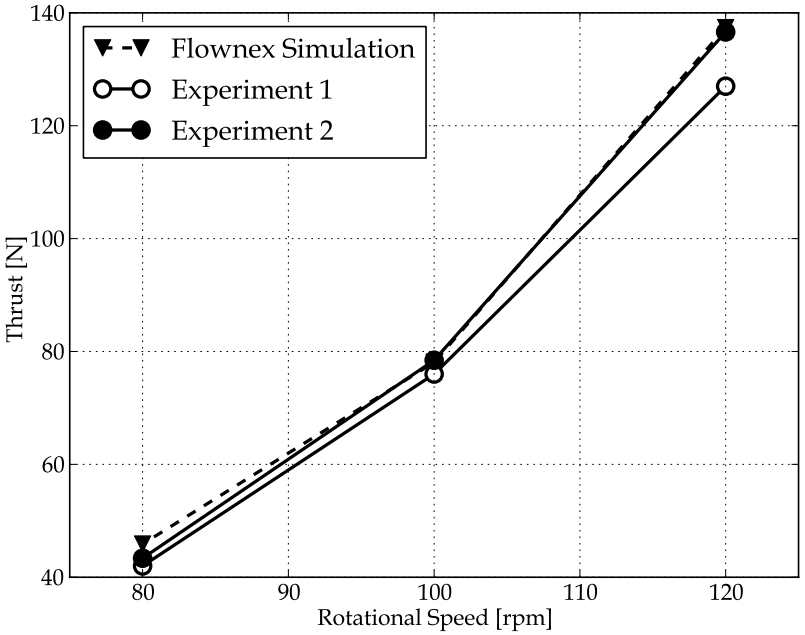

Figure 4.20: Thrust line for the baseline BMT.

Table 4.6: BMT exhaust gas temperature.

	EGT (K)		
Speed (krpm)	Experiment 1	Flownex Simulation	Difference (%)
120	1051	928	11.7
110	973	817	16.0
100	935	824	11.8
80	901	783	13.1

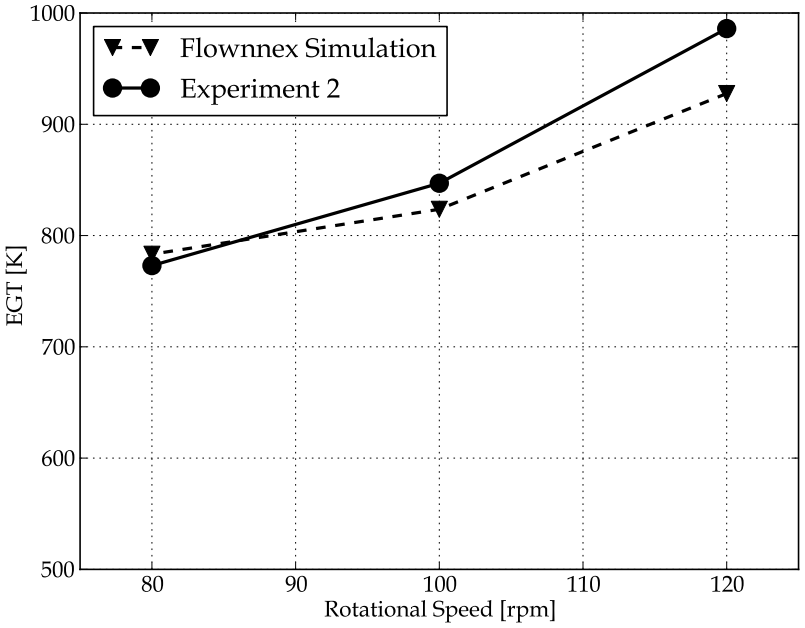

Figure 4.21: BMT experiments and Flownex simulation EGTs plot.

Having completed the standard engine simulations, its turbine stage was replaced by the turbines developed by Basson (2014) using the re-designed turbine characteristic maps described in section 4.4.3 for further analysis. This was performed to validate the engine experimental data (Smit, 2014) using the original BMT engine compressor stage with the three turbines designed by Basson (2014). The respective turbines are named as turbine 1,2 and 3. The simulation results are compared to the experimental data of the three turbine designs measured by Smit (2014). The experiments are defined as experiment A, B and C respectively.

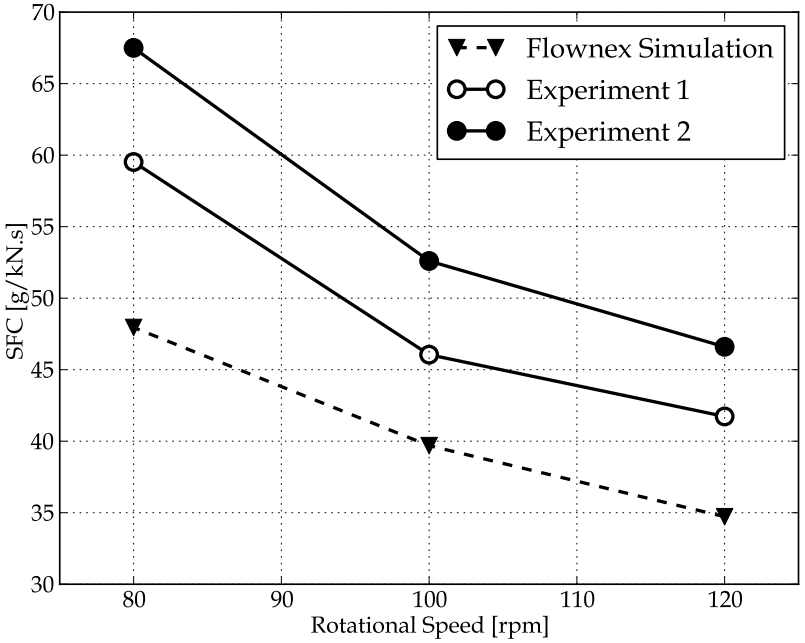

Figure 4.22: BMT specific fuel consumption comparison.

Figure 4.23 and Table 4.7 collate turbine 1 simulation results and the experimental test data. The difference between the experiment and simulation thrust is in the range of 18% to 23%. A temperature difference between 112 K and 153 K was observed when the simulation and the experimental EGTs were compared.

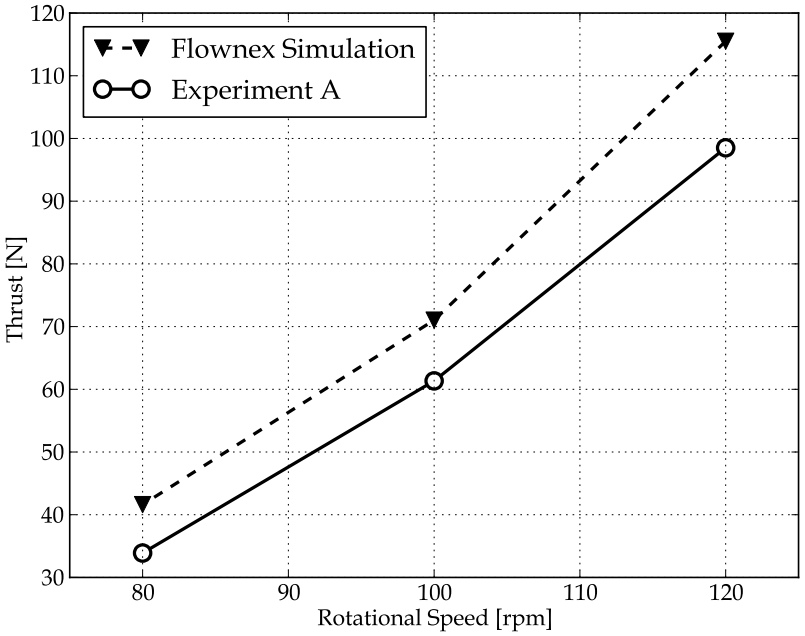

Figure 4.23: Thrust comparison (Turbine 1).

Table 4.7: Turbine 1 EGT values.

	EGT (K)		
Speed (krpm)	Experiment A	Flownex Simulation	Difference (%)
120	957	817	14.6
100	872	719	17.5
80	859	747	13.0

Figure 4.24 and Table 4.8 depict the engine performance with turbine 2. The simulation predicted thrust close the experimental thrust. The simulated thrust and the experimental test data obtained deviations in the range of 1.2% to 13%. Table 4.8 shows the comparison between the experiment and simulated EGTs. Referring to Table 4.8 the simulated EGTs were underestimated with a temperature difference between 161 K and 313 K.

Table 4.8: Turbines 2 EGT values.

	EGT (K)		
Speed (krpm)	Experiment B	Flownex Simulation	Difference (%)
120	1135	822	27.6
100	1000	765	23.5
80	883	722	18.2

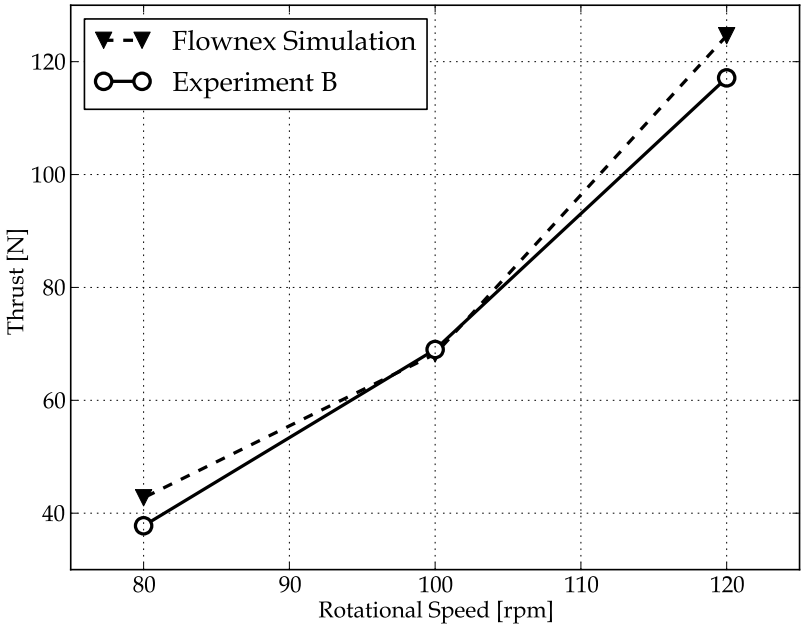

Figure 4.24: Thrust comparison (Turbine 2).

A comparison of Turbine 3 simulations and the experimental thrust values graph as a function of the rotational speeds is shown in Figure 4.25. The simulation and the experimental thrust line shows a consistent trend. A percentage difference between 4.3% and 9.2% is achieved for the thrust. Table 4.9 also displays the correlation of the EGT values for the experiment and the simulation. The simulated EGTs were underpredicted compare to the experimental EGTs. A temperature deviation of 110 K to 220 K is observed.

Table 4.9: Turbines 3 EGT values.

	EGT (K)		
Speed (krpm)	Experiment C	Flownex Simulation	Difference (%)
120	1001	781	21.9
100	869	751	13.6
80	832	722	13.2

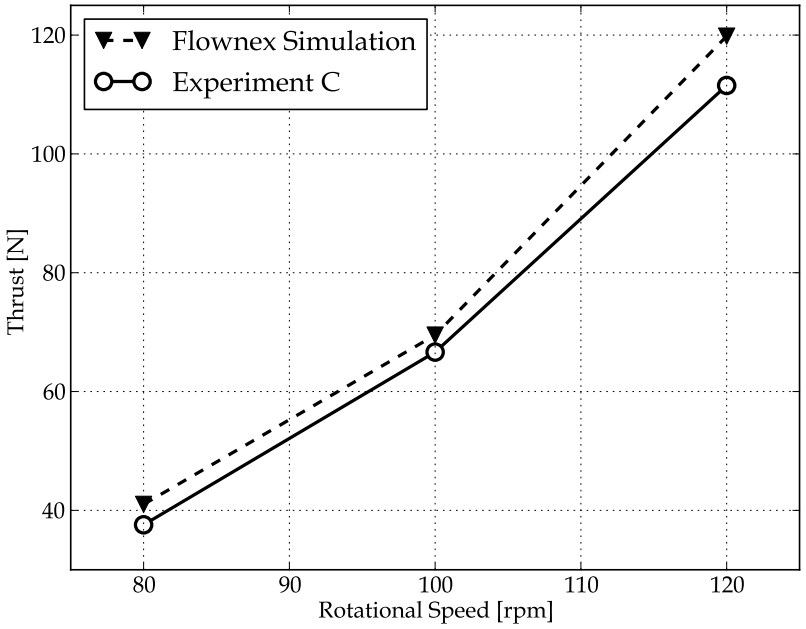

Figure 4.25: Thrust comparison (Turbine 3).

4.5 Modified Engine Simulation Results

The results of the different BMT turbine stages with De Villiers' (2014) and Burger's (2016) compressor stages as well as the results for the engine with variable turbine and nozzle area are presented in this section.

4.5.1 *Engine Arrangement with De Villiers' Compressor*

The compressor stage performance maps generated by the author discussed in section 4.4.3 were introduced into Flownex SE to investigate the engine performance. The performance analysis disclosed that the engine operates at higher turbine inlet and exhaust temperatures and lower mass flow rate at high rotational speeds when using De Villiers compressor. De Villiers faced the same problems of high EGTs during his experimental test of the engine, which prevented the engine from reaching high rotational speeds.

The performance of the engine with the De Villiers' re-designed compressor stage and the BMT turbine arrangement is given in Figure 4.26. Percentage differences in the range of 3% to 8% was obtained for the simulation and experimental thrust comparison. Figure 4.27 illustrates the correlation between the simulated results for engine configuration with Basson's re-designed turbines and the baseline turbine with De Villiers compressor stage. Comparing turbine 1 and the BMT simulation, deviations between 1.5% and 9.3% were obtained for the thrust values. The turbine 2 and 3 experimental thrust values showed a percentage difference in the range of 1.2% to 7.5% and 3.3% to 11.4% in comparison with the BMT simulated thrust values.

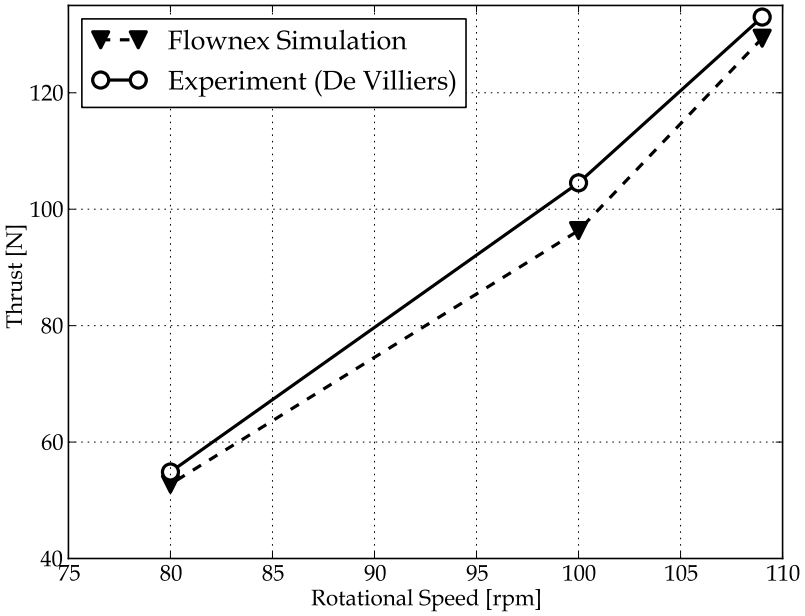

Figure 4.26: Thrust performance for De Villiers compressor.

Figure 4.28 compares and correlates the standard BMT and Basson's three turbines simulated EGTs using De Villiers's compressor stage. The BMT simulation predicted higher EGT values in comparison with the three different turbines. A percentage deviation of 0.1% to 13% is shown for the BMT and

turbine 1 simulation while turbine 2 and 3 simulated EGTs showed percentage differences of 1% to 7% and 1.4% to 10% compared to the experimental results.

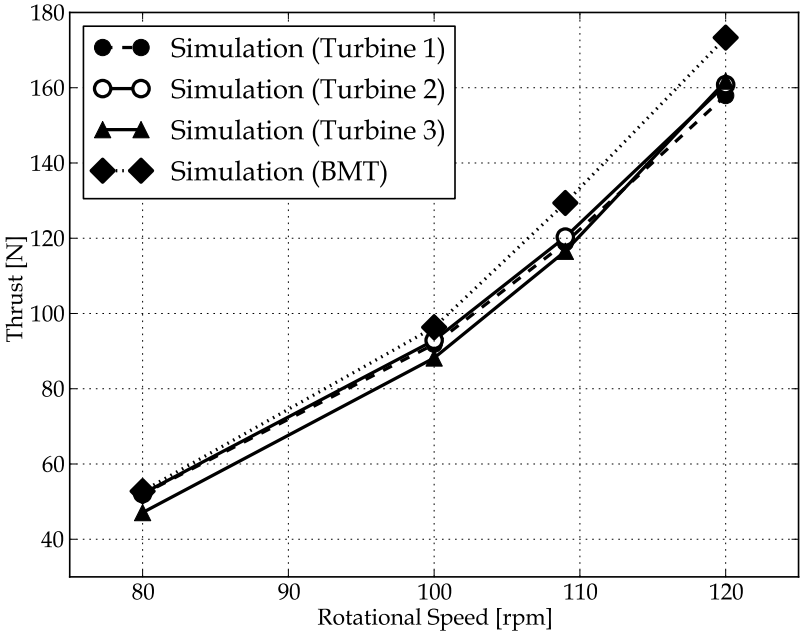

Figure 4.27: Comparison of thrust for the BMT and Basson turbines with De Villiers compressor.

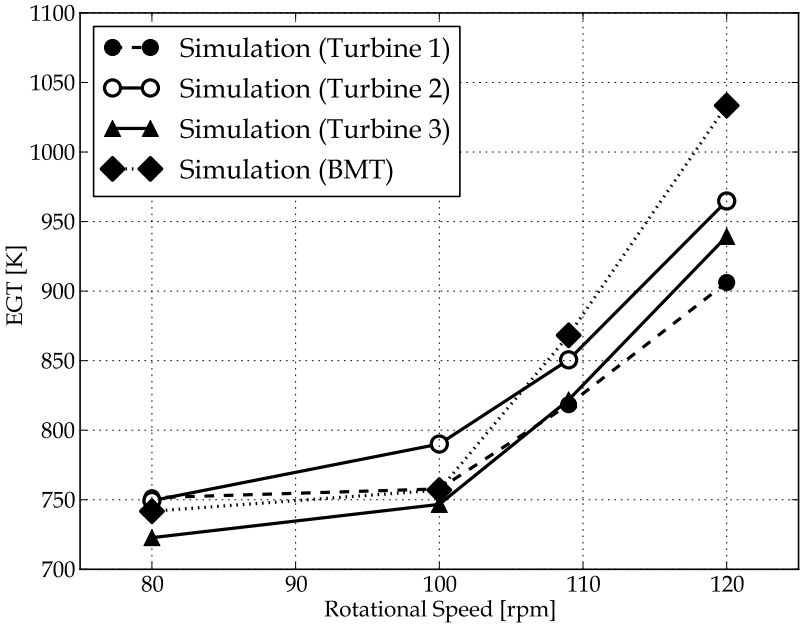

Figure 4.28: Comparison of EGTs for the BMT and Basson turbines with De Villiers compressor.

4.5.2 *Engine Configuration with Burger's Compressor*

Burger's (2016) compressor stage performance maps as presented in section 4.4.3, were imported into Flownex to assess the engine performance with the different turbine stages. The performance evaluation revealed that at higher speeds, the engine requires high fuel consumption to produce sufficient turbine power to drive the compressor. This resulted in higher TIT and EGTs which were encountered in the experimental test by Burger at the same speeds. This limited the operation of the engine at higher speeds during the experiment. Increasing the fuel consumption resulted in choking in the propelling nozzle.

Figure 4.29 depicts a graph of the simulated and experimental thrust against rotational speed obtained when using Burger's compressor stage and the standard BMT turbine stage. The comparison of the simulation and experimental thrust values showed a percentage difference between 8% and 12%. The engine thrust output obtained using Burger's compressor with the BMT and Basson's turbines is illustrated in Figure 4.30. The results of the different turbines are compared with the simulated performance of the BMT turbine and Burger's compressor.

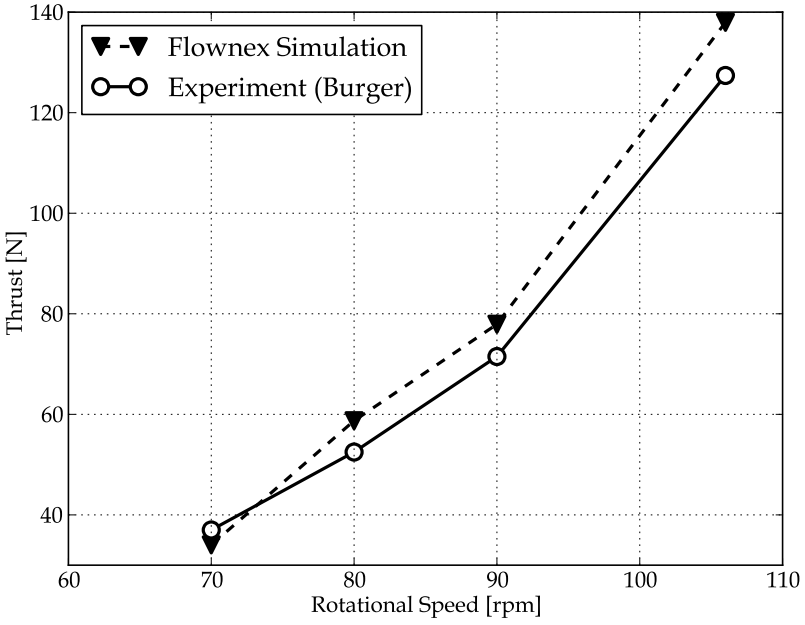

Figure 4.29: Thrust performance for Burger compressor.

The BMT and turbine 1 simulated thrust values showed differences between 1% and 10% when compared. Percentage deviations in the range of 2% to 6% and 4% to 11% were observed when the BMT thrust was compared to turbine 2 and 3 thrust. Figure 4.31 shows plot of the different turbine EGTs against rotational speed. The EGTs predicted by turbine 1 and 3 are lower than the

EGTs predicted by the BMT turbine and turbine 2. A percentage deviation between 1.2% and 13% was obtained for the BMT and turbine 1 simulation while turbine 2 and 3 and the BMT simulations obtained differences of 1% to 3.3% and 2% to 12.5% for the EGTs.

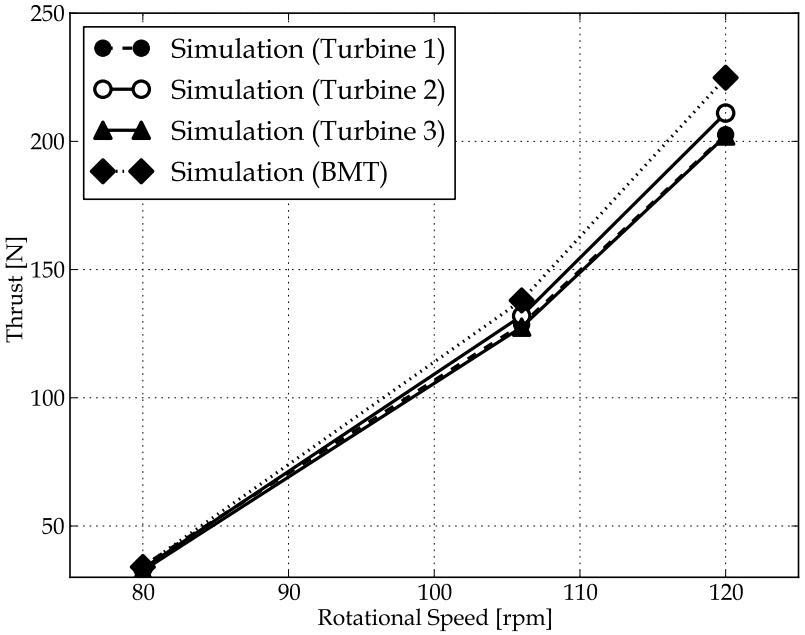

Figure 4.30: Thrust comparison for the BMT and Basson turbines with Burger compressor Burger.

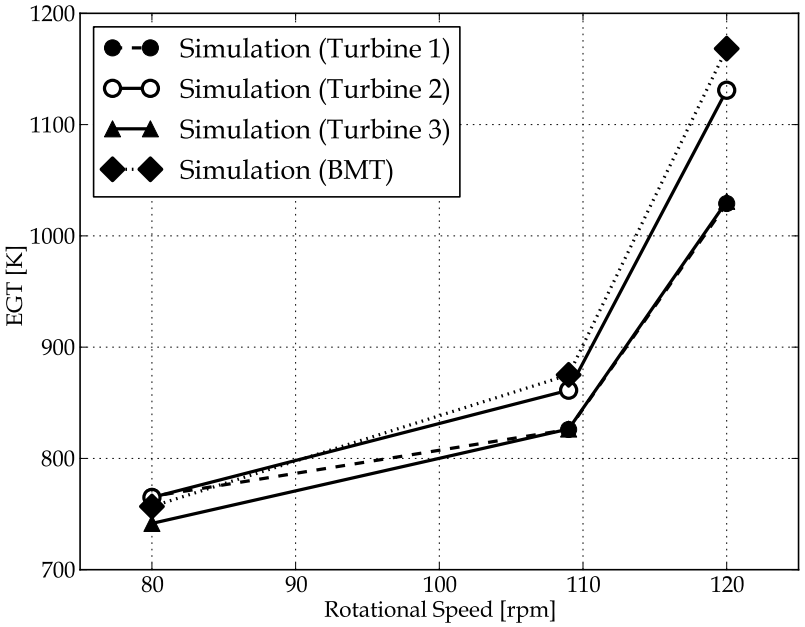

Figure 4.31: EGTs comparison for the BMT and Basson turbines with Burger compressor Burger.

4.5.3 *Engine with Variable Nozzle and Turbine Area*

The preliminary engine performance analysis using Burger and De Villiers compressor stages showed that the engine experiences high temperatures at the turbine inlet and exhaust. The engine also experiencee choking when attempting to increase the turbine power. To solve these problems, the BMT turbine characteristic area and the engine propelling nozzle area were adjusted to monitor their effects on engine performance. The maximum turbine inlet area before choke occurs is temperature dependent and increases proportionally with increasing temperature. In this regard, the turbine inlet temperature was changed to adjust the area.

An MGT's turbine inlet temperature is constrained by the strength of the turbine material. As a result of this, the turbine inlet area was increased by 3%, to accommodate MGT inlet temperature restrictions. Henceforth, this turbine will be referred to as the scaled turbine. The new scaled BMT turbine was simulated in Flownex with Burger's compressor to investigate the engine performance. The simulation was done with Burger's compressor stage due to the fact that his compressor stage outperformed De Villiers's compressor stage. The characteristic plot of the scaled turbine area and original turbine area simulations with Burger's compressor is shown in Figure 4.32. The thrust of the scaled and original turbine differed in the range of 4% to 16%. Figure 4.33 depicts the EGTs of the scaled and original turbine. A percentage difference between 5% and 10% is recorded.

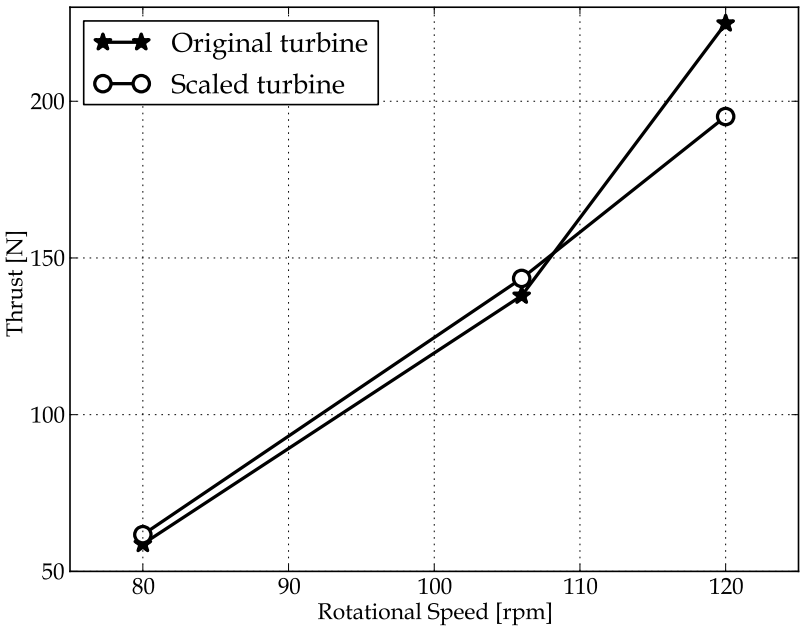

Figure 4.32: Thrust line of scaled turbine and original turbine.

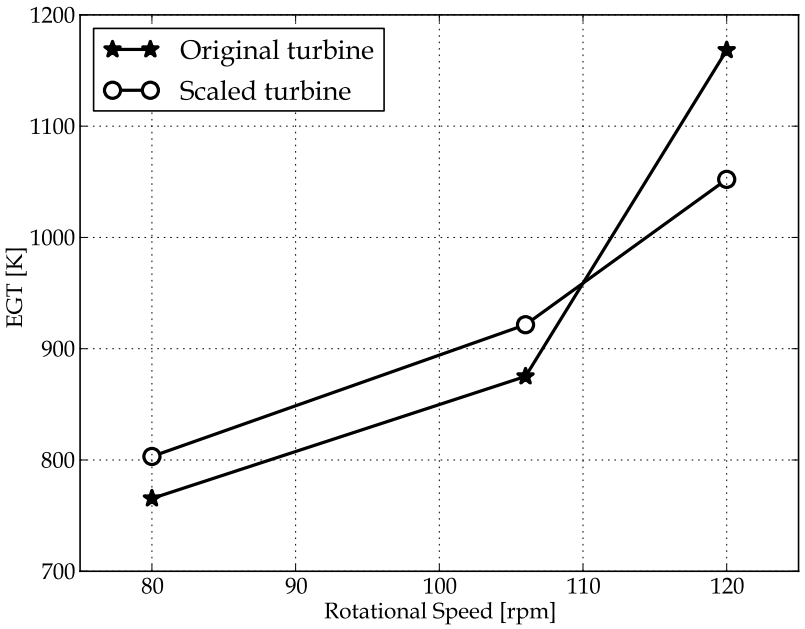

Figure 4.33: EGTs of scaled turbine and original turbine.

The propelling nozzle area of the BMT engine was then increased by 5% and 10% to see its effect on engine performance using Burger's compressor and the baseline engine turbine. The engine showed improvement in the turbine power for these increased flow areas. Beyond a 5% nozzle area increase the engine compressor efficiency and pressure ratio reduced. Therefore, a nozzle area increase of 5% was used for further engine performance modelling. Increasing the propelling nozzle area reduced the engine thrust but provided sufficient turbine power to drive the compressor. With reference to equation 4.1.13 and 4.1.16, in section 4.1.3 and 4.1.4, increasing the propelling nozzle area of the engine increases the turbine pressure ratio as well the temperature drop of the turbine. Therefore, the nozzle pressure ratio is reduced and the turbine power is increased. Figure 4.34 shows the thrust of the engine with standard and scaled nozzle area. The increased nozzle and the standard nozzle engines are compared. The percentage difference attained is between 8% and 13%. Figure 4.35 shows the EGTs of the baseline nozzle engine and the engine with scaled nozzle area. Differences in the range of 0.3% to 25% are obtained for the EGTs. The increased nozzle area showed lower exhaust gas temperature at a speed of 120 krpm.

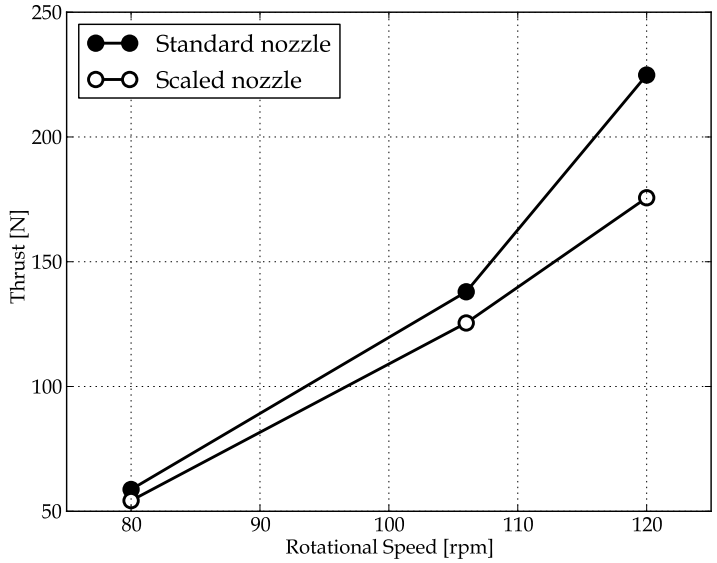

Figure 4.34: Thrust for original BMT and scaled nozzle.

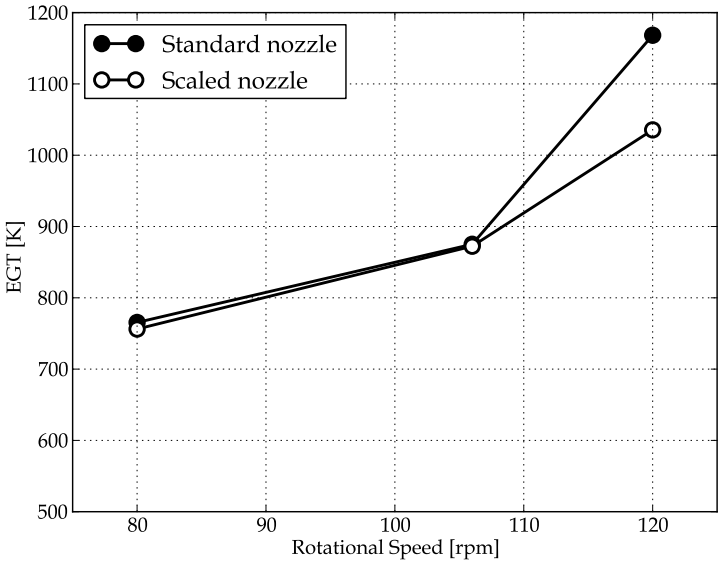

Figure 4.35: EGTs for original BMT and scaled nozzle.

4.6 Closing Remarks

The analytical and numerical procedures used for the BMT engine performance evaluations were discussed in this chapter. The sensitivity and component matching of the various compressor and turbine stages were investigated for the BMT engine. GasTurb and Flownex SE were used as numerical simulating tools for modelling the engine performance. A one-dimensional analytical calculation was also performed to study the thermodynamic characteristic behaviour of the engine. The numerical results of the different performance investigations were compared to the experimental data sets. The performance analysis showed that satisfactory matching of the engine depends on the turbine and the propelling nozzle characteristics. The baseline BMT engine simulated thrust showed a consistent trend with the experimental test results and the available BMT data.

The EGTs were underpredicted by the experimental test in comparison with the simulation EGTs. This might due to hot or cold spots in the exhaust gases or non-uniform distribution of the exhaust gases at the engine exhaust. The modified compressor stages by De Villiers (2014) and Burger (2016) were modelled with the standard BMT turbine and the different turbines designed by Basson (2014). The various performance maps published by these authors were input into the Flownex program for the engine performance investigation. It was observed that the engine arrangement using De Villiers's compressor stage operates at higher turbine inlet and exhaust temperatures and low mass flow rates.

Burger's compressor with the BMT turbine engine configuration predicted insufficient turbine power at high rotational speeds. An attempt to increase the turbine power by adding more fuel to the combustion system in order to increase the turbine power resulted in excessive turbine inlet and exhaust gas temoeratures. This resulted in choking and under-expansion of the exhaust gases in the propelling nozzle. The authors experienced high temperatures during their experimental test which prevented them from testing the engine at the design point speed. The turbine and the propelling nozzle area of the engine were also varied to look for possible improvements in the engine performance. The thrust of the engine reduced upon increasing the engine nozzle area. The simulations that made use of both increased turbine and propelling nozzle area's provided sufficient turbine power to drive Burgers's compressor at an acceptable exhaust gas temperature at high rotational speed.

Chapter 5

Turbine Mean-Line Design

A mean-line turbine design performance analysis was performed for the turbine stage of the engine based on Burger's thermodynamic compressor stage parameters at the design point. The objective was to improve the load and flow coefficients of the turbine to investigate the possibilities of engine performance gains. New turbine maps were developed and simulated with Burger's compressor to evaluate the performance of the engine. Figure 5.1 shows the mean-line design (MLD) procedure.

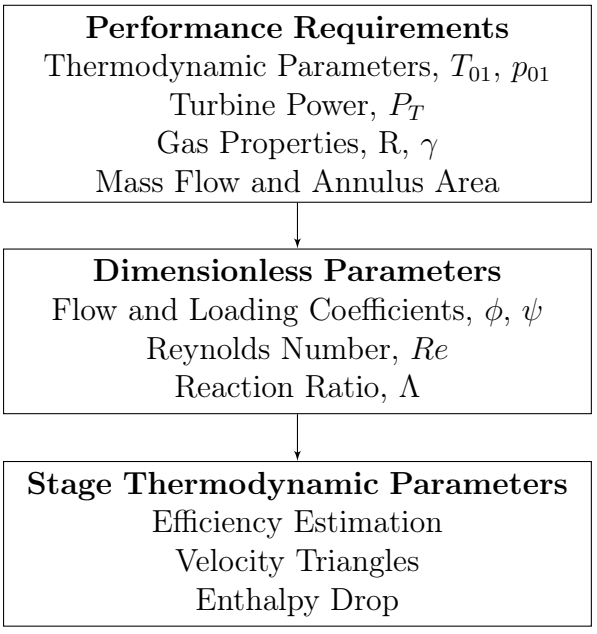

Figure 5.1: Preliminary turbine design procedure.

The MLD performance analysis is undertaken to predict the isentropic total-to-total efficiency, the velocity triangles, rotational speed and the annulus size of the turbine. The mean-line estimation of the turbine stage performance parameters did not only consider the stage efficiencies, enthalpies, pressures and temperatures but also accounted for the pressure losses in the nozzle and the rotor blade. The turbine power and the rotational speed are usually fixed by the GT compressor. The turbine stage mass flow rate, inlet temperature and pressure are predetermined by the combustion process. The turbine stage is assumed to be a normal stage therefore the inlet flow angle is assumed to be negligible and same as the turbine rotor outlet flow angle due to the absence of swirl flow at the outlet. Table 5.1 details the turbine stage requirements for the mean-line analysis (MLA).

Table 5.1: Turbine design performance parameters.

Name of Parameter	Value	Unit
Mass flow rate	0.331	kg/s
Rotational speed	120 000	rpm
Turbine inlet temperature	1200	K
Turbine inlet total pressure	390.03	kPa
Turbine power	64.11	kW
Hub radius	0.0235	m
Shroud radius	0.0315	m
Turbine inlet flow angle	0	degrees

5.1 Calculation of Design Parameters

To solve for turbine performance outputs, the dimensionless parameters of the stage have to be computed or known. The dimensionless variables govern the performance of the turbine. These quantities determine the shape of the stage velocity triangles and the flow directions. The stage work and pressure losses are highly dependent on these parameters. The most influential of these variables are the flow and power coefficient. In order to estimate the dimensionless parameters, the annulus area and the axial velocity at the turbine inlet must be known. Since the axial velocity is not known, an iteration process is used to compute the velocity. With a known inlet temperature and pressure, an initial estimate is found for the density at the turbine inlet. Using the density, mass flow rate and the annulus area, the initial axial velocity is calculated. Knowing the turbine hub and shroud radius, the annulus area is expressed as:

$$A_1 = \pi(r_s^2 - r_h^2) \tag{5.1.1}$$

The density at the inlet of the stage is computed using the stagnation temperature and pressure at the inlet. This gives an estimation of the static density at the inlet. After computing the actual static temperature with the actual axial velocity via an iteration procedure, the actual density is determined. The density is calculated as:

$$\rho_1 = p_1/RT_1 \tag{5.1.2}$$

The axial velocity and static temperature are computed using the equation:

$$C_a = \dot{m}_g/\rho_{01}A_1 \tag{5.1.3}$$

$$T_1 = T_{01} - \frac{C_a^2}{2c_{pg}} \tag{5.1.4}$$

To calculate the turbine stage flow coefficient, the turbine blade velocity at the mean radius must be used. The blade rotational velocity is computed using the given formula:

$$U = \frac{\pi N r_m}{30} \tag{5.1.5}$$

The turbine flow and work coefficient and the degree of reaction are determined as follows:

$$\phi = C_a/U \tag{5.1.6}$$

$$\psi = \frac{P_T/\dot{m}}{U^2} \tag{5.1.7}$$

$$\Lambda = (1 - \psi/2 + \phi \tan \alpha_1) \tag{5.1.8}$$

With α_1 set as zero, the degree of reaction reduces to:

$$\Lambda = (1 - \psi/2) \tag{5.1.9}$$

5.2 Velocity Vectors and Triangles

As mentioned in section 5.1 the flow and the work coefficient determines the shape and direction of flow in the turbine stages. Figure 5.2 depicts the turbine stage velocity triangle and vectors.

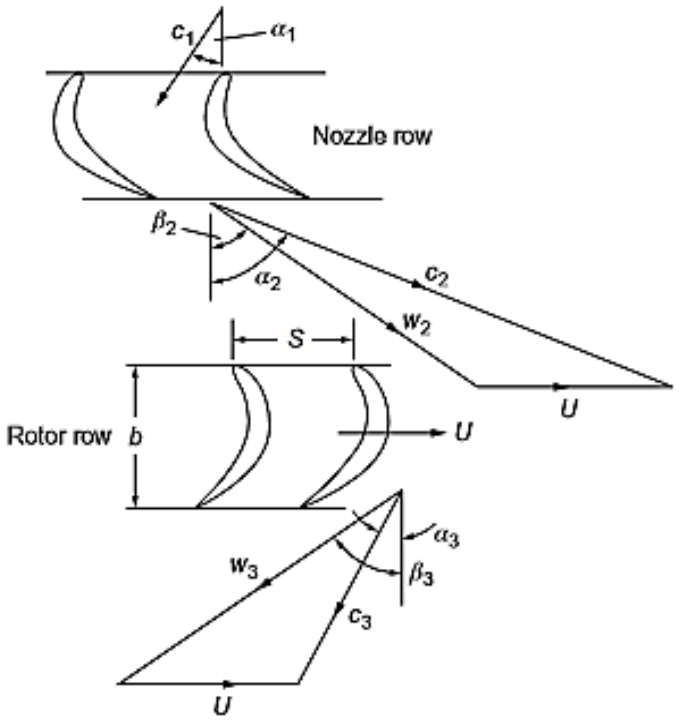

Figure 5.2: Turbine stage velocity triangle, (Dixon and Hall, 2013).

The flow angles and the velocity vectors from the stator to the rotor are computed using the dimensionless parameters as follows:

$$\alpha_2 = \arctan\left(\frac{\psi/2 - \Lambda + 1}{\phi}\right) \tag{5.2.1}$$

$$\beta_2 = \arctan\left(\frac{\psi/2 - \Lambda}{\phi}\right) \tag{5.2.2}$$

$$\beta_3 = \arctan\left(\frac{\psi/2 + \Lambda}{\phi}\right) \tag{5.2.3}$$

The gas velocities at the stator outlet and the rotor inlet and outlet are then determined as:

$$C_2 = U\sqrt{\phi^2 + (\psi/2 + 1 - \Lambda)^2} \tag{5.2.4}$$

$$C_3 = U\sqrt{\phi^2 + (\psi/2 + \Lambda - 1)^2} \tag{5.2.5}$$

Similarly, the relative and the swirl velocities at the stator and rotor are calculated using the design parameters. The stator and rotor loss coefficients are calculated using the deflection angles. The stator and rotor deflection angles are determined as:

$$\varepsilon_S = \alpha_1 + \alpha_2 \tag{5.2.6}$$

$$\varepsilon_R = \beta_2 + \beta_3 \tag{5.2.7}$$

With the deflection angles known, the loss coefficients of the stator and the rotor are then calcualted (Sayers, 1990).

$$\xi_S = 0.04 + 0.06(\varepsilon_S/100)^2 \tag{5.2.8}$$

$$\xi_R = 0.04 + 0.06(\varepsilon_R/100)^2 \tag{5.2.9}$$

Using the rotor inlet or stator outlet absolute velocity the static temperature and pressure at the rotor inlet is calculated.

$$T_2 = T_{02} - \frac{\xi_S C_2^2}{2c_{pg}} \tag{5.2.10}$$

$$p_2 = p_{02}\left(\frac{T_2}{T_{02}}\right)^{\frac{\gamma}{\gamma-1}} \tag{5.2.11}$$

The temperature drop over the stage is used to determine the outlet temperature and pressure of the rotor.

$$\Delta T_{os} = \frac{\psi U^2}{c_{pg}} \tag{5.2.12}$$

Knowing the temperature drop through the stage the stagnation and static temperature at the rotor outlet are expressed as:

$$T_{03} = T_{01} - \Delta T_{os} \tag{5.2.13}$$

$$T_3 = T_{03} - \frac{\xi_R C_3^2}{2c_{pg}} \tag{5.2.14}$$

The stagnation efficiency of the turbine stage is then calculated using the dimensionless parameters of the turbine.

$$\eta_{tt} = \frac{1}{1 + 1/2\psi[(\phi^2 + \psi^2)\xi_S + (\phi^2 + 1)\xi_R]} \tag{5.2.15}$$

The stage total-total pressure ratio is determined using η_{tt}, ΔT_{os} and T_{01}.

$$TPR_{tt} = \frac{1}{(1 - (\Delta T_{os}/\eta_{tt} T_{01}))^{\frac{\gamma}{\gamma - 1}}} \tag{5.2.16}$$

The power delivered by the turbine is calculated as:

$$P = \dot{m} U (C_{\theta 2} + C_{\theta 3}) \tag{5.2.17}$$

5.3 Turbine Stage Calculations

The stages performance parameters calculation includes the stator and rotor blade calculations. Figure 5.3 details the calculation routine for the estimation of the stage performance parameters. Detailed calculations of the stage operational output quantities are presented in Appendix B.

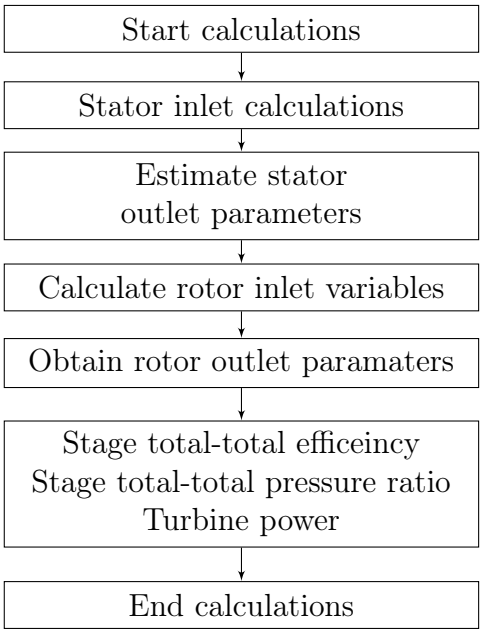

Figure 5.3: Stage calculation process.

5.4 Turbine Maps

Turbine maps can either be generated from mean-line, through flow analysis or the scaling method. When the component maps of an engine are not known, scaling method can be applied to change data from a known component maps into other characteristic maps. Using a similar approximation, the mean-line performance parameters were used to scale the existing BMT maps and Basson's turbine stage characteristic maps. The application of this method to obtain the characteristic maps of Basson's turbines are shown in Appendix B. The scaling equations (Gilani *et al.*, 2008) used to establish the performance maps are given as follows:

$$TPR = \left(\frac{TPR_{des} - 1}{TPR_{map,des}}\right)(TPR_{map} - 1) + 1 \tag{5.4.1}$$

$$\dot{m} = \left(\frac{\dot{m}_{des}}{\dot{m}_{map,des}}\right)\dot{m}_{corr,map} \tag{5.4.2}$$

$$\eta_{isen} = \left(\frac{\eta_{des}}{\eta_{map,des}}\right)\eta_{map} \tag{5.4.3}$$

Figures 5.4 and 5.5 illustrate the relationship between the scaled map and the mean-line design value. The MLD value of the re-designed turbine compares well with the scaled map. The scaled maps were introduced into the Flownex environment for performance modelling to ascertain whether the engine characteristic will show improved performance.

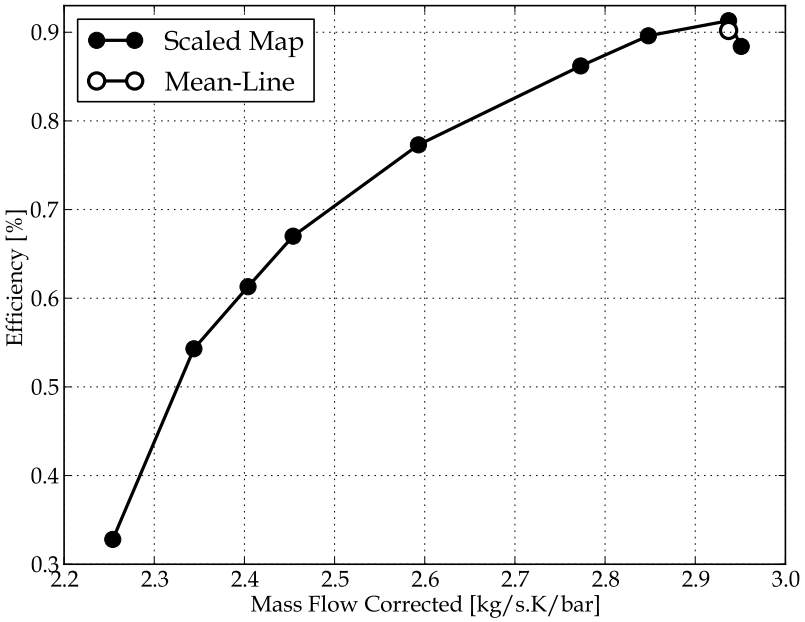

Figure 5.4: Efficiency vs corrected mass flow rate.

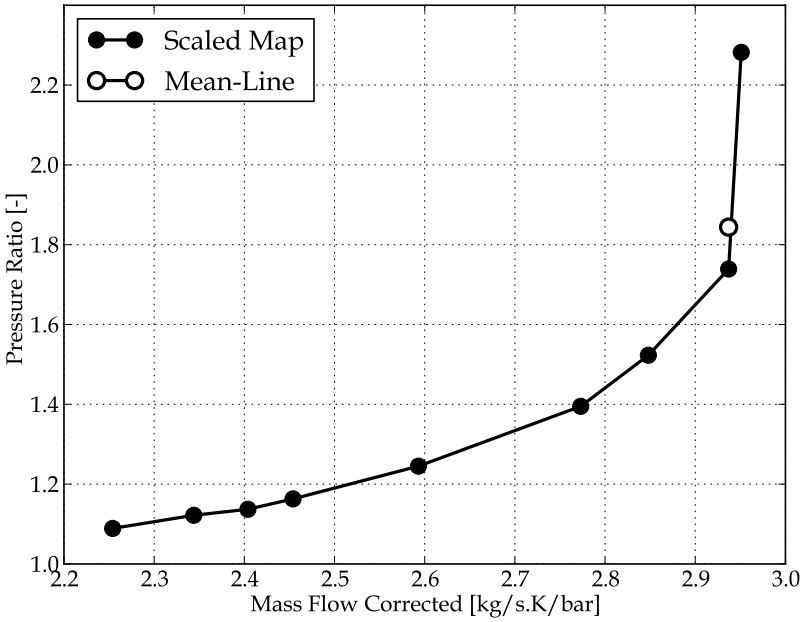

Figure 5.5: Pressure ratio vs corrected mass flow rate.

5.5 Results

The performance outputs of the stage mean-line analysis and the Flownex numerical results of the engine with the modified turbine and Burger's com-

pressor are presented in this section. The simulation of the MGT with the new turbine maps showed that increasing the load and flow coefficient of the turbine has the potential of increasing the turbine power and hence the performance of the engine. Table 5.2 depicts the results provided by the turbine mean-line evaluation.

Table 5.2: Mean-line results.

Name of Parameter	Value	Units
Total-to-total Pressure Ratio	1.834	-
Total-to-total Isentropic Efficiency	0.902	%
Flow Coefficient	0.611	-
Loading Coefficient	1.622	-
Degree of Reaction	0.189	-
Rotor Inlet Flow Angle (α_2)	69.34	Degrees
Rotor Inlet Blade Angle (β_2)	45.49	Degrees
Rotor Outlet Blade Angle (β_3)	58.55	Degrees

Burger's (2016) extrapolation predicted a thrust value of 220 N while the simulation for the new turbine with Burger's compressor predicted a thrust of 188 N for good matching of the engine at the design speed. Figure 5.6 and 5.7 describe the performance of the BMT engine with the modified turbine and the old BMT turbine using Burger's compressor stage. A percentage difference between 1% and 17% were obtained for the thrust of the engine. The modified turbine predicted lower thrust value at the design point compared to the old turbine but with sufficient turbine power at a reasonable fuel flow rate to drive the engine compressor. As shown in Figure 5.7, the modified turbine stage predicted lower exhaust gas temperature values compare to the old turbine. A temperature difference in the range of 40 K to 175 K was established for the exhaust gas temperature.

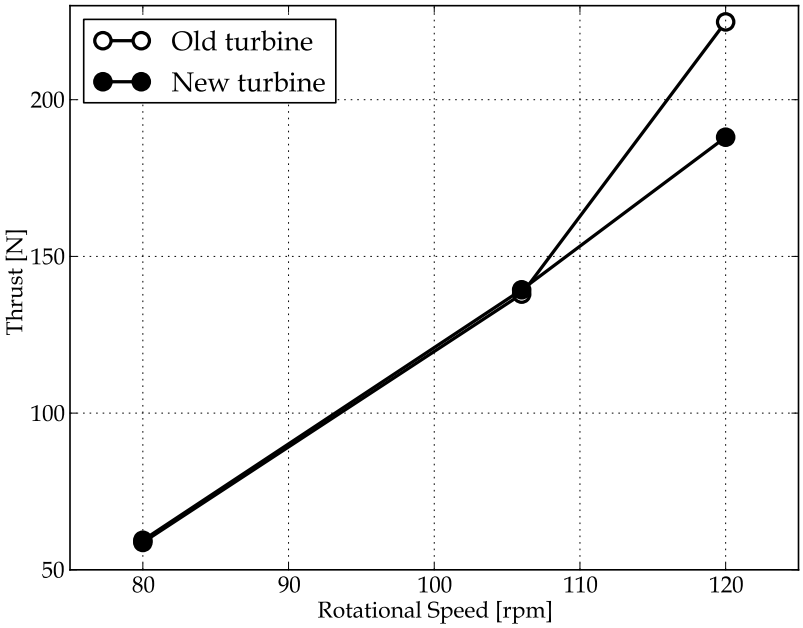

Figure 5.6: BMT thrust performance.

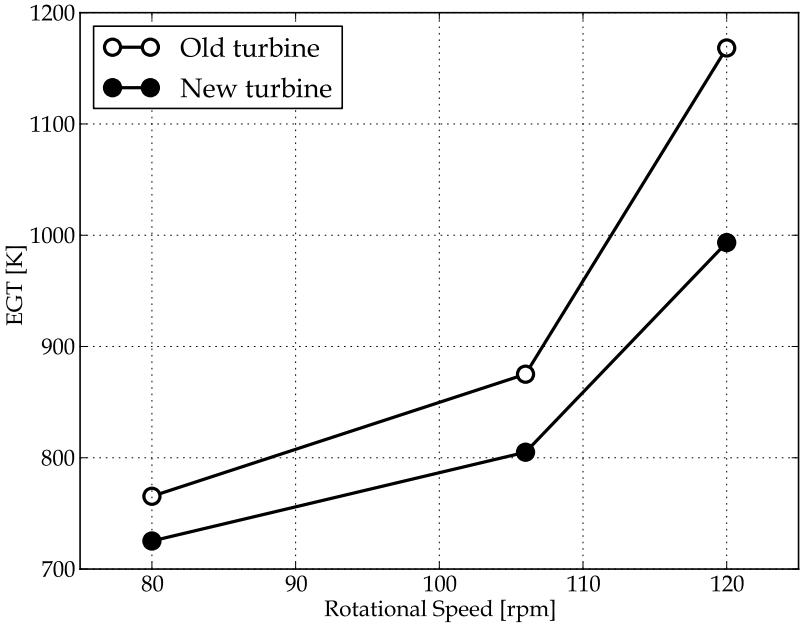

Figure 5.7: BMT EGT performance.

5.6 Closing Remarks

The turbine mean-line performance analysis was discussed in this chapter. This involved computation of the design parameters which dictates the performance

of the turbine stage. The scaling method of generating characteristic maps from existing engine turbine maps using the mean-line operating parameters is also presented. The mean-line analysis predicted high load and flow coeficients compared to the load and flow coefficients used by Basson (2014). A low degree of reaction value was estimated by the mean-line analysis. The higher the stage load coefficient, the lower the value of degree of reaction and the less the pressure drop in the turbine rotor. Therefore, the tangential velocity of the flow through the blades is increased and reduces the flow acceleration in the rotor.

The simulation results for the scaled characteristic maps showed improvement in the engine performance. The new turbines showed that with improved load and flow coefficient, the turbine power is isufficiently enhanced so as to provide sufficient power to drive the engine compressor. The modified turbine simulation predicted a thrust lower than the thrust predicted by the old BMT turbine at the design point but with sufficient turbine power require to drive the engine compressor. A percentage difference in the range of 1% to 17% and a temperature difference between 40 K and 175 K were obtained for the engine thrust and EGTs.

Chapter 6

Discussion, Conclusions and Recommendations

6.1 Discussions

To enhance the performance of a micro gas turbine, each engine component should be efficient to provide the required mass flow and generate the required power to drive the engine with minimum fuel input. Furthermore, having knowledge of the operating characteristics of the engine elements facilitates matching of the engine components and the potential of predicting the operating range and improving engine performance.

It was observed that the EGTs measured from the two exhaust temperature probes of the experimental test showed a large difference. Based on the discussions presented in chapter 3, it was decided to use the results from the thinner probe for future comparisons. The turbine inlet temperature also recorded low temperatures compared to the available engine turbine inlet temperature. The turbine inlet temperature is affected by non-uniform radial and circumferential temperature profile as well as radiation heat losses present at the turbine inlet and therefore the turbine inlet temperature is not considered realiable.

Performance modelling of the engine with the baseline engine turbine stage and the modified compressor stages exhibited insufficient turbine power to drive

the compressor. It was evident that the modified compressors have high power and need a turbine with a similar power to drive it. The addition of an extra mass of fuel into the combustion unit in order to increase the turbine inlet temperature to raise the turbine power generates excessive turbine inlet and exhaust temperatures without increasing the mass flow rate of air through the engine.

In practice, this excessive temperature is detrimental to the integrity of the MGT's turbine material. Consequently, to increase the TIT to higher temperature limits, the turbine material needs to be investigated and improved. Larger axial turbines use bleed air from the compressor which circulates through air channels in the turbine blades to cool them (Farokhi, 2014). MGTs do not apply these cooling techniques, and are therefore vulnerable to high temperatures. The material used to manufacture MGT turbine blades is Inconel IN713LC, a nickel-based super-alloy. Figure 6.1 shows the characteristic behaviour of Inconel IN 713 LC. As shown in the figure, the material strength decrease under high temperatures. Therefore, limiting the turbine inlet temperatures to a maximum between 1000 K and 1100 K is likely to give better operating performance and minimum risk to the turbine blades.

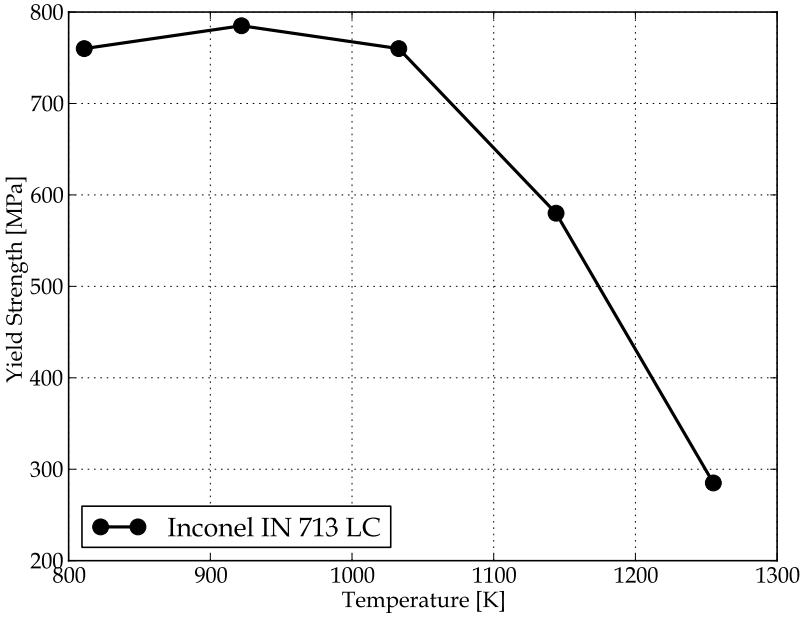

Figure 6.1: Effects of temperature on the yield strength of Inconel IN 713 LC, (Basson, 2014).

Increasing the turbine flow area of the engine to ensure satisfactory performance showed that it requires the area of other expansion units to be increased. Varying the turbine area has the tendency to increase the engine thrust but does not improve the power output of the turbine at lower input temperatures.

The engine propelling nozzle area was adjusted to study its effects on engine output. When the propelling nozzle area is increased the non-dimensional mass flow through the turbine is also increases and hence the turbine pressure ratio increases. This then reduces the nozzle pressure ratio and fixes the engine operating line to produce satisfactory turbine power. The engine output thrust is reduced by increasing the nozzle area. The numerical simulation showed that further increases in the nozzle area beyond a certain percentage redefines the compressor operating point and subsequently decreases the engine compressor pressure ratio and efficiency.

The turbine mean-line analysis predicted high flow and load coefficients. Increasing the load and flow coefficient of an MGT turbine design can increase the turbine power but reduces the efficiency for a given engine frontal area. For jet engines, a minimum weight and small frontal area are considered important, unlike industrial gas turbines (Cumpsty, 2003). Therefore, high flow and load coefficients give a shorter compact turbine but with reduced efficiency (Sayers, 1990). The degree of reaction of the turbine was quite low which implies low turbine rotor pressure loss. The degree of reaction defines the static pressure loss in the rotor with respect to the turbine stage static pressure loss and influences the turbine efficiency. A low degree of reaction value is associated with high stage loading coefficient.

In conclusion, the engine performance modelling showed that for accurate matching of the BMT engine, the turbine stage power should match the power required by the compressor. The new turbine simulations in chapter 5 also showed that with improved turbine performance parameters, the turbine can generate sufficient power to drive the compressor. Therefore, the turbine stage performance should be considered when re-designing new compressor stages for the engine.

6.2 Conclusion

The performance assessment of the BMT 120 KS engine using the component matching method was undertaken in this thesis. Using both analytical and numerical calculations, a parametric and component sensitivity analysis was performed for the engine with the different engine elements. The results from the project could give prior information for the design and matching of the BMT engine components for satisfactory operation.

The project presented a detailed overview on MGTs in chapter two. Research efforts that have been performed to improve the performance output of micro gas turbine engines were explored. The various existing GT performance

modelling and simulation methods used to effectively and efficiently predict the operating range of gas turbines were also covered. The advantages and disadvantages of the linear and non-linear modelling and computation methods with regards to a gas turbine's effective operation were explored and discussed.

Chapter three provided the experimental procedure and operational performance data measurements of the BMT baseline engine. The calibration and data acquisition from the measuring instruments were discussed. The outcomes of the experiment showed consistent trends with the available BMT engine data although the turbine inlet and exhaust temperature measurements of the engine showed wide discrepancies. Good correlation was established between the engine thrust performance and mass flow rate sets of data.

In chapter four, the engine cycle analysis was described. A detailed hand cycle analytical calculation was performed as a benchmark for the BMT thermodynamic cycle investigations. Using GasTurb and Flownex simulation programs the baseline BMT engine operational characteristics were evaluated at the on-design and off-design operating points. Further analysis was carried out with Flownex SE to study component matching of the various engine constituents using established performance maps of the components. This involved a matching analysis of the baseline engine elements and the re-designed compressor and turbine stages of the engine. It was observed from the sensitivity evaluation results that the engine experiences high EGTs at high speeds when employing the baseline engine turbine and the modified compressor stages. The turbine area of the baseline engine was increased to find the performance gain possibilities of the engine. The results disclosed that variation of the turbine characteristic area does not influence the engine turbine power at lower inlet temperature. The propelling nozzle of the engine was altered to modulate the turbine power of the engine. With an increase in the nozzle area the engine provided adequate turbine power to drive the compressor at a reduced fuel flow rate at acceptable EGTs and thrusts.

A turbine mean-line performance analysis of the baseline BMT engine based on Burger's compressor design point parameters was detailed in chapter five of the study. The mean-line parameters were used to scale the existing engine turbine maps for further performance modelling and simulation in Flownex SE. The generated scaled map showed a good trend with the engine turbine characteristic maps and other performance maps in literature. The simulated results with the modified BMT turbine map showed good improvement of the engine turbine power, thrust and EGTs. The new turbine simulations predicted that the engine can generate a thrust of approximately 190 N for accurate matching of the engine components.

6.3 Recommendation for Future Work

The main objective of the thesis was to evaluate the performance of the BMT 120 KS engine by assessing the causes of high fuel consumption and high exhaust and turbine temperatures and the engine's inability to reach the design speed with the re-designed compressor stages.

The various engine studies demonstrated that increasing the engine propelling nozzle area has the potential of increasing the engine turbine power and hence reducing the effects of high fuel consumption. Consequently, it is suggested that the engine propelling nozzle area should be adjusted to modulate the turbine power. In conjunction with this, the experimental test rig engine should be fitted with an elongated variable converging nozzle area for further study of the engine's performance.

It was evident from the sensitivity matching analysis that the modified compressors have a high power requirement and therefore requires a turbine that can produce power to match the compressor's power demand. The turbine stage of the engine should be designed with improved load and flow coefficients. Both an emperical and CFD turbine design with improved power and flow coefficients should be performed. The measurement of engine EGT's should be further investigated using radiative shielded thermocouples.

The EGTs showed different temperature readings which might be due to hot or cold areas in the exhaust gases. The presence of hot or cold areas in the exhaust gases could be probably due to the un-equal mixing of air and fuel in the combustor. Therefore, the engine combustion chamber performance should be modelled using CFD in order to establish whether there are indeed hot or/and cold areas in the exhaust gases.

Appendices

Appendix A

BMT Engine Analytical Calculations

A.1 Assumptions

1. Free vortex flow (Conservation of angular momentum)
2. Adiabatic work done
3. Half the pressure loss occurs in the diffuser and the other half in the impeller.

A.2 Compressor Inlet

The calculations are iterated. The annulus area of the compressor is determined using the hub and shroud radius at the impeller inlet.

$$A = \pi(r_s^2 - r_h^2) = 0.00188 \text{ m}^2 \tag{A.2.1}$$

Knowing the atmospheric pressure and temperature the density at the inlet of the engine can be calculated. The engine is a test rig or stationary engine, hence the free stream conditions are equal to the engine inlet stagnation properties. The Mach number and the free stream velocity of the engine are negligible in this instance. The density is found using the relation:

$$\rho_2 = \frac{p_2}{RT_2} = 1.12503 \text{ kg/m}^3 \tag{A.2.2}$$

An initial estimate of the velocity is calculated using the calculated density. The actual velocity as well as the actual static density, pressure and temperature are calculated making use of an iteration procedure. The following set of equations is used to determined the parameters.

$$C_2 = \frac{\dot{m}_a}{\rho_2 A_2} = 136.170 \text{ m/s} \tag{A.2.3}$$

$$T_2 = T_{02} - \frac{C_2^2}{2c_p} = 278.774 \text{ K} \tag{A.2.4}$$

$$p_2 = p_{01}\left(\frac{T_2}{T_{02}}\right)^{\frac{\gamma}{\gamma-1}} = 90.122 \text{ kPa} \tag{A.2.5}$$

$$M_2 = \frac{C_2}{\sqrt{\gamma RT_2}} = 0.4068 \tag{A.2.6}$$

A.3 Impeller Outlet

To compute the impeller outlet performance quantities the impeller blade velocity and flow area have to be known or determined. The blade velocity and area are computed as:

$$U = \frac{\pi r_{2'} N}{30} = 439.822 \text{ m/s} \tag{A.3.1}$$

$$A_{2'} = 2\pi r_{2'} b = 0.001319 \text{ m}^2 \tag{A.3.2}$$

The velocities and the temperatures, as well as the pressures at the impeller outlet, are calculated using the outlined equations.

$$C_{\theta 2'} = U - C_{r2'} \tan \beta_{2'} = 368.432 \text{ m/s} \tag{A.3.3}$$

$$C_{2'} = \sqrt{C_{\theta 2'}^2 + C_{r2'}^2} = 388.0070 \text{ m/s} \tag{A.3.4}$$

$$T_{02'} = T_{02'} - \frac{U_2 C_{\theta 2'}}{c_p} = 425.2562 \text{ K} \tag{A.3.5}$$

$$T_{2'} = T_{02'} - \frac{C_2^2}{2c_p} = 350.3560 \text{ K} \tag{A.3.6}$$

The impeller outlet ratio, static pressure and density are denoted by:

$$p_{2'} = \frac{p_{02'}}{p_{02}} \frac{p_{2'}}{p_{02'}} p_{02} = 180.3657 \text{ kPa} \tag{A.3.7}$$

$$\rho_{2'} = \frac{p_2}{RT_{2'}} = 1.79375 \text{ kg/m}^3 \tag{A.3.8}$$

$$M_{2'} = \frac{C_2}{\gamma R T_{2'}} = 1.0341 \tag{A.3.9}$$

Due to the assumption of adiabatic flow in the diffuser the stagnation temperature at the impeller represents the total compressor stage temperature. Hence the total-to-total compressor stage efficiency is found as:

$$\eta_c = \frac{T_{02}(CPR^{\frac{\gamma-1}{\gamma}} - 1)}{T_{02'} - T_{02}} = 0.81498 \tag{A.3.10}$$

Assuming that half pressure loss occurs in the impeller and the other half in the diffuser the impeller efficiency is given by:

$$\eta_{imp} = [1 - 0.5(1 - \eta_c)] = 0.90749 \tag{A.3.11}$$

$$IPR = [1 + \eta_{imp}(T_{02'}/T_{02} - 1)]^{\frac{\gamma}{\gamma-1}} = 3.5182 \tag{A.3.12}$$

A.4 Diffuser Leading Edge

The diffuser leading edge parameters were calculated using the following equations.

$$A_{din} = 2\pi r_{din} b_{din} = 0.001487 \text{ m}^2 \tag{A.4.1}$$

$$C_{\theta din} = \frac{C_{\theta 2'} r_2}{r} = 348.5174 \text{ m/s} \tag{A.4.2}$$

$$C_{din} = \sqrt{C_{\theta din}^2 + C_{rdin}^2} = 363.3112 \text{ m/s} \tag{A.4.3}$$

$$T_{din} = T_{02} - \frac{C_d^2 in}{2c_p} = 359.6026 \text{ K} \tag{A.4.4}$$

$$p_{din} = \frac{p_{din}}{p_{0din}} \frac{p_{0din}}{p_{01}} p_{01} = 197.558 \text{ kPa} \tag{A.4.5}$$

$$\rho_{din} = \frac{p_{din}}{RT_{din}} = 1.8862 \text{ kg/m}^3 \tag{A.4.6}$$

$$C_{rdin} = \frac{\dot{m}}{\rho_{din} A_{din}} = 102.6189 \text{ m/s} \tag{A.4.7}$$

A.5 Diffuser throat

In order to compute the compressor diffuser thermodynamic quantities, the following relations were used.

$$A_{th} = 2\pi r_{th} b_{th} = 0.001608 \text{ m}^2 \tag{A.5.1}$$

$$C_{\theta th} = \frac{C_{\theta 2} r_2}{r} = 322.3786 \text{ m/s} \tag{A.5.2}$$

$$C_{th} = \sqrt{C_{\theta th}^2 + C_{rth}^2} = 334.1988 \text{ m/s} \tag{A.5.3}$$

$$T_{th} = T_{02} - \frac{C_{th}^2}{2c_p} = 369.7052 \text{ K} \tag{A.5.4}$$

$$p_{th} = \frac{p_{th}}{p_{0th}} \frac{p_{0th}}{p_{01}} p_{01} = 217.6754 \text{ kPa} \tag{A.5.5}$$

$$\rho_{th} = \frac{p_{th}}{RT_{th}} = 2.03243 \text{ kg/m}^3 \tag{A.5.6}$$

$$C_{rth} = \frac{\dot{m}}{\rho_{th} A_{th}} = 88.0957 \text{ m/s} \tag{A.5.7}$$

A.6 Diffuser Trailing Edge

Using the same iteration procedure used in the previous sections the diffuser trailing edge parameters were determined as follows.

$$A_{dout} = 2\pi r_{dout} b_{dout} - n t_v b_{dout} = 0.001365 \text{ m}^2 \tag{A.6.1}$$

$$C_{dout} = \frac{C_{rth}}{\cos \alpha_{dout}} = 88.2686 \text{ m/s} \tag{A.6.2}$$

$$T_{dout} = T_{02} - \frac{C_{dout}^2}{2c_p} = 421.3955 \text{ K} \tag{A.6.3}$$

$$p_{dout} = \frac{p_{dout}}{p_{0dout}} \frac{p_{0dout}}{p_{01}} p_{01} = 308.1154 \text{ kPa} \tag{A.6.4}$$

$$\rho_{dout} = \frac{p_{dout}}{RT_{dout}} = 2.5402 \text{ kg/m}^3 \tag{A.6.5}$$

$$C_{rdout} = \frac{\dot{m}}{\rho_{dout} A_{dout}} = 82.9980 \text{ m/s} \tag{A.6.6}$$

A.7 Combustor

The combustion chamber describes the heat addition process of the engine thermodynamic cycle. The process is expressed using an energy and mass balance equation. Using this principle the maximum engine cycle temperature is determined as:

$$T_{04} = T_{03} + \frac{f \eta_b HV}{c_{pg}} = 984.8898 \text{ K} \tag{A.7.1}$$

The combustion outlet or the turbine inlet pressure is computed as:

$$p_{04} = p_{03}(1 - \Delta p) = 286.335\text{kPa} \tag{A.7.2}$$

The corresponding static pressure and temperature are determined as:

$$T_4 = T_{04} - \frac{C_4^2}{2c_{pg}} = 977.6539 \text{ K} \tag{A.7.3}$$

$$p_4 = p_{04}\left(\frac{T_4}{T_{04}}\right)^{\frac{\gamma_g}{\gamma_g - 1}} = 278.0125 \text{ kPa} \tag{A.7.4}$$

A.8 Turbine and Nozzle

Taking into account the mechanical efficiency and using the turbine isentropic efficiency the total pressure and the temperature at the turbine outlet can be related by the following equation.

$$T_{05} = T_{04} - \frac{\dot{m}_a c_p}{\dot{m}_g \eta_m c_{pg}}(T_{03} - T_{02}) = 864.2626 \text{ K} \tag{A.8.1}$$

$$p_{05} = p_{04}\left[1 - \frac{(1 - T_{05}/T_{04})}{\eta_T}\right]^{\frac{\gamma_g - 1}{\gamma_g}} = 153.6680 \text{ kPa} \tag{A.8.2}$$

With a known stagnation and static temperature at the nozzle outlet the velocity of the exhaust gases is represented as:

$$u_e = \sqrt{2c_{pg}(T_{08} - T_8)} = 444.5730 \text{ m/s} \tag{A.8.3}$$

A.9 Performance Parameters

The engine output thrust and specific fuel consumption are determined using the given equation.

$$F_{net} = \dot{m}_a u_e = 128.0370 \text{ N} \tag{A.9.1}$$

$$SFC = \frac{\dot{m}_f}{F_{net}} = 37.2548 \text{ g/kNs} \tag{A.9.2}$$

Appendix B

Turbine Mean-Line Calculations

The turbine mean-line properties are mathematically formulated using the equations discussed below. An iteration procedure is used to compute the parameters. With a known turbine hub and shroud radius, the annulus area of the turbine at the mean radius is calculated

$$A = \pi(r_s^2 - r_h^2) = 0.0013823 \text{ m}^2 \tag{B.0.1}$$

Using the atmospheric pressure and temperature, an initial estimate is determined for the static density at the turbine inlet in order to calculate the axial velocity of the flow into the turbine.

$$\rho_1 = \frac{p_1}{RT_1} = 1.1333 \text{ kg/m}^3 \tag{B.0.2}$$

Having computed the density of the flow, the axial velocity is then calculated as:

$$C_a = \frac{\dot{m}_g}{A\rho_1} = 211.29 \text{ m/s} \tag{B.0.3}$$

Knowing the estimated axial velocity, the static temperature and pressure at the stator inlet are determined. Using an iteration process, the actual velocity and static condition at the inlet are evaluated.

$$T_1 = T_{01} - \frac{C_a^2}{2c_{pg}} = 1180.55 \text{ K} \tag{B.0.4}$$

$$p_1 = p_{01}\left(\frac{T_1}{T_{01}}\right)^{\frac{\gamma_g}{\gamma_g - 1}} = 383.97 \text{ kPa} \tag{B.0.5}$$

In order to calculate the dimensionless parameters the rotational velocity of the turbine has to be known or determined. The blade speed is expressed as:

$$U = \frac{\pi r_m N}{30} = 345.57 \text{ m/s} \tag{B.0.6}$$

Using the blade speed and the axial velocity of the flow through the turbine the flow coefficient of the turbine is found as:

$$\phi = \frac{C_a}{U} = 0.611 \tag{B.0.7}$$

With the known power or specific work of the turbine and the blade rotational velocity the loading coefficient of the turbine is determined. The power coefficient can also be evaluated using the temperature drop through the stage and the specific heat of hot air.

$$\psi = \frac{P_T/\dot{m}}{U^2} = 1.622 \tag{B.0.8}$$

The turbine degree of reaction combines the blade loading and flow coefficient as well as the flow angle at the inlet of the turbine. A normal stage was assumed for the turbine hence the flow angle of the turbine was assumed to be negligible. Using these quantities the degree of reaction is computed from the relation:

$$\Lambda = (1 - \psi/2 + \phi \tan \alpha_1) = 0.189 \tag{B.0.9}$$

The flow directions or the velocity triangles are then calculated using the following equations

$$\alpha_2 = \arctan\left(\frac{\psi/2 - \Lambda + 1}{\phi}\right) = 69.34^\circ \tag{B.0.10}$$

$$\beta_2 = arctan\left(\frac{\psi/2 - \Lambda}{\phi}\right) = 45.49^\circ \tag{B.0.11}$$

$$\beta_3 = arctan\left(\frac{\psi/2 + \Lambda}{\phi}\right) = 58.55^\circ \tag{B.0.12}$$

The non-dimensional velocities at the stator to the rotor are then calculated using the these equations.

$$C_2 = U\sqrt{\phi^2 + (\psi/2 + 1 - \Lambda)} = 599.01 \text{ m/s} \tag{B.0.13}$$

$$W_{\theta 2} = U(\psi/2 - \Lambda) = 301.39 \text{ m/s} \tag{B.0.14}$$

$$C_{\theta 2} = U(\psi/2 + 1 - R) = 560.51 \text{ m/s} \tag{B.0.15}$$

The deflection angles at the stator and rotor are determined using the relations

$$\varepsilon_S = \alpha_1 + \alpha_2 = 69.34^\circ \tag{B.0.16}$$

$$\varepsilon_R = \beta_2 + \beta_3 = 104.04^\circ \tag{B.0.17}$$

Using the computed deflection angles, the loss coefficients in the stator and the rotor are then computed.

$$\xi_S = 0.04 + 0.06(\varepsilon_S/100)^2 = 0.068 \tag{B.0.18}$$

$$\xi_R = 0.04 + 0.06(\varepsilon_R/100)^2 = 0.104 \tag{B.0.19}$$

Using the velocity at the rotor inlet and the stator outlet the static temperature and pressure at the rotor inlet is calculated.

$$T_2 = T_{02} - \frac{\xi_S C_2^2}{2c_{pg}} = 1187.89 \text{ K} \tag{B.0.20}$$

$$p_2 = p_{02}\left(\frac{T_2}{T_{02}}\right)^{\frac{\gamma}{\gamma-1}} = 386.36 \text{ kPa} \tag{B.0.21}$$

To determine the rotor outlet temperature and pressure the temperature drop per the stage is used.

$$\Delta T_{os} = \frac{\psi U^2}{c_{pg}} = 168.725 \tag{B.0.22}$$

Using the the temperature drop through the stage the stagnation and static temperature and pressure at the rotor outlet is expressed as:

$$T_{03} = T_{01} - \Delta T_{os} = 1031.85 \text{ K} \tag{B.0.23}$$

$$T_3 = T_{03} - \frac{\xi_R C_3^2}{2c_{pg}} = 1028.16 \text{ K} \tag{B.0.24}$$

$$p_{03} = p_{01}\left(\frac{T_{03}}{T_{01}}\right)^{\frac{\gamma_g}{\gamma-1}} = 212.89 \text{ kPa} \tag{B.0.25}$$

The total-to-total efficiency of the turbine stage is then calculated using the dimensionless parameters of the turbine.

$$\eta_{tt} = \frac{1}{1 + 1/2\psi[(\phi^2 + \psi^2)\xi_S + (\phi^2 + 1)\xi_R]} = 0.902 \tag{B.0.26}$$

The total-to-total pressure ratio of the turbine stage is determined as:

$$TPR_{tt} = \frac{1}{(1 - (\Delta T_{os}/\eta_{tt} T_{01}))^{\frac{\gamma}{\gamma - 1}}} = 1.834 \tag{B.0.27}$$

B.1 Turbine Maps

The various turbine maps developed by applying the scaling method to Basson's turbine stages are presented.

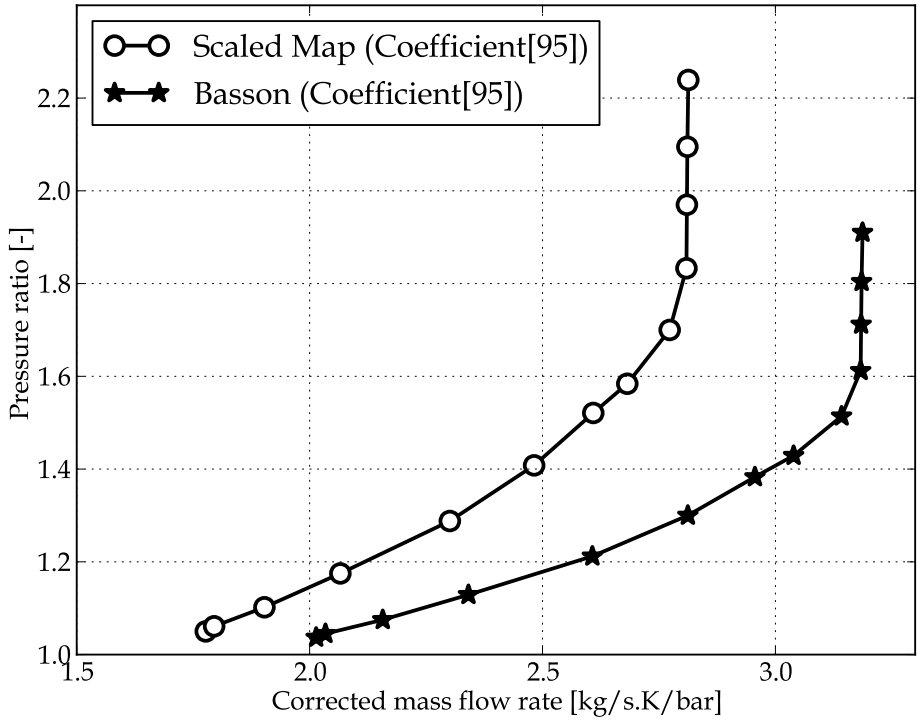

Figure B.1: Pressure ratio vs corrected mass flow rate.

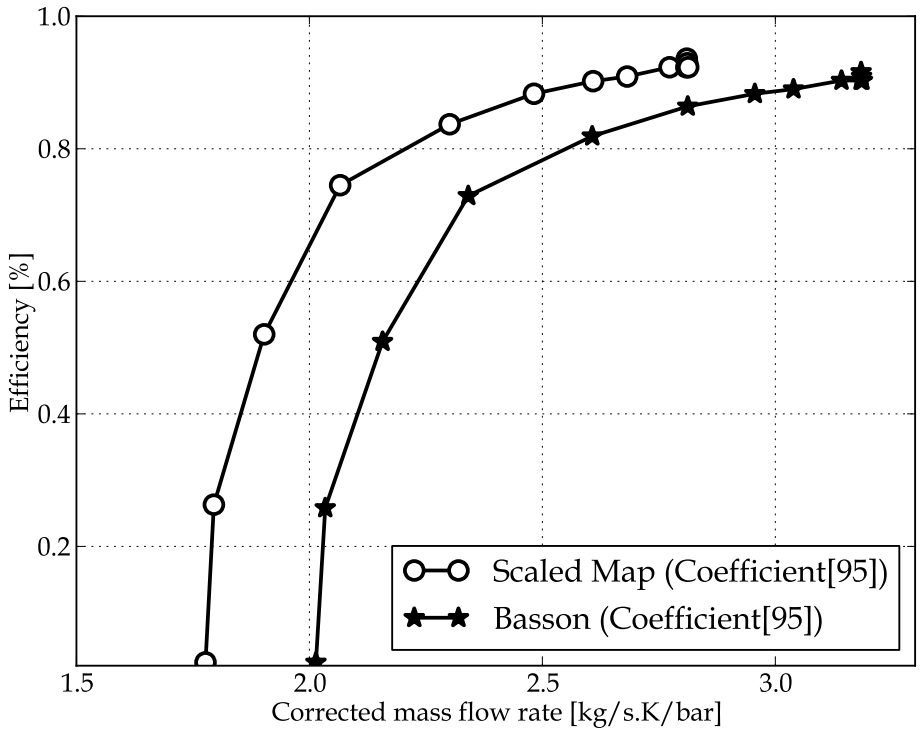

Figure B.2: Efficiency vs corrected mass flow rate.

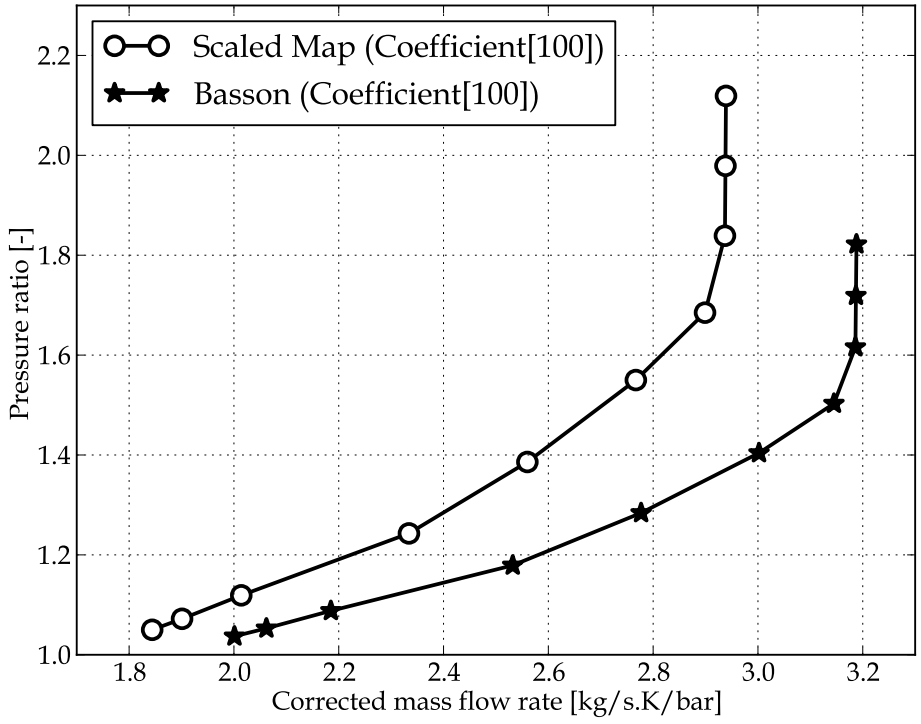

Figure B.3: Pressure ratio vs corrected mass flow rate.

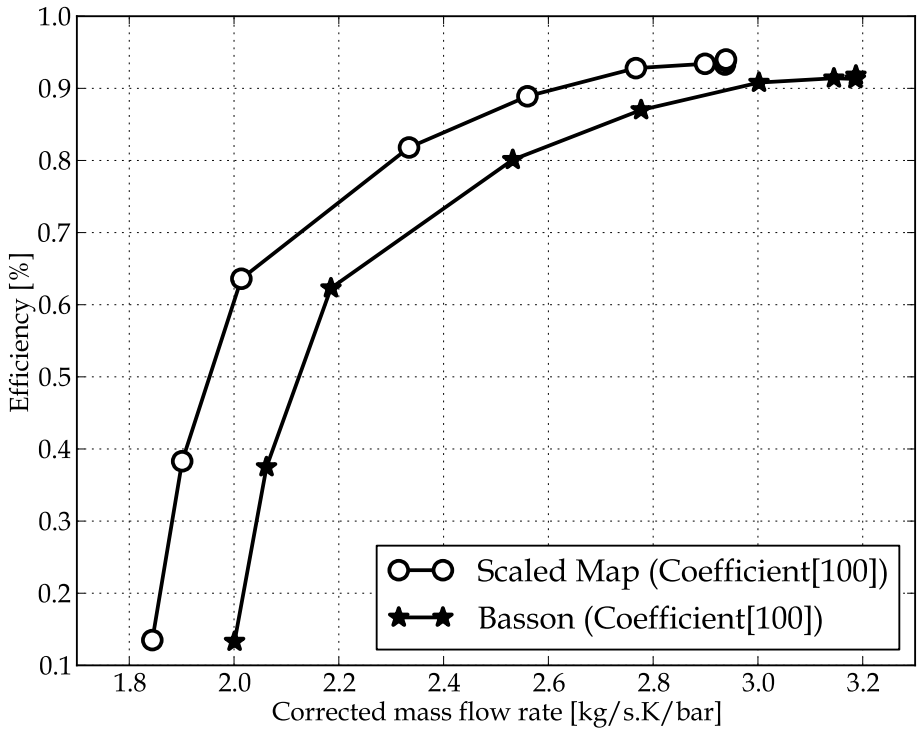

Figure B.4: Efficiency vs corrected mass flow rate.

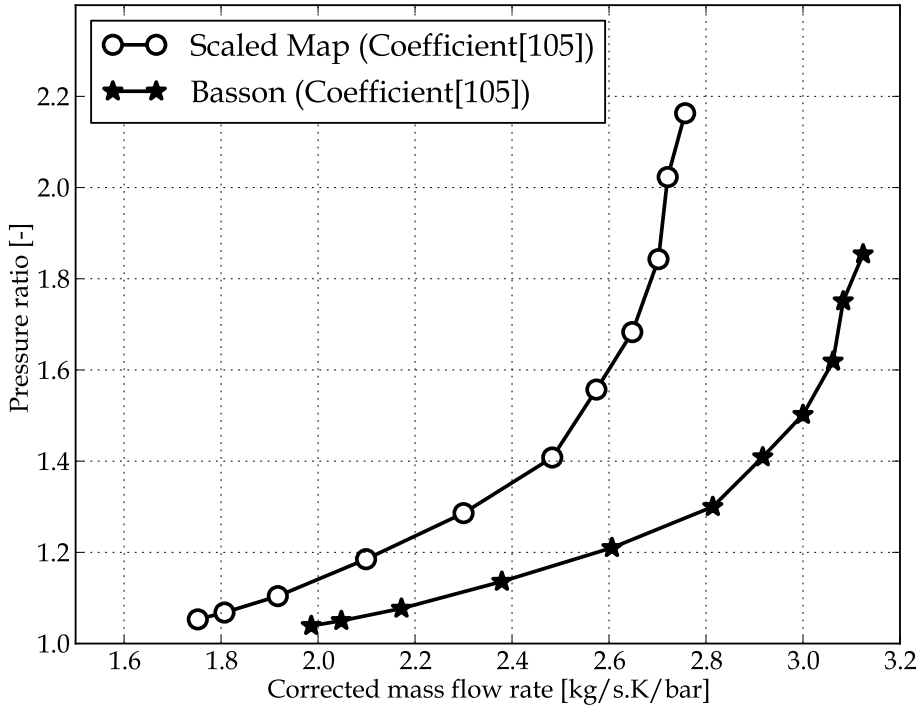

Figure B.5: Pressure ratio vs corrected mass flow rate.

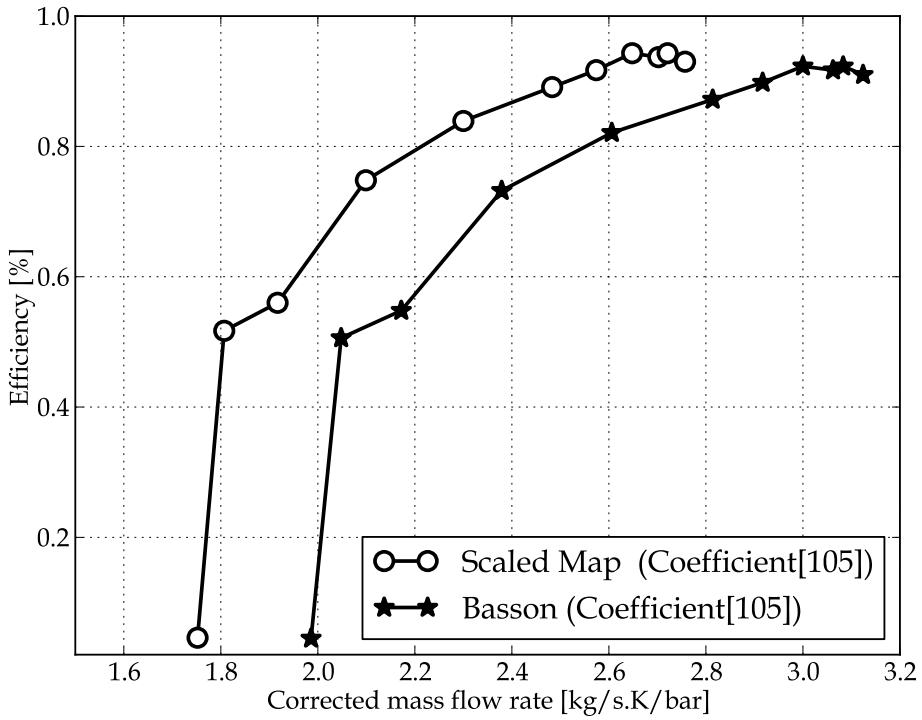

Figure B.6: Efficiency vs corrected mass flow rate.

Appendix C

Experimental Setup

The engine test was undertaken on the gas turbine test rig in the Department of Mechanical and Mechatronic Engineering's combustion and gas turbine test laboratory. Figure C.1 shows a schematic of the test bench. The test bed is made of two thick U-shaped aluminium frames placed on top of each other. The test bed is installed with a set of linear bearing which allows the runner bed with the engine to move for thrust measurement. The test facility is equipped with a bell- mouth at the engine inlet. The bell mouth measures the air mass flow into the engine and ensures laminar distribution of the airflow at the engine intake.

1. Test Facility Inlet
2. Bell-Mouth
3. Circular Duct
4. Base Bed
5. Runner Bed
6. Engine
7. Thrust Load Cell
8. Engine Outlet

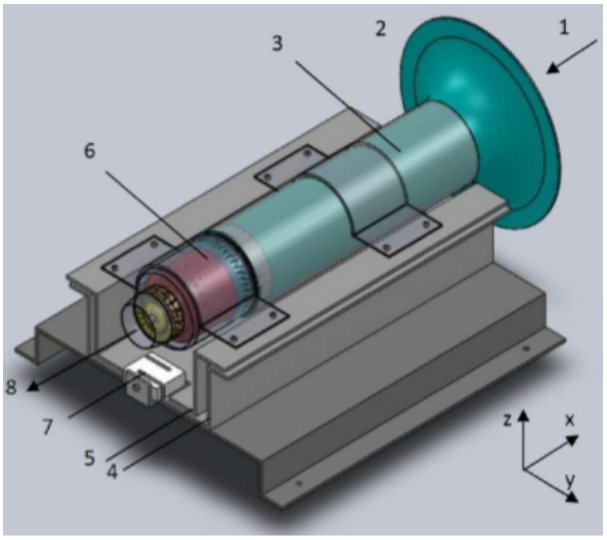

Figure C.1: Test bench, (Krige, 2012).

C.1 Calibration of Measuring Devices

The individual pressure transducers were calibrated using a mechanical hand pump and analogue pressure measuring gauge. The pressure transducers were calibrated at a minimum pressure of 100 kPa and a maximum pressure of 500 kPa. The HBM P8AP pressure transducers shown in Figure C.3 is connected to the HBM QuantumX MX840A data logger shown in Figure C.2 for recording the data. Catman software was used to interpret and record the pressure readings.

Figure C.2: Data logger.

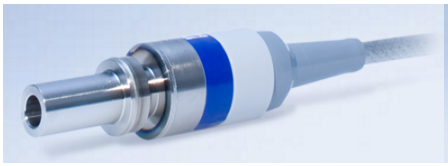

HBM P8AP Pressure Sensor

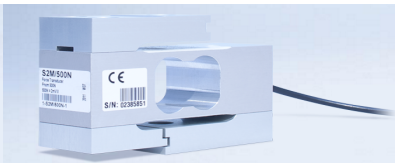

HBM RCC S2M/500N Thrust Sensor

HBM U9C Fuel Consumption Sensor

Figure C.3: Measuring sensors.

Likewise, the thrust and fuel consumption load cells shown in Figure C.2 were also connected to the spider data logger for data interpretation and measurement. The reference thermocouple and K-type thermocouples are connected to the HBM QuatumX MX1609, where the output of each thermocouple is displayed on the PC.

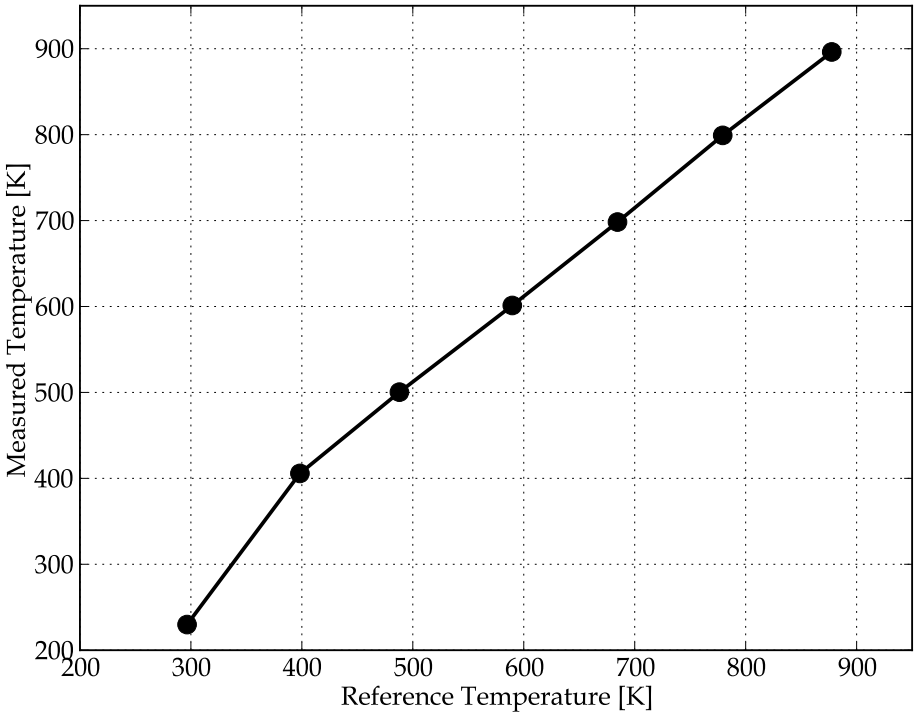

Figure C.4: Temperature calibration.

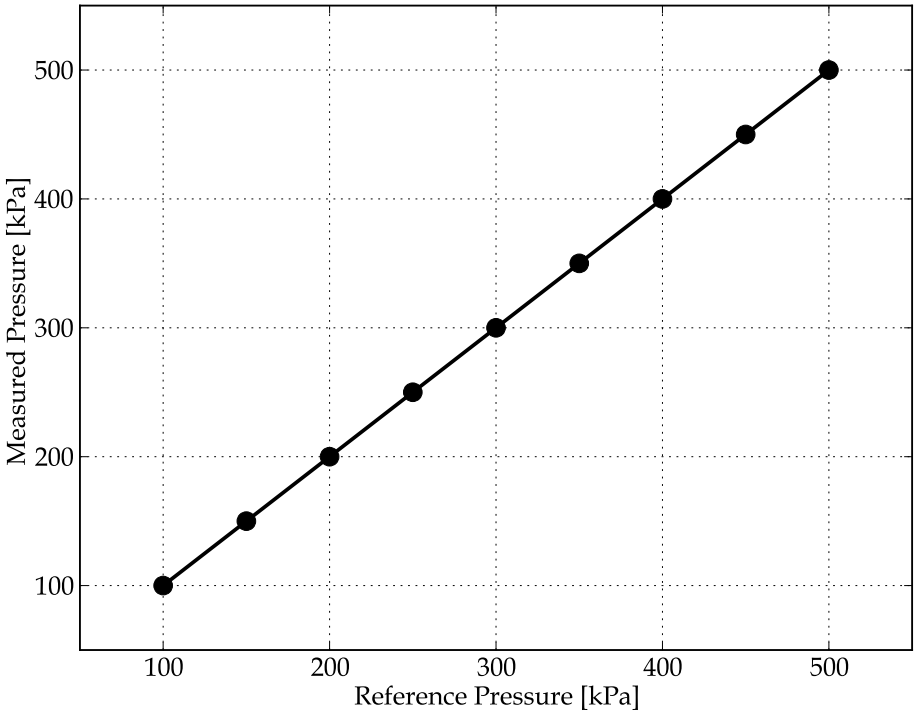

Figure C.5: Pressure calibration.

C.2 Test Procedure

The engine experimental test procedure involves the following sequence:

1. Mount the complete assemble BMT engine on the test rig bed.
2. Fix the engine inlet pressure measuring lines (tubes).
3. Attach the bell-mouth to the inlet of the engine.
4. Connect the measuring temperature probes and pressure sensors to their respective positions on the engine.
5. Mix MGT lubrication oil with the Kerosene fuel in a container and position it on the fuel load cell.
6. Connect the fuel lines from the fuel tank to the engine.
7. Turn on the GSU and do a pre-check run for lubrication of the engine bearings and check for easy flow of fuel.
8. Measure the laboratory environment ambient conditions.
9. Start the engine using the GSU and gradually increase the speed until the desired speed is attained.
10. Throttle the engine to idling and shut it down.
11. Save the recorded performance data for further analysis.

Appendix D

Engine Components

The BMT engine individual components are presented in this section. The components include the compressor and turbine stage as well as the combustion chamber.

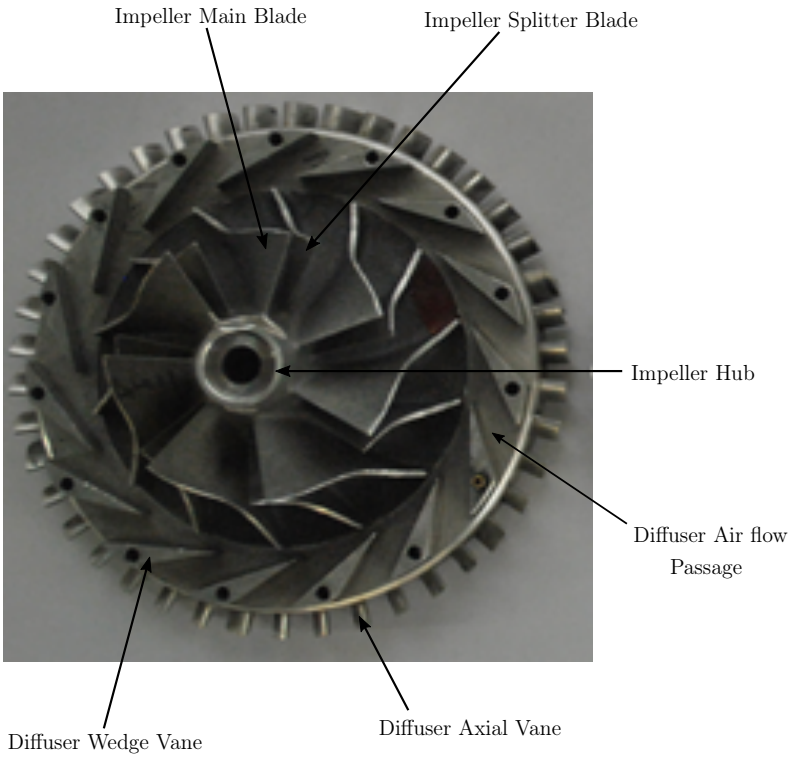

Figure D.1: BMT engine compressor stage (Impeller and diffuser).

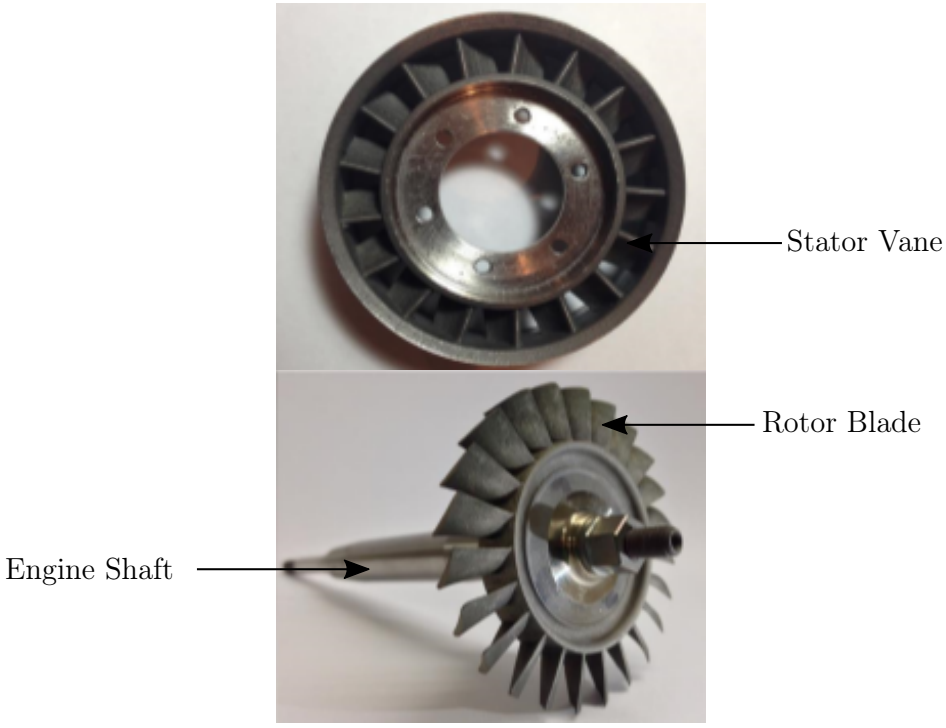

Figure D.2: BMT engine turbine stage (Stator and rotor).

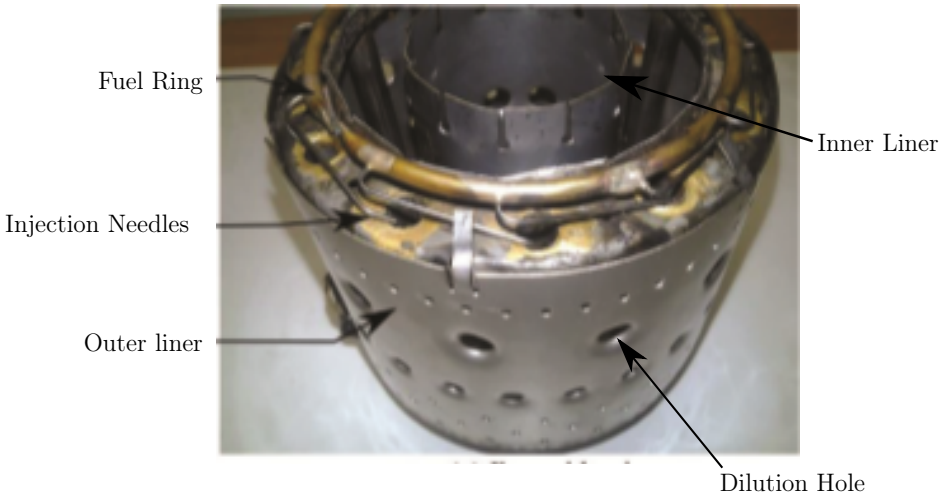

Figure D.3: BMT engine combustion chamber.

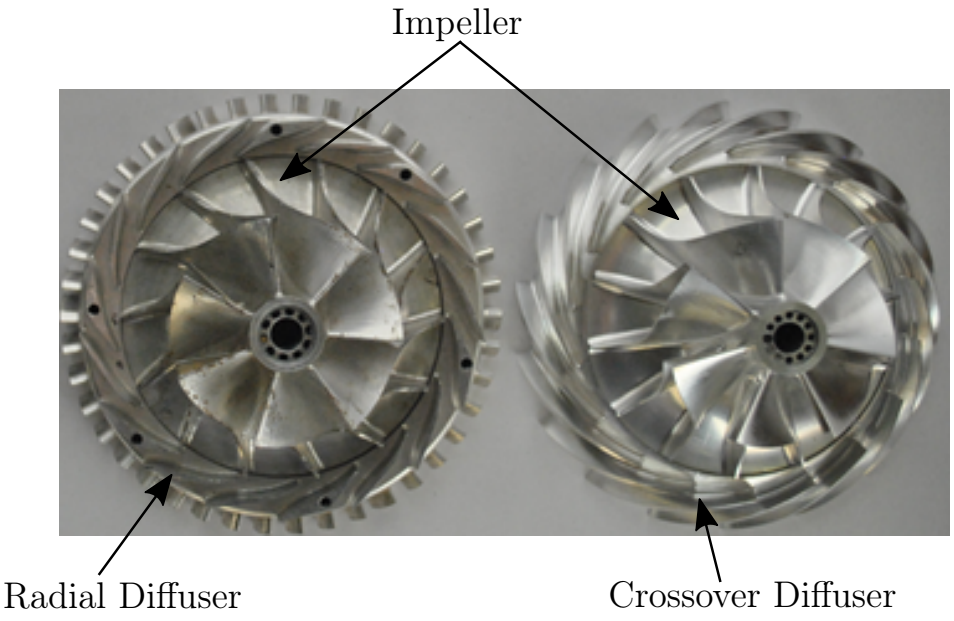

Figure D.4: BMT redesigned compressor stages. (Krige and Burger)

List of References

Abdel-Fattah, A.M. and Frith, P. (1995). Derivation of axial compressor stage characteristics from the overall performance map. In: *Proceedings of the 12th Australasian Fluid Mechanics Conference*, pp. 8–15.

Akbari, P. and Müller, N. (2003). Performance investigation of small gas turbine engines topped with wave rotors. *AIAA Pap*, vol. 4414.

Amirante, R., Catalano, L., Dadone, A. and Daloiso, V. (2007). Design optimization of the intake of a small-scale turbojet engine. *Computer Modeling in Engineering and Sciences*, vol. 18, no. 1, p. 17.

Armstrong, J. and Verstraete, D. (2014). Semi-constant volume combustion in a micro gas turbine. In: *Fourth Australasian Unmanned Systems Conference*.

Asgari, H. (2014). *Modelling, Simulation and control of gas turbines using artificial neural networks*. Ph.D. thesis, University of Canterbury.

Badami, M., Nuccio, P. and Signoretto, A. (2013). Experimental and numerical analysis of a small-scale turbojet engine. *Energy Conversion and Management*, vol. 76, pp. 225–233.

Baird, A. (2011). *Operators Manual for the BMT120KS Series Turbine Engine.*

Bakalis, D.P. and Stamatis, A.G. (2012). Data analysis and performance model calibration of a small turbojet engine. *Proceedings of the Institution of Mechanical Engineers, Part G: Journal of Aerospace Engineering*, vol. 226, no. 12, pp. 1523–1533.

Bar, W. and Czarnecki, M. (2009). Design-point, off-design meanline performance analysis and cfd computations of the axial turbine to micro gasturbine engine. *Journal of KONES*, vol. 16, pp. 9–16.

Basson, J.G.T. (2014). *Design methodology of an axial-flow turbine for a micro jet engine.* Master's thesis, Stellenbosch University.

Bauwens, P. (2015). *Gas path analysis for the MTT micro turbine.* Ph.D. thesis, TU Delft, Delft University of Technology.

Becker, C.P. (2015). Development of velocity and temperature probes for a micro gas turbine. Tech. Rep., Stellenbosch University.

Bringhenti, C. and Barbosa, J.R. (2004). Performance study of a 1 mw gas turbine. In: *Proceedings of the 10th Brazilian Congress of Thermal Sciences and Engineering, ENCIT, Brazil Soc. of Mechanical Sciences and Engineering–ABCM, Rio de Janeiro, Brazil, Nov.*

Brohez, S., Delvosalle, C. and Marlair, G. (2004). A two-thermocouples probe for radiation corrections of measured temperatures in compartment fires. *Fire Safety Journal*, vol. 39, no. 5, pp. 399–411.

Burger, C.J. (2016). *Design Procedure of a Compact Aerodynamic Crossover Diffuser for Micro Gas Turbine Application*. Master's thesis, Stellenbosch University.

Cerri, G., Salvini, C., Procacci, R. and Rispoli, F. (1993). Fouling and air bleed extracted flow influence on compressor performance. In: *ASME 1993 International Gas Turbine and Aeroengine Congress and Exposition*, pp. V03CT17A027–V03CT17A027. American Society of Mechanical Engineers.

Chaudhari, K., Kulshreshtha, D. and Channiwala, S. (2012). Design and cfd simulation of annular combustion chamber with kerosene as fuel for 20 kw gas turbine engine. *combustion*, vol. 2, no. 6.

Cohen, H., Rogers, G. and Saravanamuttoo, H. (1996). H, 1996, gas turbine theory.

Cumpsty, N. (2003). A simple guide to the aerodynamic and thermodynamic design and performance of jet engines.

De Villiers, L.C.B. (2014). *Design of a Centrifugal Compressor for Application in Micro Gas Turbines*. Master's thesis, Stellenbosch University.

Dixon, S.L. and Hall, C. (2013). *Fluid mechanics and thermodynamics of turbomachinery*. Butterworth-Heinemann.

El-Sayed, A.F. (2008). *Aircraft propulsion and gas turbine engines*. CRC Press.

Farokhi, S. (2014). *Aircraft propulsion*. John Wiley & Sons.

Figliola, R.S. and Beasley, D.E. (2015). *Theory and design for mechanical measurement*. John Wiley and Sons.

Flack, R. (1990). Analysis and matching of gas turbine components. *International Journal of Turbo and Jet Engines*, vol. 7, no. 3-4, pp. 217–226.

Gao, J.-h. and Huang, Y.-y. (2011). Modeling and simulation of an aero turbojet engine with gasturb. In: *Intelligence Science and Information Engineering (ISIE), 2011 International Conference on*, pp. 295–298. IEEE.

Gieras, M.M. (2012). Computational study of an aerodynamic flow through a micro-turbine engine combustor. *Journal of Power Technologies*, vol. 92, no. 2, p. 68.

Gilani, S.I.-u.-H., Baheta, A.T., Majid, M.A.A. and Amin, M. (2008). Thermodynamics approach to determine a gas turbine components design data and scaling method for performance map generation. In: *International conference on plant Equipment and reliability, Selangor, Malaysia.*

Guidez, J., Roux, P., Poirson, N., Jourdanneau, E., Orain, M. and Grisch, F. (2009). Investigation of combustion in miniaturised combustor for application to micro gas turbines. In: *Progress in Propulsion Physics*, vol. 1, pp. 469–480. EDP Sciences.

Iancu, F., Piechna, J., Dempsey, E. and Müller, N. (2005). Ultra-micro wave rotor investigations. *Technical Digest PowerMEMS*, pp. 93–96.

Jie, C. and Guoping, H. (2010). Redesign of an 11 cm-diameter micro diffuser. *Chinese Journal of aeronautics*, vol. 23, no. 3, pp. 298–305.

Krieger, G.C., de Campos, A.P., Sacomano Filho, F.L. and Souza, R.C.d. (2012). A swirler stabilized combustion chamber for a micro-gas turbine fuelled with natural

gas. *Journal of the Brazilian Society of Mechanical Sciences and Engineering*, vol. 34, no. 4, pp. 441–449.

Krige, D. (2012). *Performance evaluation of a micro gas turbine centrifugal compressor diffuser*. Master's thesis, Stellenboosch University.

Krivcov, A., Shabliy, L. and Baturin, O. (2014). Gas-dynamic modeling of gas turbine engine components collaborative workflow. *Open Mechanical Engineering Journal*, vol. 8, pp. 445–449.

Kurzke, J. (2012). *Design and Off-Design Performance of Gas Turbines*.

Leylek, Z., Anderson, W.S., Rowlinson, G. and Smith, N. (2013). An investigation into performance modeling of a small gas turbine engine. In: *ASME Turbo Expo 2013: Turbine Technical Conference and Exposition*, pp. V05AT23A007–V05AT23A007. American Society of Mechanical Engineers.

Li, Y. (2002). Performance-analysis-based gas turbine diagnostics: A review. *Proceedings of the Institution of Mechanical Engineers, Part A: Journal of Power and Energy*, vol. 216, no. 5, pp. 363–377.

Ling, J., Wong, K. and Armfield, S. (2007). Numerical investigation of a small gas turbine compressor. In: *16th Australasian Fluid Mechanics Conference (AFMC)*, pp. 961–966. School of Engineering, The University of Queensland.

M-Tech (2015). *General User Manual*. www.flownex.com.

MacIsaac, B. and Langton, R. (2011). *Gas Turbine Propulsion Systems*, vol. 49. John Wiley & Sons.

Meyers, B. (2016). Personal communication.

Mirza-Baig, F. and Saravanamuttoo, H. (1991). Off-design performance prediction of turbofans using gasdynamics. In: *ASME 1991 International Gas Turbine and Aeroengine Congress and Exposition*, pp. V002T02A034–V002T02A034. American Society of Mechanical Engineers.

NASA (2016). Ideal brayton cycle.

Available at: `https://www.grc.nasa.gov/www/k-12/airplane/brayton.html`

Pachidis, V., Pilidis, P., Talhouarn, F., Kalfas, A. and Templalexis, I. (2006). A fully integrated approach to component zooming using computational fluid dynamics. *Journal of engineering for gas turbines and power*, vol. 128, no. 3, pp. 579–584.

Pinkel, B. and Karp, I.M. (1947). A thermodynamic study of the turbojet engine.

Procacci, R. and Rispoli, F. (1995). *Off design performance evaluation of deteriorated variable geometry axial flow compressors*. ASME.

Rahman, N. and Whidborne, J.F. (2008). A numerical investigation into the effect of engine bleed on performance of a single-spool turbojet engine. *Proceedings of the Institution of Mechanical Engineers, Part G: Journal of Aerospace Engineering*, vol. 222, no. 7, pp. 939–949.

Sayers, A.T. (1990). *Hydraulic and compressible flow turbomachinery*. Cape Town, McGraw-Hill London.

Smit, F.V. (2014). Investigating the design of the turbine stage of a specific micro-gas turbine engine. Tech. Rep., Stellenbosch University.

Snyder, P.H. and Fish, R.E. (1996). Assessment of a wave rotor topped demonstrator gas turbine engine concept. In: *ASME 1996 International Gas Turbine and Aeroengine Congress and Exhibition*, pp. V001T01A009–V001T01A009. American Society of Mechanical Engineers.

Söhret, Y., Turan, Ö. and Karakoç, T.H. (2015). Analysis of combustion efficiency for turbofan engine combustor using matlab. *International Journal of Engineering and Technology*, vol. 7, no. 2, p. 86.

Stamatis, A. (2011). Evaluation of gas path analysis methods for gas turbine diagnosis. *Journal of Mechanical Science and Technology*, vol. 25, no. 2, pp. 469–477.

Suchocki, T., Lampart, P. and Klonowicz, P. (2014). Numerical investigation of a gtm-140 turbojet engine. *Open Engineering*, vol. 5, no. 1.

Suraweera, J.K. (2011). *Off-Design Performance Prediction of Gas Turbines without the use of Compressor or Turbine Characteristics*. Master's thesis, Carleton University Ottawa.

Thirunavukarasu, E. (2013). Modeling and simulation study of a dynamic gas turbine system in a virtual test bed environment.

Tomita, J.T. and Barbosa, J.R. (2003). A model for numerical simulation of variable stator axial flow compressors. In: *Proceedings of 17th International Congress of Mechanical Engineering–COBEM*.

Toro, C.A.G., Wong, K. and Armfield, S. (2008). Computational study of a micro-

turbine engine combustor using large eddy simulation and reynolds averaged turbulence models. *ANZIAM Journal*, vol. 49, pp. 407–422.

Trebunskikh, T., Ivanov, A. and Dumnov, G. (2012). Floefd simulation of microturbine engine. In: *Proceedings of Applied Aerodynamics Conference on Modelling & Simulation in the Aerodynamic Design Process*.

Tsoutsanis, E., Meskin, N., Benammar, M. and Khorasani, K. (2015). Transient gas turbine performance diagnostics through nonlinear adaptation of compressor and turbine maps. *Journal of Engineering for Gas Turbines and Power*, vol. 137, no. 9, p. 091201.

Van Der Merwe, B.B. (2012). *Design of a Centrifugal Compressor Impeller for Micro Gas Turbine Application*. Master's thesis, Stellenbosch University.

Verstraete, D., Hendrick, P., Djanali, V., Ling, J., Wong, K. and Armfield, S. (2010). Micro propulsion activities at the university of sydney. In: *Proceedings of the Powermems 2010 Conference*.

Walsh, P.P. and Fletcher, P. (2004). *Gas turbine performance*. John Wiley & Sons.

Wilson, J. and Paxson, D.E. (1993). Jet engine performance enhancement through use of a wave-rotor topping cycle. Tech. Rep., NASA.